The Physical Connection between Cosmic Gas Flows, Supermassive Black Holes Growth, and Galaxy Evolution

Natalie Nicole Bran Sanchez

A dissertation
submitted in partial fulfillment of the
requirements for the degree of

Doctor of Philosophy

University of Washington

2022

Reading Committee:

Jessica Werk, Chair

Thomas Quinn

Charlotte Christensen

Program Authorized to Offer Degree:

Astronomy

University of Washington

Abstract

The Physical Connection between Cosmic Gas Flows,
Supermassive Black Holes Growth,
and Galaxy Evolution

Natalie Nicole Bran Sanchez

Chair of the Supervisory Committee:
Associate Professor Jessica Werk
Astronomy

The circumgalactic medium (CGM) represents a key interface in the processes of galactic evolution. Here, the gas which enters galaxies through mergers and filaments and the gas expelled from a disk through stellar and black hole feedback intersect, maintaining a reservoir that will shape a galaxy throughout its lifetime. However, due to the diffuse and difficult-to-observe nature of this gaseous region, the degree to which galactic processes impact it are still uncertain, making the CGM a natural laboratory for testing the impact of different feedback models. The CGM of Milky Way-mass galaxies are the best targets for these analyses as these galaxies lie at the turnover mass during which galaxies switch from being dominated by stellar processes and become dominated by supermassive black hole (SMBH) or active galactic nucleus (AGN) processes.

My focus of my thesis work is in exploring the impact of supermassive black hole (SMBH) feedback on the evolution of Milky Way-mass (MW-mass) galaxies in hydrodynamic simulations. We use simulations from the N-body+Smoothed particle hydrodynamics code, ChaNGa, and include a 25 Mpc cosmological volume, ROMULUS25, and a suite of "genetically modified" (GM) galaxies. These GM galaxies originate from nearly identical initial conditions resulting in minor modifications to their accretion histories that maintain the large scale structure and final halo mass of the original simulation. We find that (1) the

SMBH propagates metals from the disk out into CGM, (2) the mass of metals retained by the galaxy depends on its deviation from the M-sigma relation, and (3) black hole accretion histories can be influenced by larger scale galaxy accretion physics, which work in tandem to quench star formation.

TABLE OF CONTENTS

LIST OF FIGURES

Figure Number Page

LIST OF TABLES

ACKNOWLEDGMENTS

In this section, I hope to properly thank all of the communities, institutions, and people who have invested in my success. I am the child that the village of my community has raised, and I am deeply thankful to so many for the love, support, friendship and mentorship that I have experienced while becoming the scientist and the doctor that I am today. I know I will not be able to fit absolutely everyone here (or else this thesis will become thousands of pages long), but I will do my best.

In roughly (academic) chronological order, I want start by thanking the Santa Monica College Astronomy O3 Club and its founder, Professor Gary Fouts. It was in this class that I first decided to pursue astronomy as a career, and I can't imagine what my life would be if I had not taken this first astronomy class in community college. At Cal Poly Pomona, I'd like to thank the CAMPARE and Cal-Bridge program for supporting me in an REU that represented my first experience as a researcher at the University of Arizona. Professor Matt Povich and Professor John Bieging were great mentors for my research on the M17 nebula and I thank them for the experience that led me to decide to pursue grad school in astronomy. I'd also like to thank Professor Alex Rudolph for his incredible support both as an undergraduate student in CAMPARE and through the years since. He has provided wisdom and encouragement throughout my time as a graduate student, and I am so excited to return to California this Fall and join him in his work with Cal-Bridge as a postdoc mentor. I continued my journey as a student in the Fisk-Vanderbilt Masters-to-PhD Bridge Program and I am so thankful for the continued support of this program both during my time in Nashville and as I moved to Seattle. I met wonderful and lifelong mentors during my two years in the program including Dr. Jillian Bellovary (LET'S GO MUSIC CITY!! NRG!),

Dr. Jedidah Isler (I never apologize during talks anymore!), and Dr. Dina Stroud (Where in the world do we meet up for dinner next?). Thank you all so much for the times we shared. Some of the friends I'd like to highlight in this period of my life are Blake Silberman, Thanh Ngyuyen, Anoush Kazarians, Jessica Maldonado, Abigail Searfoss, and Richard Galvez. It's been anywhere from six years to a decade since we met in physics classrooms and laughed (or cried) over shared meals, but I am still so thankful for all of you. A special thank you to Sirose Loyola and Kirsten Labastida for being the most fabulous and joyful girl gang anyone could ask for. We never went to school together. Life just threw us together a we chose to share our weeb-y wackiness forever and for that I will always be grateful.

Having completed this thesis at the University of Washington, this section of acknowledgements will be necessarily thorough. I've built such a life here over the last six years and it has been filled with the most wonderful people.

To every single graduate student that I overlapped with, I appreciate you even if our time was short. To name just a few, thank you to my dear office mates: Dr. Brett Morris, Debby Tran, and Samantha Gilbert; to the board game crew: Heather Nuhfer, Paul Morrissey, Phoebe Sanderbeck, and Colin Papsworth; to the Old Fogies: Hannah Bish, Diana Windemuth, Michael Blatnik; to all of GCAP, but especially Myles McKay, Brianna Thomas, Lupita Tovar, and Bethlee Lindor; and to the grad students who have moved on to become my mentors in research and in life: Michael Tremmel and Grace Telford. You are all stars, and I'm so thankful to have been a part of your constellation.

Thank you to Night Lunch, Seattle's Premiere and ONLY All-Astronomy Rock Band. Screaming into a microphone for four hours every weekend is the only thing that kept me sane for so many years. I love you boys forever. CAMP NIGHTLUNCH COMETH.

A huge thank you to my thesis committee. All of you are not only committee members, but have been incredible mentors over the last six years. Professor Charlotte Christensen, you didn't have to be my co-advisor from three thousand miles away, but you did. Thank

you so much for all your computational wisdom and helping me become a better mentor myself. Professor Thomas Quinn, you've always shared your seemingly infinite knowledge of the simulations with humility and kindness. I never felt bad asking you questions (sometimes more than once!) and I appreciate everything I've learned from you about creating my own universe. Professor Julianne Dalcanton, I have learned so much about galaxies from you but what I'm more thankful for is the way that you would twitter message me to make sure things were alright when I was struggling with the other hard things in life. I'll never stop appreciating your guidance and support. Finally, Professor Jessica Werk, I could write an entire new acknowledgement section about our time together, but I will restrain myself. Suffice it to say, thank you so much for believing in me, even when I stopped believing in myself. I know that as one of your first graduate students, I made you *werk* hard sometimes, but I see in myself now the ways that you have fostered my growth (even when I ran off in different directions). Thank you for preparing me for the life of an astronomer, and for your amazing cameos at Whine Time Karaoke.

Finally, I want to thank my family. To my mother, Lili Williams, and my step-father, Bob Williams, who support me will all their love from another country. I'm so glad you were able to be there when I defended my PhD, and I can't wait to lay on beaches together again soon. To Luis Sanchez, who gave me my name. I literally wouldn't be here without you and your support in college. I appreciate you and our relationship. To Alan Sims, I'm pretty sure your dad isn't supposed to be one of your best friends, but here we are. Thank you for answering every phone call and talking me through the hard times in life. To Jason Poe, you'll probably never read this, but I still appreciate you, Big Bit. To Dr. Lia Medeiros, if you're wondering why you're not featured earlier it's because you are officially family. You're the sister I never knew I needed. To you all, I love you so much.

And especially, thank you to Trevor who I can now officially call my husband. You and Pod are my family. I'm so excited to see the next step of our journey together. I already

said all the important bits in my wedding vows just last week, so I'm not going to blather on about how much I love you. You know. No leave, only stay.

Last of all, and inspired by the woman at UW graduation whose acknowledgements said only "The person I should thank most for my achievements is me," I want to thank you, Natalie Nicole Sanchez. You're reading this sometime in the future and hopefully living out all the dreams that I have for you. Thank you for going to community college and taking a chance on stars and space. Thank you for living in pool houses and sleeping in cars and getting through undergrad. Thank you for joining roller derby in Nashville and getting that first tattoo. Thank you for deciding to study simulations even though you thought "I'm too dumb to do theory." Thank you for making the hard choice and moving to Seattle. Thank you for choosing yourself, for making music and sharing it loudly, for laughing and crying, for building new friendships and keeping the only ones. I am here in this moment putting the final touches on this thesis because of every choice and every sacrifice you made. It was good and it was hard and it was worth it.

I love you, future Nicole. I hope you're still choosing it all.

DEDICATION

to Toodle and Pod

Chapter 1

A BRIEF HISTORY OF THE (SIMULATED) UNIVERSE

A bright screen which shows a heroine frozen mid-run through an avenue of dark trees. The dramatic beating of a drum and screeching strings momentarily silenced. The shape of a monster in silhouette against the dark blue sky. A scene meant to inspire shock and terror. By hitting the pause button on a scary movie such as this one, a viewer can admire the technical skills required to make such movie magic. A cinematographers skilled eye. A costumers skilled hands. More recently, the impressive (and only sometimes subtle) impact of special effects.

However, it is only if you were to rewind this tale returned backwards in time from the precipice of this monster's attack, that you could learn the history of this moment. The reason our characters have been drawn to the woods. The motivation of the heroine. The evolution of the monster. All of the pieces that bring this story to life.

So what does this have to do with astronomy?

Well, as a theoretical astronomer, I am, in a sense, much like a movie director. I create stories, or *theories*, about the evolution of galaxies and the way that the universe works by stepping moment by moment through movies, that is *simulations*.

For decades, simulations have been a necessary tool for understanding the underlying physics of the universe. These simulations allow us to continue the work of unpacking the results of observational surveys by giving us a glimpse into the history of galaxy formation. Returning to our metaphor, we can imagine the glowing spiral disk galaxy, Andromeda (seen in Figure 1.1), as the ending to our movie. (If it helps to imagine Spock or Han Solo flying in the foreground, please do.) A key benefit of studying galaxies in this manner come from out ability to *rewind* our galaxy back through time, to witness the gas flowing in and out, the

Figure 1.1: An image of Andromeda taken by David Dayag. Also known as Messier 31, Andromeda is the closest galaxy to our own Milky Way and the two are expected to collide within the next $\sim$ 5 billion years. Schiavi2020

colliding of galaxies with each other, and any other explosive and exciting events throughout a galaxies life, or evolution. By combining the powers of these galaxy simulations with observations, both in the creation of these simulations and afterwards by comparing them to observations, we deepen our understanding of the universe and all the underlying physical mechanisms at play.

Throughout my work, I use cosmological simulations to understand the evolution of galaxies. Cosmological simulations include information about the cosmology, i.e. large scale structure and dynamics, of the universe within which our galaxies form and evolve. There are two main types of these cosmological simulations: volumes and zoom-ins. Volumes simulate a fraction of the universe[1] and contain hundreds to thousands of galaxies, allowing us to draw

[1]For example, a common size for a dark matter-only volume is 50 Mpc on a side. That is 10^{10}, or 10 billion, times the size of our solar system. I.e. these simulations are quite large.

conclusions from the statistical sample of galaxy populations. Meanwhile, zoom-in galaxy simulations focus on one main or central galaxy and trace its individual history through time, while simulating the surrounding environment at a courser resolution. Due to the differences in scales, zoom-in galaxies often have the benefit of being higher resolution, but they lack the capability to draw statistically significant conclusions like from volumes. In my work, I combine the power of both cosmological volumes and zoom-in galaxies to draw precise conclusions that maintain cosmological context.

In particular, I use N-Body/smooth particle hydrodynamic (SPH) simulations which use discrete particle to represent dark matter, gas, and stars. This method relies on the assumption that gas, on large scales, behaves as a fluid, and solves the equations of hydrodynamics using Lagrangian methods. There are other methods used to simulate galaxies, such as adaptive mesh refinement (AMR), an Eulerian method, which represents the galaxy in the form of a mesh or grid wherein each cell tracks the gas properties in the corresponding region of space[28;29;162]. Each box in the grid represents an individual particle with its specific properties, and due to the nature of the grid-based system, each component of the grid can selectively increase or decrease resolution. More recently, moving mesh, a combination of Eulerian and Lagrangian techniques, has also been applied to galaxy formation studies[296]. While each of these methods have their strengths and their caveats, I will mostly focus on the details of SPH simulations and characteristics that are broadly consistent across the different types.

The process of accurately simulating a galaxy is complicated and through time has been fraught by missing components and a lack of computational power. Some of the first galaxy formation simulations, which were limited by early computational methods, focused only on dark matter halos.[2] These simulations, though limited in scope, led important strides in understanding halo population models[239], the assembly of massive clusters[364], and the

[2]Semi-analytical models, which combine numerical dark matter-only simulations with analytical models for the baryons, have and continue to bridge part of the divide between high computational expense and resolution limitations[41;63;116;146;294].

growth of large scale structure[1;82]. Since this first wave of galaxy simulations the scale has increased from a few thousand particles to over a trillion[238], and exponentially increased our understanding of the physics driving galaxy evolution. Nevertheless, the current scale of resolution demands that some of the physical mechanisms in our simulations be implemented through "sub-grid" physical models which attempt to capture the relevant physics at sub-resolution scales. For example, one commonly used method to model the accretion of SMBHs is to use Bondi-Hoyle accretion[34], Thus, as the resolution of these simulations increases and better, more accurate sub-grid physical models are created with each new generation, our understanding of the universe grows as well.

It was only within this last decade or so that simulations began to reproduce observed galaxy relations[113;134;151;275;299;322;344;353]. One essential difficulty arising from the many different and co-dependent mechanisms at play in galaxy evolution.

1.1 The Prescriptions of Galaxy Simulations

Some of the key models and sub-grid prescriptions[3] in galaxy simulations include: gas cooling, star formation, stellar feedback/energy ejection, supermassive black hole formation and accretion, active galactic nuclei feedback, magnetic fields, and more recently, cosmic rays.

Gas cooling processes such as hydrogen and helium line cooling, Bremsstrahlung, inverse Compton, and metal line cooling are a critical model within galaxy simulations as they directly impact the formation of stars. However, resolution effects can limit the implementation of some models. For example, at the resolution of the cosmological volume, ROMULUS25[322] ($M_{gas} \sim 10^5$, $M_{DM} \sim 10^5$, See Section 2.2 for additional details), we are unable to resolve individual star formation regions. Therefore, the inclusion of a full treatment for metal cooling results in over-cooling within a galaxy and creates an unrealistic interstellar medium[56].

[3]Depending on the resolution of the simulation, the physics that impacts the different components can not be directly implemented hence the implementation for a "sub-grid" model. For example, in the resolution of the ROMULUS25 cosmological volume (See Section 2.2), star particles are created with a mass of $\sim 10^4$ $M_\odot$ meaning that each particle must represent a stellar *population*. Therefore, we apply an initial mass function to each particle which determines how many individual stars and of what mass are represented within each star particle.

At higher resolutions, such as those of the Justice League[11] ($M_{gas} \sim 10^4$, $M_{DM} \sim 10^4$), the inclusion of a full prescription for metal cooling is possible. Thus, while gas cooling is a physical process which does not require a sub-grid implementation, whether a simulation can resolve different gas phases determines which cooling processes can be applied.

Star formation is naturally a key component in galaxy formation. Stars form from gas particles which can be subject an array of specific criteria in terms of density[275;353], temperature[322], environment within gravitationally bound regions[134;278], gas prone to gravitational instability (or Jeans Length criteria), and other requirements. An efficiency rate of 1% is supported by observations[31;171] for gas to convert into stars per expected rate of gravitational collapse (i.e. free fall time), and star formation rates are typically use a Kennicutt-Schmidt relation,

$$\frac{dM_*}{dt} = \frac{\epsilon M_g}{t_{ff}}, \tag{1.1}$$

where dM_*/dt is the stellar mass production rate, ϵ is the efficiency constant (usually a value between 0.01 and 1 constrained by observations), M_g is the mass of the gas particle, and t_{ff} is the free fall time. After star particles are formed, stellar evolution is tracked including supernova ejecta (typically Type Ia and Type II and more recently neutron star mergers) and the metal enrichment of the surrounding gas[210;342;367]. The metal yields assumed in simulations are determined through stellar evolution calculations and can often be a source of uncertainty.[4]

The injection of energy and momentum into the local environment by stellar winds and supernova or by active galactic nuclei (AGN) is known collectively as stellar feedback or AGN/supermassive black hole (SMBH) feedback. Feedback plays a critical component in the growth and evolution of galaxies. My work in particular has centered on the analysis of feedback prescriptions, with a focus on SMBH or AGN feedback, and how this feedback impacts the gas inside and around galaxies. However, the implementation of sub-grid models for feedback processes can vary widely between galaxy simulations which motivates both my

[4]This uncertainty has been an important caveat in my work, as shown in Chapters 2 and 4.

past and ongoing work as well as the continued progress needed to better understand the coupling of feedback energy to gas physics.

1.2 Feedback, feedback, feedback

Decades of observations have shown that large scale gas outflows driven by energetic processes in the disk of a galaxy are a critical component in galaxy evolution. Stellar feedback[292] from supernova and stellar winds is an important source of energy for driving outflows through radiation pressure, thermal pressure, and cosmic rays[48;109;335]. Additionally, SMBHs, during their growth phase as AGN, can drive powerful winds that evacuate gas from the center of their host galaxy[160] and quench star formation[59;86;88;265]. There is a variety of observational evidence for stellar feedback driven outflows[37;262] and observations of outflows driven by AGN[247;316], but a deeper understanding of the underlying physics driving these outflows is still necessary.

Current stellar feedback methods have a variety of implementations but have two main forms when it comes to supernova energy expulsion: thermal or kinetic. In the case of thermal stellar feedback, nearby gas is heated after supernova events and, to avoid excessive cooling, radiative cooling will be shut off for a specific amount of time (typically $\sim 10^7$ yr)[303]; gas will be heated to high enough temperatures that radiative cooling is ineffective for $\sim 10^7$ yr[66]; or thermal energy will be tracked in a seperate hot phase[156;295]. In other cases, kinetic energy must thermalize before being radiated away. Newer models also include other feedback channels such as the energy and moment injected via stellar winds and the photoionization and radiation pressure of nearby young, massive stars[4;129;290;304]. Stellar feedback must not only drive galactic-scale outflows to contend with observations, but this process is likely also necessary to account for the low baryon retention in galaxies[20;200] (See Chapter 4 for further discussion). However, studies have shown stellar feedback is ineffective in shutting off star formation in the high mass galaxy regime[41;55;354]. Nevertheless, additional work is necessary to determine which stellar feedback models drive more accurate and realistic galaxy evolution.

Supermassive black hole feedback, also called AGN feedback, is well accepted to be more effective at regulating star formation in more massive galaxies ($M_* > 3 \times M_\odot$)[76;231;285;292], as well as regulating the accretion and growth of the SMBH itself. Furthermore, theoretical studies have shown that AGN feedback is a necessary component in full cessation of star formation, or quenching, of galaxies, especially at the high mass end[79;151;189;236;266]. SMBH feedback is typically split into two modes, quasar and radio mode, to account for the related phenomena observed from AGN jets including electromagnetic radiation, relativistic jets, and non-relativistic outflows which are less collimated[168]. Quasar mode feedback, or the radiatively efficient mode, injects energy and momentum while assuming the bolometric luminosity is proportional to the accretion rate[75;297], eg:

$$L_r = \epsilon_r \dot{M}_{BH} c^2, \tag{1.2}$$

where L_r is the bolometric luminosity, ϵ_r is the radiative efficiency, $\dot{M}_{BH}$ is the mass accreted by the black hole, and c is the speed of light. Then, the feedback energy is

$$\dot{E} = \epsilon_f L_r = \epsilon_f \epsilon_r \dot{M}_{BH} c^2 \tag{1.3}$$

where ϵ_f is the feedback efficiency, which assumes some fraction of the luminosity can couple thermally and isotropically to surrounding gas.

Comparatively, radio-mode or "mechanical" feedback, which is driven by highly-collimated jets of relativistic particles, is thought to be important to the regulation of star formation.[86;192;282;284;354] This mode occurs when the SMBH is accreting at lower accretion rates, but despite being launched at a few times the Schwarzchild radius can extend out to tens of kpc from the galaxy. SMBHs may also provide a "preventative feedback" mode during which impacted gas will maintain high entropy and long cooling times that continue to suppress star formation. Similar to stellar feedback however, the implementation of AGN feedback is widely contested and variable between simulations. The details of feedback remains uncertain such as whether SMBHs heat up gas needed for star formation or eject it and how this

process scales at different masses and redshift[377]. Predictions from these different simulations need further validating before we can determine the true nature of feedback energy. Recent studies of the circumgalactic medium (CGM) have shown that the gaseous halo around a galaxy may be particularly sensitive to feedback processes in a galaxy. Though observations of this diffuse region are still difficult, accurately simuating the gas in the CGM may be the key to solving the myster of feedback.

1.3 The CGM and You

Observations of the circumgalactic medium, the halo of gas around a galaxy, show that it must be impacted by feedback processes in the stellar disk (See Tumlinson, Peeples and Werk (2017) for a recent review[330]). Accretion from the metal-poor intergalactic medium (IGM) is unable to account for the amount of cold gas and the high metal content observed in the CGM[332]. However, McQuinn & Werk (2018)[194] explain that the energy deposited onto halo gas by black holes and supernovae appears too low to explain the multi-phase gas seen in the CGM. Nearly an order of magnitude more feedback energy than we observe is necessary to account for the vast quantities of material, like OVI ions, in the CGM. We require a better understanding of both stellar and AGN feedback to determine the role they each play in regulating and quenching star formation and enriching the CGM with gas and metals.

The CGM of Milky Way-mass (MW-mass) galaxies is a critical laboratory in which the effects of all of these feedback processes are entangled. Galaxies in this mass range (virial mass, $M_{vir(z=0)} \sim 10^{12}$) live at the knee of the stellar mass–halo mass relation, the transition between galaxies dominated by stellar feedback and higher mass galaxies dominated by AGN processes. With their gas being impacted by both stellar and SMBH feedback, it is crucial to study the CGM of MW-mass galaxies.

By examining the impact of feedback processes on the CGM of Milky Way-mass galaxies in cosmological volumes and zoom-in simulations, my work aims to resolve these different yet deeply interconnected questions about the formation of galaxies:

1. What role does SMBH feedback play in quenching galaxies in Milky Way-mass simulations? (Chapter 2)

2. How well do our simulations match the observational properties of the galaxies in CGM surveys? What processes, such as stellar or SMBH feedback, impact the amount of O VI in the CGM of our simulated galaxies? (Chapter 3)

3. Finally, where do the metals in a galaxy flow through and end up after being impacted by different processes? (Chapter 4)

You'll find the answers to these questions and more in the following chapters.

Chapter 2

ONE TWO QUENCH: A DOUBLE MINOR MERGER SCENARIO

Portions of this chapter were originally published in collaboration with Michael Tremmel, Jessica K. Werk, Andrew Pontzen, Charlotte Christensen, Thomas Quinn, Sarah Loebman, and Akaxia Cruz in the April 2021 edition of The Astrophysical Journal (Sanchez, N. N., Tremmel, M., Werk, J. K., et al. 2021, The Astrophysical Journal, 911, 116; 2021

Summary

Using the N-body+Smoothed particle hydrodynamics code, ChaNGa, we identify two merger-driven processes—disk disruption and supermassive black hole (SMBH) feedback—which work together to quench L* galaxies for over 7 Gyr. Specifically, we examine the cessation of star formation in a simulated Milky Way (MW) analog, driven by an interaction with two minor satellites. Both interactions occur within ∼100 Myr of each other, and the satellites both have masses 5 to 20 times smaller than that of their MW-like host galaxy. Using the genetic modification process of[260], we generate a set of four zoom-in, MW-mass galaxies all of which exhibit unique star formation histories due to small changes to their assembly histories. In two of these four cases, the galaxy is quenched by $z = 1$. Because these are controlled modifications, we are able to isolate the effects of two closely-spaced minor merger events, the relative timing of which determines whether the MW-mass main galaxy quenches. This one-two punch works to: 1. fuel the supermassive black hole (SMBH) at its peak accretion rate; and 2. disrupt the cold, gaseous disk of the host galaxy. The end result is that feedback from the SMBH thoroughly and abruptly ends the star formation of the galaxy by $z \approx 1$. We search for and find a similar quenching event in ROMULUS25, a hydrodynamical $(25\,\mathrm{Mpc})^3$ volume simulation, demonstrating that the mechanism is common enough to occur even in a small sample of MW-mass quenched galaxies at $z = 0$.

2.1 Introduction

Benchmark astronomical surveys, such as the Sloan Digital Sky Survey (SDSS) and the Cosmological Evolution Survey (COSMOS), have revealed how the bi-modality in galaxy properties evolves over redshift e.g.[15;23;44;139;208;308]. Actively star-forming galaxies and non-star-forming, "passive" galaxies occupy two distinct regions of parameter space in color magnitude diagrams and exhibit distinct morphologies e.g.[338;371] and stellar populations e.g.[104;148;179;191;362]. Theoretical studies have been able to reproduce the bimodal galaxy distributions in SFR[91], morphology[291], and color[144;214]; however, no theoretical consensus has yet emerged to explain the increase of quenched galaxies observed from $z \sim 1$ to present day[24;140].

The general decline in star formation rate towards $z \sim 0$ has been well-described by observational studies e.g.[179;218], and this process is almost certainly influenced by a decrease in cool gas supply in the local universe e.g.[243]. However, there are many large-scale and small-scale processes that can impact the star formation properties of a galaxy.

Peng et al. 2010[230] describes two main quenching pathways: environmental[13;16;147] and mass[149] quenching. Examples of such quenching processes include halo quenching or starvation —two types of mass-quenching—each cite a specific source driving their quenching.

For example, halo quenching relies on the long cooling times of high-temperature ($\sim 10^6$ K) halo gas[146;246;292]. As IGM gas enters a high mass ($M_{\rm halo} \gtrsim 10^{11}$ $M_\odot$) galaxy through filaments, it shock heats to the virial temperature of the galaxy[70;158], ultimately depriving galaxies of their star-forming fuel. However, within these massive halos, star formation suppression through this mode can be less efficient in high baryon fraction galaxies[26] and cool gas may still permeate through shocked regions and accrete onto the galaxy[45;73;213].

Similarly, the process which includes the physical removal and suppression of the gaseous fuel of a galaxy is called "starvation" and occurs in both low and high mass galaxies. In low mass galaxies with small gravitational potential wells, star formation feedback processes —such as stellar winds, radiation, and energy ejected via supernovae —are powerful enough

to strip galaxies of some or all of their gas[72;173]. In more massive galaxies, AGN feedback is a likely culprit for ejecting the cool gas from a galaxy disk through powerful outflows[59;86;88;90] and enriching the circumgalactic medium (CGM) with metals formed in the disk[214;266;309]. In some cases, the AGN feedback energy can be strong enough to expel gas out of the CGM into the ICM[224]. Additionally, the large scale cooling regulation which occurs in the CGM may drive gas back towards the galaxy, which can then further fuel the AGN, in a self-regulating galactic fountain[10;54;105;216;318;345]. Nevertheless, the AGN alone may not be capable of fully quenching a galaxy[75;236;329], and observations of highly star-forming galaxies can still show significant AGN activity[46;202;211;256;287].

In both of these cases, halo quenching and starvation, the main source of quenching comes from a specific physical driver—long cooling times and feedback processes—while observational evidence shows that these sources of quenching can be disrupted by other galactic properties such as AGN feedback in bright SF galaxies. Furthermore, additional studies find that the combination of halo quenching and the AGN activity driving starvation can work together to reduce star formation in some galaxies[42;188]. In our study, we focus on the combination of physical processes which drive galaxy quenching through galaxy mergers. A third quenching process described by Peng et al. 2010[230], merger quenching is mostly independent of mass and is typically associated with a major merger resulting in the cessation of star formation in a galaxy[62;103;297;317]. However, we uniquely investigate this type of quenching through a series of minor merger interactions, rather than as the result of a single major merger.

We use a carefully constructed set of initial conditions to study merger-driven quenching within a controlled environment. Our study follows that of Pontzen et al. 2017[236] (hereafter, P17) which investigates quenching by black hole feedback and merger effects in tandem. P17 utilize the 'genetic modification' technique GM,[260] to create a suite of cosmological simulations of Milky Way-mass (MW-mass) halos at $z = 2$ with assembly histories that have been modified in controlled ways. The environment and assembly history of each galaxy in the suite was nearly identical, except for a significant merger event with varying mass ratio

(1:10, 1:5, and 2:3) occurring at $z < 2$. The resulting physical state of the main galaxy ranges from star forming to temporarily-quenched to permanently quenched due to the interplay between the major merger and SMBH feedback. In the permanently-quenched case (2:3), P17 show that the combined effort of the merger and the SMBH feedback work together to halt star formation: the merger disrupts the disk while the AGN feedback ejects and heats some, but not all, of the cold disk gas. It is the lack of an orderly disk that prevents further star formation despite some cool gas remaining in the galaxy.

We follow the methods of P17 to investigate quenching in a new suite of genetically modified MW-mass galaxies at $z = 0$. However, we note that P17 examines the major mergers likely to occur at high-z for more massive halos, while we focus on MW-mass galaxies which have more quiet recent histories, like our own MW. In this study, we examine the influence of a more minor modification within these simulations and show that two minor mergers can lead to a unique form of quenching in MW-mass galaxies.

This paper is organized as follows: Section 2.2 details our set of simulations and describes the genetic modification process. Section 2.3 reports our findings and results. In Section 2.4, we summarize our results and discuss the broader implications of our findings.

2.2 Simulation Parameters

To create our sample of galaxies, we used the modern SPH code, Charm N-body GrAvity solver ChaNGa[196]. ChaNGa inherents the same physical models as Gasoline[350;351] and includes the following physical prescriptions: cosmic UV background[119], star formation using an IMF given by[169], blastwave supernova feedback[226;305] for more details including both SNIa and SNII[313;369]. SNII feedback imparts 10^{51} ergs of thermal energy per supernova onto surrounding gas particles. Low temperature metal line cooling[280;303;352] is included to allow gas below $10^4 K$ to cool proportionally to the metals in the gas. Gas above this threshold cools only via H/He, Bremsstrahlung, and inverse Compton. No high temperature metal cooling is included due to the resolution of our simulations which does not resolve individual star forming regions See[324] for more detailed discussion.

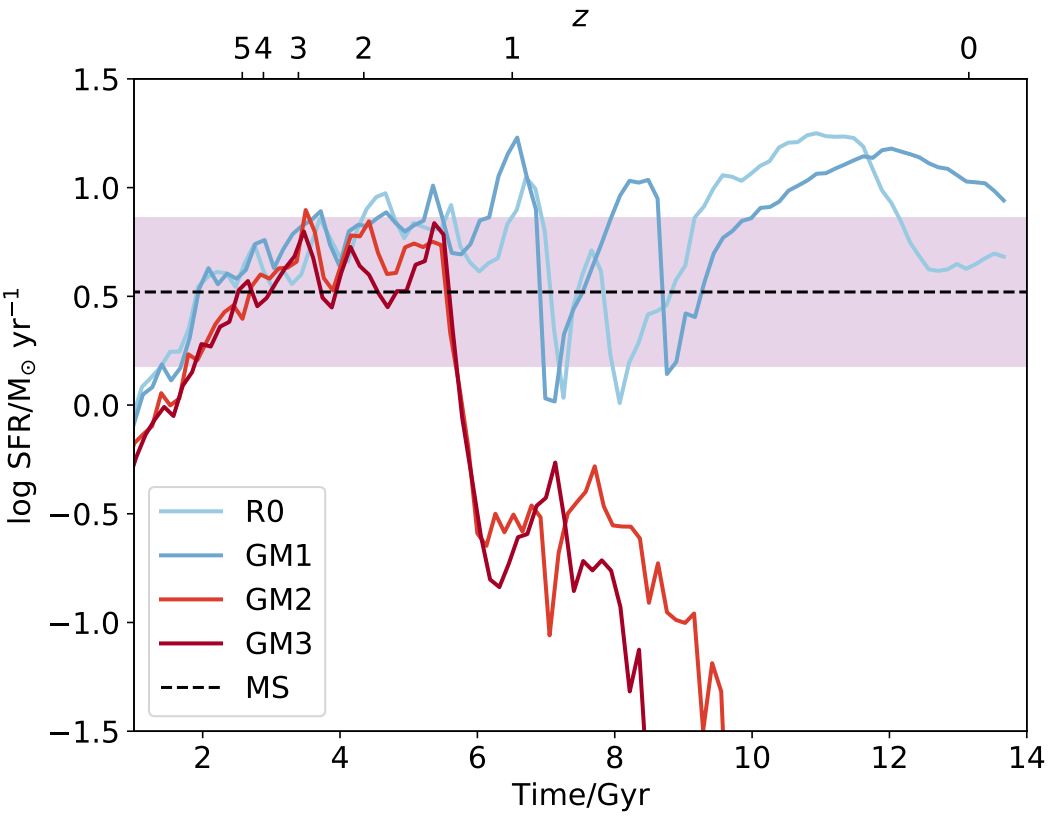

Figure 2.1: Star formation histories of our 4 GM galaxies. The star forming galaxies, R0 and GM1, are shown in dark and light blue; the quenched galaxies, GM2 and GM3, are shown in dark and light red; and the main sequence star formation rate, for $M_{star} = 5 \times 10^{10} M_{\odot}$ at z = 0, is shown in purple[363]. All 4 of our galaxies begin with very similar ICs which have been genetically modified to shrink the mass of a satellite which enters the main halo at $z = 1$. Despite their similar beginnings, two of the galaxies, R0 and GM1, remain star forming through their lives, while the others, GM2 and GM3, quench just after $z = 1$ and remain that way until $z = 0$ (~ 8 Gyr).

Our simulations use an improved set of black hole (BH) prescriptions including formation, accretion, and dynamical friction[323]. SMBH seeds form from dense, extremely low metallicity gas particles which allows BHs to form early in low mass halos, as predicted by the majority of theoretical models. Sub-grid models for SMBH accretion and dynamical friction have been implemented, including realistic SMBH mergers and dynamical evolution. SMBH dynamics are accurately followed down to sub-kpc scales[321]. In particular, the subgrid model for accretion takes into account angular momentum support from nearby gas particles. This model

allows for more physical growth compared to strictly Bondi-Hoyle accretion and does not require additional assumptions or free parameters. Angular momentum support is included in the accretion equation:

$$\dot{M} \propto \frac{\pi (G M_{BH})^2 \rho c_s}{(v_\theta^2 + c_s^2)^2}, \tag{2.1}$$

where ρ is the density of the surrounding gas, c_s is the sound speed, and v_θ is the rotational velocity of the surrounding gas. The quantity v_θ is informed by the angular momentum support of this gas on the smallest, resolvable scale. Additionally, a density dependent boost factor is implemented to avoid underestimating SMBH accretion rates due to resolution affecting temperature and density calculations of nearby gas. Using the prescription of Booth et al. 2009[36], the standard Bondi rate is scaled by a density dependent factor, $(n_{gas}/n_*)^\beta$, where n_* is the star formation density threshold and β is a free parameter. Combined, the density dependent boost factor and inclusion of angular momentum support results in the full equation from Tremmel et al. 2017[323]:

$$\dot{M} = \alpha \times \begin{cases} \frac{\pi (GM)^2 \rho}{(v_{\rm bulk}^2 + c_s^2)^{3/2}} & \text{if } v_{\rm bulk} > v_\theta \\ \\ \frac{\pi (GM)^2 \rho c_s}{(v_\theta^2 + c_s^2)^2} & \text{if } v_{\rm bulk} < v_\theta \end{cases}; \tag{2.2}$$

$$\alpha = \begin{cases} \left(\frac{n}{n_{th,*}}\right)^\beta & \text{if } n \geq n_{th,*} \\ \\ 1 & \text{if } n < n_{th,\star} \end{cases}$$

where v_{bulk} is the smallest relative velocity of the SMBH's 32 nearest gas particles. Thus, in cases where bulk motions dominate over rotational motion, the formula reverts to Bondi-Hoyle.

Thermal SMBH feedback energy is determined by the accreted mass, $\dot{M}$, and imparted

on the nearest 32 gas particles according to a kernel smoothing:

$$E = \epsilon_r \epsilon_f \dot{M} c^2 dt, \tag{2.3}$$

where $\epsilon_r = 0.1$ and $\epsilon_f = 0.02$ are the radiative and feedback efficiency, respectively. Accretion is assumed to be constant over one black hole timestep, dt. Cooling is shut off immediately after AGN feedback events for a short ($\sim 10^{4-5}$ years) time. These choices were calibrated against dozens of zoom-in simulations to broadly reproduce observed galaxy and SMBH scaling relations. Furthermore, this SMBH feedback prescription is shown to produce large scale outflows[236;324]. For more details on the SMBH prescriptions, see Tremmel et al. 2017[323].

Our simulations were each run with the same ΛCDM cosmology, $\Omega_m = 0.3086$, $\Omega_\Lambda = 0.6914$, $h = 0.67$, $\sigma_8 = 0.77$[3], and have a Plummer-equivalent softening length of 250 pc (a spline kernel of 350 pc is used). Initial conditions were generated using genetIC[307].

2.2.1 Halo and Merger Identification

Individual halos are selected using the post-processing tool Amiga Halo Finder, which selects halos using an overdensity criteria and grid based system which iteratively removes particles that are gravitationally unbound from prospective halos[107;163;164]. Virial mass, M_{vir}, and virial radii, R_{vir}, are determined using a spherical top-hat collapse technique. Halos are traced backwards through time from $z = 0$ to previous snapshots, following the halo from the previous snapshot which contains the majority of the same particles using the analysis tools pynbody[234] and TANGOS[235].

Merger ratios are defined at infall, during the snapshot just before the center of the satellite halo has first passed into the virial radius of the main halo (Table 2.1), and are calculated as $q = M_{vir,halo}/M_{vir,satellite}$. Larger infall ratios indicate mergers with smaller satellite galaxies.

These following zoom-in simulations were first described in Sanchez et al. 2019[266], which compared the O VI column densities within these galaxies to observations from the COS-Halos Survey. This previous study examined the effects of star formation history and SMBH

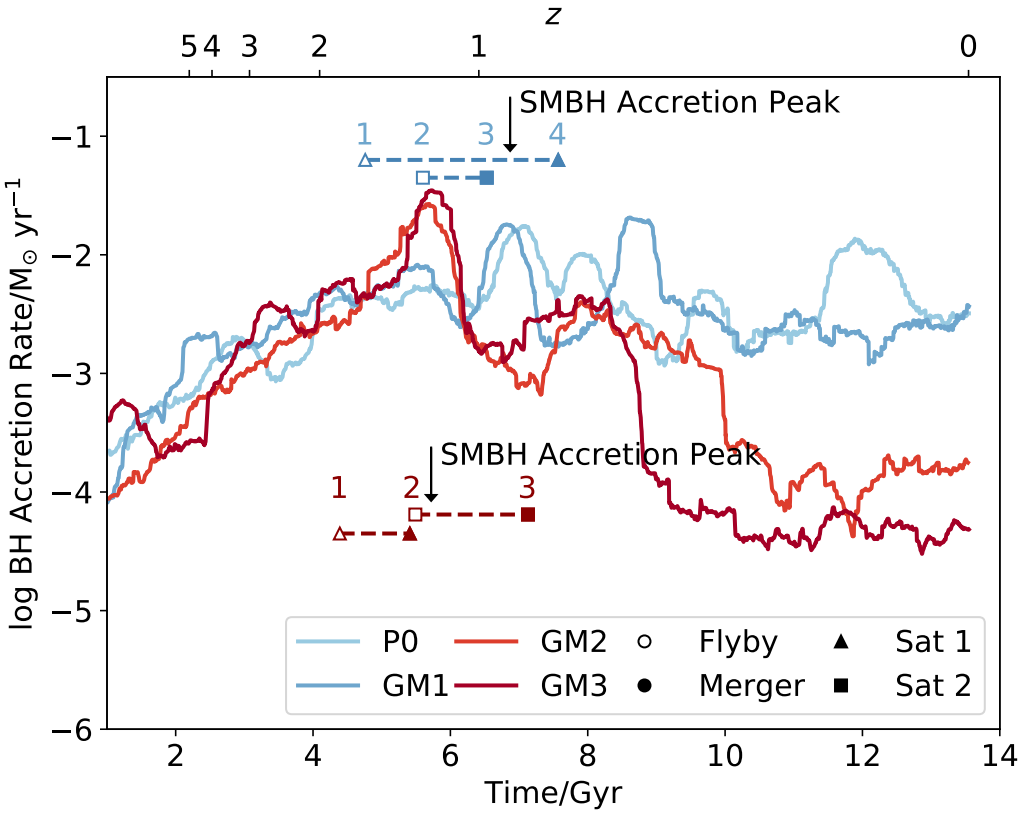

Figure 2.2: SMBH accretion rates for our four GM galaxies across time averaged using a rolling mean of 450 Myrs. The peak of accretion and feedback energy occurs earlier in both quenched galaxies, within ~ 100 Myr of the double satellite interaction ($z \sim 1$). The timing of the satellite interactions are indicated in blue for the star forming galaxies, and red for the quenched cases. Triangles connected with a dashed line indicate the interaction period of the first satellite, from initial flyby (open marker) to time of its merger with the main halo (solid marker). For the second satellite interaction, open and closed squares indicate the initial flyby and time of merger, respectively. See Table 2.1 for flyby and merger times.

feedback on the circumgalactic medium. They found that while differences in the star formation histories of the galaxies didn't result in significant variations in the amount of O VI in the CGM of these galaxies, SMBH feedback was a significant driver of the metals into the CGM.

2.2.2 The Genetic Modifications

We selected a Milky Way-mass "Organic" galaxy, henceforth R0, ($M_{halo} = 9.9 \times 10^{11}$ M$_\odot$) from an initial, dark-matter only cosmological volume which had uniform resolution and was 50 Mpc on a side. R0 was selected for the Large Magellanic Cloud-mass (LMC-mass, $M_{sat} = 2 \times 10^{10}$ M$_\odot$) satellite galaxy which was contained within its virial radius at $z = 0$, and was otherwise isolated (>2 Mpc) from other MW-mass galaxies. Once selected, we define a Lagrangian region associated with this halo to create the "zoom-in" simulation of our R0 galaxy using the technique of Katz et al. 1993[145]. This zoom-in R0 includes baryons and their related physics while only re-simulating a few virial radii from the main halo at the highest resolution ($M_{gas} = 2.1 \times 10^5$ M$_\odot$, $M_{DM} = 1.4 \times 10^5$ M$_\odot$) while large scale structure at farther distances are simulated only in DM at a much coarser resolution.[1]

To create the subsequent "genetically modified" galaxies, we used the method of Roth et al. 2016[260] to modify the initial conditions of R0 by decreasing the mean over-density associated with the particles in the LMC-mass satellite which was present in R0 at $z = 0$. With this method, we created three GM galaxies (GM1, GM2, and GM3), each modified to result in a subsequently smaller satellite mass see Table 1; [266]. The benefit of this method is that it allows us to fix the large scale structure and the final mass of the main halo ($M_{vir} \sim 10^{12} M_\odot$) while varying specific aspects of the halos assembly history. The simulations resulted in a set of four galaxies which, despite controlling for large scale environment and only slightly modifying the assembly of the halo, have varying baryonic evolution. Two of these galaxies, R0 and GM1, are star forming, disk galaxies, similar to the Milky Way, while two of these galaxies, GM2 and GM3, unexpectedly become quenched at $z \sim 1$ (Figure 2.1).

Simulation snapshots of particle data had varying cadences with medians of 700 Myr and 200 Myrs for R0 and GM1, respectively, and 400 Myrs for both GM2 and GM3. Additional static images were created on the fly during each simulation with a cadence of 3 Myrs.

While first introduced in Sanchez et al. 2019[266], two of these zoom-in simulations (GM2

[1]Correction: Sanchez et al. 2019[266] states that the DM mass is 3.4×10^5 M$_\odot$ which is the DM mass resolution for ROMULUS25 not the GM galaxies.

and GM3) were additionally discussed in Cruz et al. 2020[65], which examined the effect of self-interacting dark matter models on SMBH growth histories. Though the effects of varying assembly and star formation have been explored in these papers, no thorough treatment describing the quenching in these galaxies has yet been put forth. The purpose of the present paper is to explore the physical processes driving quenching in these galaxies.

2.2.3 The ROMULUS25 *Cosmological Volume*

ROMULUS25[323] hereafter R25 is a 25 Mpc cosmological volume that includes galaxies between halo masses of 10^9 —10^{13} $M_\odot$. The galaxies in R25 have been shown to lie along the M_{BH}-M_*, stellar mass-halo mass, and M_{BH}-σ relations[252], and are consistent with observations of of star formation and SMBH accretion histories at high redshift[323]. Furthermore, Tremmel et al. 2017[323] shows that SMBH physics plays a necessary role in reproducing MW-mass galaxy evolution and quenching in high mass galaxies. R25 has a mass resolution of $M_{gas} = 2.1 \times 10^5$ $M_\odot$ and $M_{DM} = 3.4 \times 10^5$ $M_\odot$ for gas and DM particles, respectively.

For our study, we examine a set of 26 MW-mass galaxies which have final halo masses, M_{halo}, between 5×10^{11} and 2×10^{12} $M_\odot$ and which are not satellites of a more massive halo at $z = 0$. Our M_{halo} measurements use the corrections of Munshi et al. 2013[204].

2.3 Results

2.3.1 Differences in Merger Timings

Due to the constraints that maintain the final mass of the main halo while changing the LMC satellite mass, the genetic modification technique affects the timing of accretion throughout the evolution of the galaxy. In GM2 and GM3, our two quenched cases and those with the smallest satellite masses, the accretion of satellites onto the main galaxy must occur faster and therefore earlier to maintain the final mass of the main halo. Consistently, SMBH accretion also peaks earlier ($z \sim 1.18$), nearly 1 Gyr before the peak of SMBH accretion in the two star forming cases, R0 and GM1 (Figure 2.2, discussed in detail below). The

differences in timing and order of the minor mergers which occur are key to understanding the effect of the quenching in these two galaxies.

We note that the variations between the two star forming galaxies themselves are minimal. Similarly, the two quenched cases have timing and sequence that are closely similar (Table 2.1). For that reason, we will generalize to two cases: the star forming case and the quenched case.

Figure 2.3 illustrates the differences in the order and timing of the minor mergers in the star forming (*Upper Panels*) and quenched cases (*Lower Panels*). In the star forming case, (1) satellite 1 and satellite 2 are both infalling towards the galaxy of the main halo by $t \sim 4.7$ Gyr, when satellite 1 does a flyby of the main galaxy. (2) Satellite 2 then does a flyby nearly

Table 2.1: Timing of the Minor Merger Scenarios*

Sim	Sat 1 Infall Ratio q	Sat 1 Flyby** Gyr	Sat 1 Merger** Gyr	Sat 2 Infall Ratio q	Sat 2 Flyby** Gyr	Sat 2 Merger** Gyr	SMBH Accretion Peak Gyr
R0	5.4	4.76	7.57	13.6	5.60	6.53	6.95
GM1	7.3	4.69	7.39	14.6	5.40	6.35	6.74
GM2	8.2	4.43	5.42	18.9	5.44	6.80	5.59
GM3	9.5	4.39	5.41	17.9	5.49	7.13	5.84

*Details about satellite interactions in our four GM galaxies, including infall merger ratios, flyby times, merger times, as well as the time of the peak accretion rate of the SMBH. Infall merger ratios, q, are defined as $M_{vir,halo}/M_{vir,satellite}$ at the simulation output before the satellite enters the main halo.

**Flyby and merger times were determined by visual examination of ppm image files created on the fly during simulation with a cadence $\sim$ 3 Myr.

Table 2.2: Properties of Zoom-In Galaxies Prior to Minor Merger Interactions

Sim (z)	Halo Mass ($M_\odot$)	Gas Mass ($M_\odot$)	Stellar Mass ($M_\odot$)	Cold Gas ($M_\odot$)	Dense Gas ($M_\odot$)	R_{vir} (kpc)
R0 (1.18)	5.7×10^{11}	7.1×10^{10}	1.3×10^{10}	4.1×10^{9}	7.0×10^{9}	122.8
GM1 (1.32)	4.9×10^{11}	6.0×10^{10}	1.2×10^{10}	3.7×10^{9}	7.0×10^{9}	110.0
GM2 (1.32)	5.1×10^{11}	6.4×10^{10}	9.1×10^{9}	5.0×10^{9}	4.6×10^{9}	111.4
GM3 (1.32)	5.0×10^{11}	6.0×10^{10}	7.5×10^{9}	5.0×10^{9}	3.3×10^{9}	110.5

*Details about the simulations prior to the start of the minor merger interactions at $z \sim 1$, including total virial halo mass, total gas mass, total stellar mass, cold gas mass and dense gas mass, all in the main halo. Virial radius of each halo is also included. The properties of R0 are shown at $z \sim 1.18$ due to the limited number of simulation outputs available for this simulation. The properties of the three other simulations are shown at $z \sim 1.32$.

a Gyr later at $t \sim 5.5$ Gyr. (3) Satellite 2 merges another Gyr after that at $t \sim 6.4$ Gyr. (4) Finally, satellite 1 merges last at nearly $t \sim 7$ Gyr.

In the quenched case, the order and timing of these same interactions are markedly different. (1) Satellite 1 does its flyby nearly half a Gyr earlier ($t \sim 4.4$ Gyr) than in the star forming case, consistent with the earlier, faster accretion expected from the galaxies with the most significantly shrunken satellite mass. (2) A Gyr after the flyby of satellite 1, satellite 1 merges with the main halo at $t \sim 5.4$ Gyr and the flyby of satellite 2 quickly follows, occurring within the next 100 Myr. In the quenched case, (3) satellite 2 is the last to merge, a little more than 1.5 Gyr after the double interaction preceding it. The specific order and timing between these interactions are what set the stage for the stark result of quenching in this galaxy rather than continued star formation.

Figure 2.4 includes a series of gas density maps spanning the time of these interactions. GM1, our star forming case, is shown on the left, while GM2, our quenched case is on the right. At t $\sim$ 5.2 Gyr in the star forming case (*Upper Left*), satellite 1 has completed its

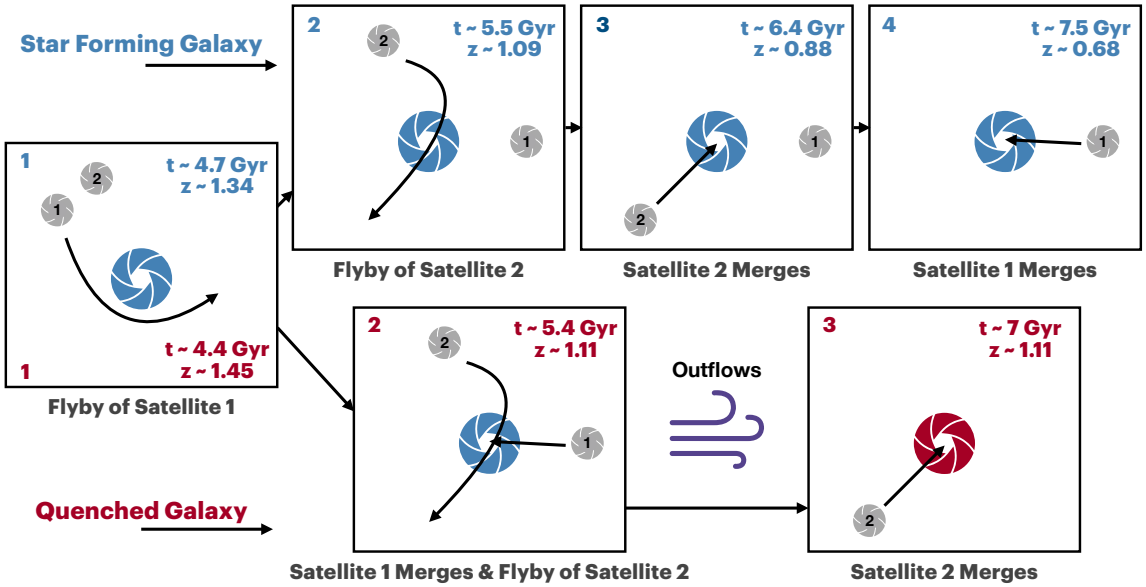

Figure 2.3: Diagram detailing the order of the satellite merger scenario in the star forming (*Upper*) and quenched (*Lower*) cases. In the star forming case, the satellite interactions occur in this order: flyby of satellite 1, flyby of satellite 2, then the merger of satellite 2, and finally satellite 1 merges last. In the quenched case, the order of these interactions is different. Satellite 1 still interacts with a flyby first, however it then merges with the main halo within a Gyr. Shortly after (<100 Myr), the flyby of satellite 2 occurs. Additionally, in the quenched case, the time when satellite 1 merges and satellite 2 does its flyby is shortly followed by the peak of SMBH accretion in these galaxies (a few 100 Myrs).

flyby of the main galaxy and is still moving away from it, while satellite 2 is infalling. At this time, our quenched GM2 (*Upper Right*) has experienced the same interaction. However, by t $\sim$ 5.6 (*Middle Left Panel*), satellite 2 in GM1 has completed its flyby of the main galaxy and satellite 1 is falling back towards it returning from its initial flyby. In contrast (*Middle Right Panel*), satellite 1 in GM2 has fully merged with the main halo by this time, with satellite 2 having completed its flyby as well. Finally, at t $\sim$ 5.9 (*Bottom Left Panel*), both GM1 satellites are now infalling back towards the main galaxy. In GM2, (*Bottom Right Panel*), satellite 2 alone is infalling and will complete its merger in about another Gyr.

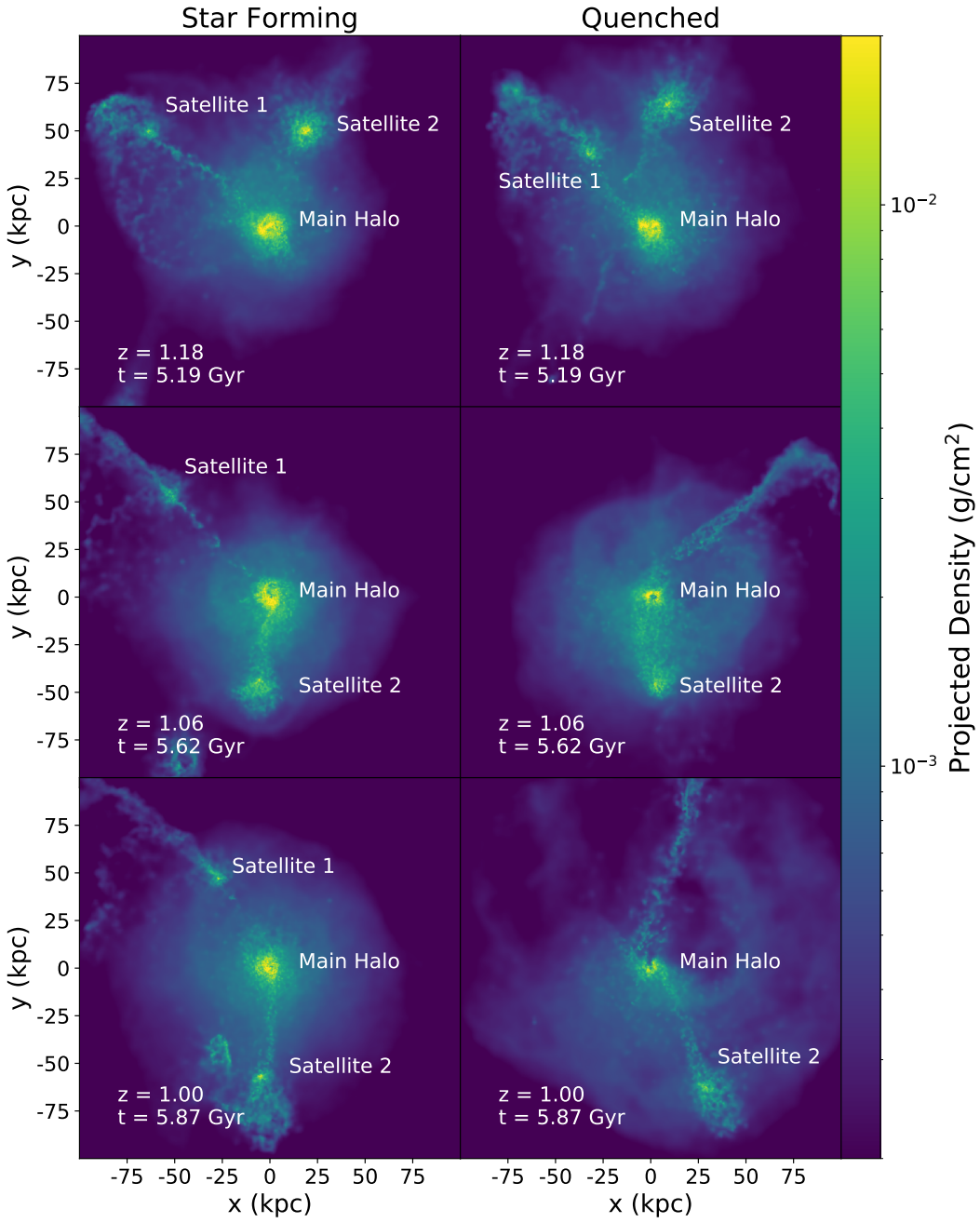

Figure 2.4: Gas density maps of the star forming galaxy, GM1, and quenched galaxy, GM2, during their minor satellite interactions. *Left:* In GM1, satellite 1 and 2 are both infalling at z = 1.18 (*Top Panel*). About a half a Gyr later (*Middel Panel*), satellite 2 has completed its flyby and satellite 1 is still infalling towards the main halo. By $z = 1$, both satellites are making their way toward the main halo where they will finally merge around t $\sim$ 7.5 and t $\sim$ 6.5 for satellite 1 and 2, respectively. *Right:* In GM2, one of our quenched galaxies, the order and timing of these interactions have some key differences. At $z = 1.18$ (*Top Panel*), like in the star forming GM1, the main halo of GM2 has experienced the flyby of satellite 1, while satellite 2 is still in its initial infall. However by $z = 1.06$ (*Middel Panel*), satellite 1 has fully merged with the main halo and satellite 2 has completed its flyby, in contrast to the star forming case which still shows both satellites. Finally at $z = 0$ (*Bottom Panel*), satellite 2 is infalling back towards the main halo and will merge with it in about 1.5 Gyr.

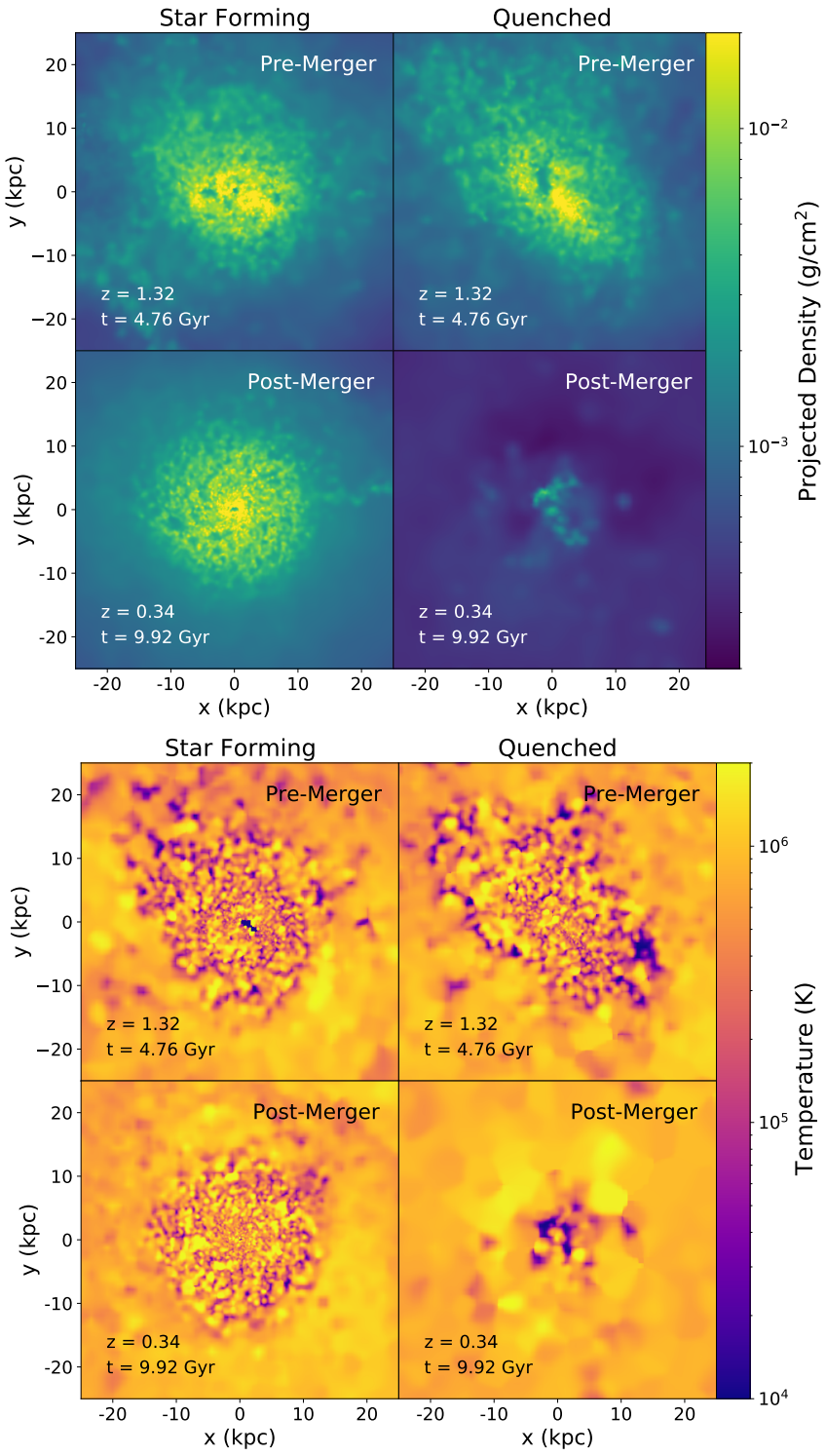

Figure 2.5: Gas density (*Upper*) and temperature maps (*Lower*) of the star forming galaxy, GM1, and quenched galaxy, GM2. The upper panels show both galaxies long before the minor merger interactions which quenched GM2 while both galaxies experience a time of disk stability. The lower panels of each galaxy show them at a time long after the interaction has impacted the galaxies, showing the stable disk that GM1 has maintained through the series of interaction at $z = 1$ and the complete lack of disk and cold gas in GM2.

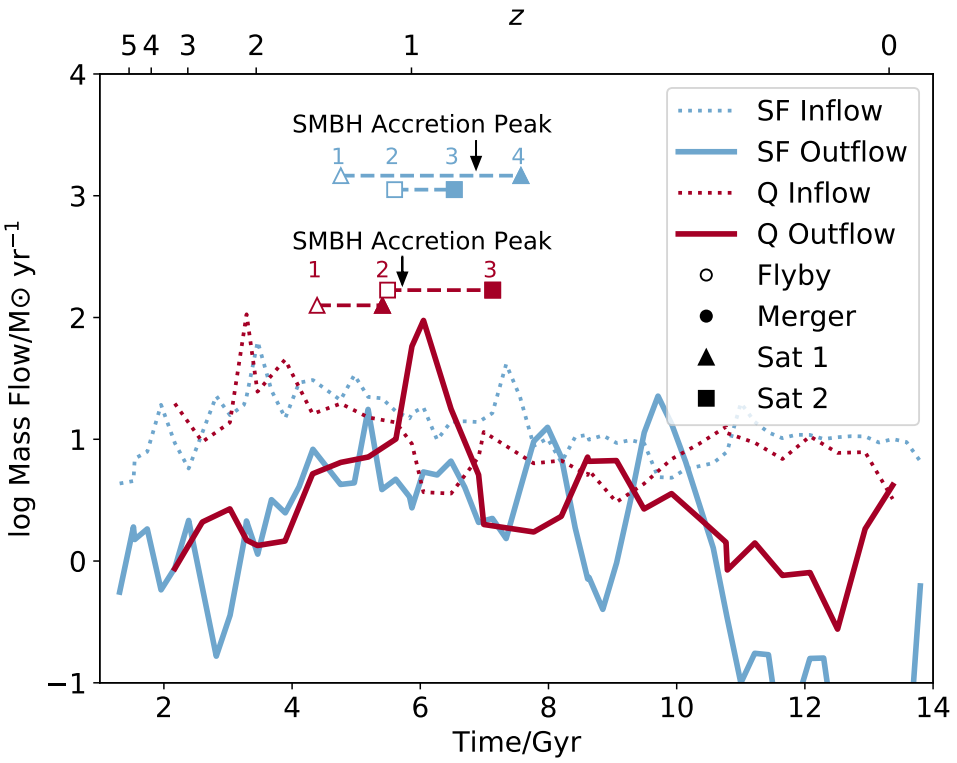

Figure 2.6: The mass flow as a function of time in GM1, the star forming case, and GM2, the quenched case. Blue lines denote GM1, one of our star forming galaxies, and red lines denote GM2, one of the quenched cases. Dotted lines indicate inflow at the virial radius, while solid lines indicate outflow at the virial radius. The minor satellite flybys and mergers are indicated as in Figure 2.2. A significant outflow occurs at $z \sim 1$, directly following the minor satellite interaction (when satellite 1 merges and satellite 2 follows with a flyby) and the peak in SMBH accretion.

2.3.2 Satellite Interactions and SMBH Feedback

While we've shown that these interactions do not have a large effect on the star forming cases, R0 and GM1, both GM2 and GM3 experience significant outflows at $z \sim 1$, quenching the galaxy completely for the rest of the simulation (Figure 2.6). Outflows and inflows are calculated by measuring the velocity of the gas passing through a shell at the virial radius with thickness of $0.1R_{vir}$. While the inflow rates of the galaxies generally follow a similar shape (dotted lines), a clear and significant difference is present in the outflows (solid lines). While there is no large outflow in the star forming case (blue solid line), in the quenched case there is a large outflow (red solid line) directly following the minor satellite interactions

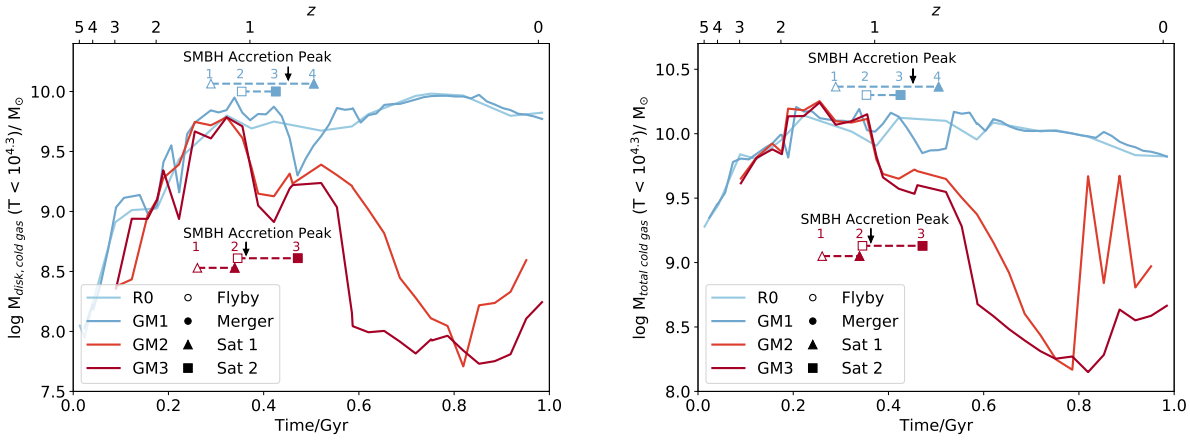

Figure 2.7: Cold disk gas ($T < 2 \times 10^4$ K, $R < 0.1R_{vir}$) and cold gas mass ($T < 2 \times 10^4$ K, $R < R_{vir}$) in our GM galaxies. *Left:* Prior to ~ 6 Gyr, the amount of cold gas in the disk of the star forming and quenched galaxies is not significantly different. *Right:* Similarly, we see consistent amounts of total cold gas mass in all 4 of the halos prior to this time. However, in both figures, once the minor satellite interactions occur (red filled triangle and open red square) and the SMBH accretion rate peaks in GM2 and GM3 (lower down-turned black arrow), the majority of this cold gas is removed in a large outflow from the disk (Figure 2.6). Line colors, styles, and marker styles as in (Figure 2.2).

and SMBH accreiton peak at $t \sim 6$ Gyr. These outflows expel most of the gas from the disk, removing the fuel supply for further star formation (Figure 2.7).

We investigate the galaxy properties during the time just before quenching in GM2 and GM3 to understand why they quench while the others do not. Specific characteristics of the merger do not appear to be drivers of the quenching (Table 2.2). No significant differences arise between the primary halos with regards to the total virial mass, gas mass, or stellar mass at the time of the merger or leading up to it. There is also no significant difference between the amount of cold ($< 2\times 10^4$ K) gas in the disk or the entire halo (Figure 2.7). We do not find significant differences between the properties of the star forming and quenched galaxies prior to $z = 1$ (Figure 2.8), instead determining that the main difference between these GM simulations is directly related to the timing of their satellite interactions.

Figure 2.2 not only shows the accretion rate of the SMBH at the center of each GM main galaxy, but additionally the timing and sequence of the satellite interactions are marked. In the star forming cases (solid lines in blue), the mass of the SMBH continues to grow during

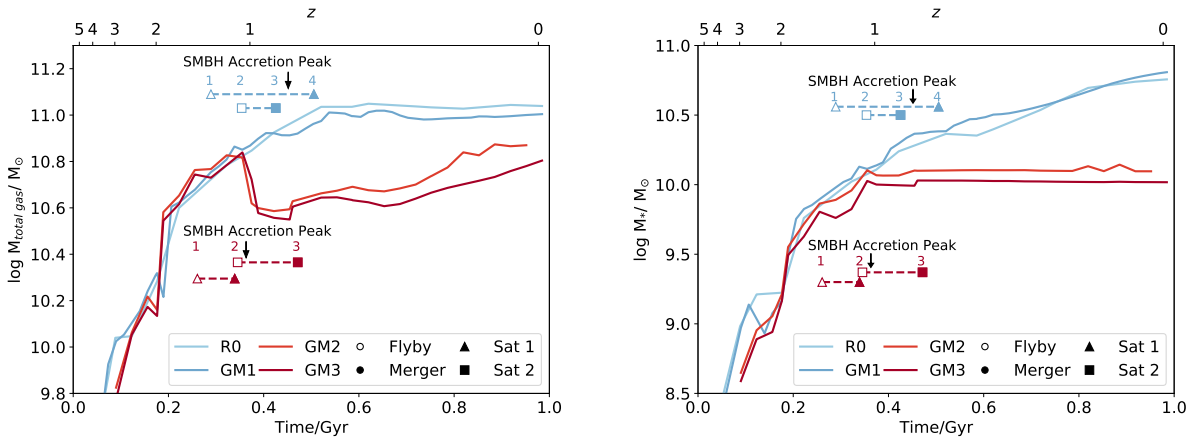

Figure 2.8: The total gas and total stellar mass for the 4 GM galaxies. Prior to ~ 6 Gyr, there is little variation in either the total gas mass (*left*) or stellar mass (*right*) the star forming or quenched galaxies. The key difference affecting the overall properties of the galaxies after $z \sim 1$ is the timing between the minor mergers. Line colors, styles, and marker styles as in (Figure 2.2). The timing between the mergers in the star forming case (~ 1 Gyr) is significantly longer than that of the quenched case (~ 100 Myr) in which the timing of the minor merger interaction coincides with the peak of SMBH accretion in the quenched case.

the times of the mergers ($z \sim 1$) and the first peak of SMBH accretion occurs at $t \sim 6.8$ Gyr. This peak in accretion coincides closely with the merger of satellite 2, but without disrupting star formation. In comparison, the peak of SMBH accretion in the quenched cases occurs at $t \sim 5.8$ Gyrs, following both the merger of satellite 1 and flyby of satellite 2 within a few Myrs. This set of interactions is followed by a significant outflow at $t \sim 6$ Gyr, after which the galaxies remain quenched for the rest of their lives.

Given no significant differences in the physical characteristics of the galaxies, or their SMBHs, prior to the series of interactions that occur at $z \sim 1$, we then look to the dynamics of the disk to better understand how the differences in galaxy accretion history arise. Figure 2.9 shows the circularity parameter (j_z/j_{circ}, see Keller et al. 2015[155] and Simons et al. 2019[288] and references therein) of cold gas ($T < 2 \times 10^4$ K) for the star forming, R0, and quenched, GM2. The galaxy disk is first oriented on the total angular momentum of the gas within 5 kpc of the galaxy center. Then for each cold gas particle within 20 kpc, the circularity parameter is calculated as ratio of its specific angular momentum component perpendicular to the disk (j_z) and the specific angular momentum for the theoretical circular

orbit of that particle in its current potential (j_{circ}). Values of j_z/j_{circ} closer to 1 indicate gas that is rotationally supported in a disk, while gas with $j_z/j_{circ} < 0.5$ is dispersion dominated. Gas prior to the merger (*upper panels*) is stable and mostly rotationally supported in both galaxies. Difference arise after the mergers occur (*lower panels*). We see that GM1 (*bottom left panel*), our star forming case, retains a stable disk which has become compacted after the merger[71]. While GM2 (*bottom right panel*), our quenched case, has cold gas which is no longer rotationally supported in a disk (j_z/j_{circ} values closer to 0). This difference is a key component in our result.

2.3.3 The Quenching Combination

In both the GM cases where the galaxy quenches after $z = 1$, the difference in the satellite merger combination is present. Additionally, the earlier accretion of satellite 1 feeds the SMBH with its gas, resulting in an earlier peak of SMBH accretion than in the SF galaxies. We determine that the subsequent disruption of the disk in these quenched cases —through the minor merger interaction of the merger and subsequent flyby —allows the resulting SMBH feedback (from the peak of SMBH accretion) to eject a majority of the cold gas in the disk (Figure 2.7). This one-two punch combination of minor satellite interactions, in tandem with the SMBH feedback, works to quench the galaxies until $z = 0$. In short, to quench these galaxies, the combination of fuel given to the SMBH by satellite 1 and the disruption of the main galaxy disk by both satellite interactions results in SMBH-driven outflows strong enough to quench the galaxy until $z = 0$.

Our result is broadly consistent with that of POntzen et al. 2017[236]. Their results from a different set of genetically modified galaxies show that a disk instability resulting from an interaction is necessary for a galaxy to quench. Another requirement for quenching is the presence of a SMBH, and in particular they concluded that continuous bursts of feedback were necessary to maintain their quenched galaxies. Sanchez et al. 2019[266] further refined the latter requirement by examining R0 and the same GM galaxies explored in this paper, both with and without BHs. Unlike in P17 however, we find that a single burst of SMBH

is enough to quench two of our galaxies for nearly 8 Gyr without further episodes of SMBH feedback. We attribute these varying results to the differences in redshift and galaxy mass in each study, ours exploring lower mass galaxies at low redshift.

2.3.4 Quenching Galaxies in a Broader Context

Each of our quenched galaxies has an interaction timescale of $\sim$ 100 Myrs between when satellite 1 merges and satellite 2 does its subsequent flyby. The timescale between the mergers of each satellite in the quenched cases are on the order of 1 Gyr (bottom panels in Figure 2.3). In contrast, the order and timing of the flybys and mergers are markedly different for the two cases in which star formation does not cease. While in these cases satellite 2 merges before satellite 1, these distinct events are separated by a similar 1 Gyr (top panels, Figure 2.3). We use the timing constraints above to guide an analysis of quenching in the larger, cosmological simulation, ROMULUS25[323]. The purpose of this analysis is to understand the role of minor mergers in quenching MW-mass galaxies, which has thus far been unexplored.

To constrain how likely this type of event might be in the (z <2) universe, we examine a population of MW-mass galaxies from the cosmological volume R25. While a larger DM-only volume may provide a more statistically significant measurement for how often these minor mergers occur in MW-mass galaxies overall, we choose instead to select our additional sample from R25. First, it provides a larger, uniform sample of isolated MW-mass galaxies with the same physics and resolution as the GM simulations. Second, as we are interested in determining whether the combination of minor mergers and the effects of the SMBH can result in a quenched galaxy similar to what we see in the GM suite, a larger DM-only simulation would not be sufficient due to the lack of baryonic physics.

From R25, we examined 26 MW-mass galaxies, 8 of which are quenched by $z = 0$. To create this sample, we selected all the MW-mass galaxies in R25 with $M_{\rm vir}$ between $5 \times 10^{11} M_{\odot}$ and $2 \times 10^{12} M_{\odot}$ at $z = 0$ that were not satellites of a more massive halo. There were 26 MW-mass galaxies with these characteristics, each with varying star formation and accretion histories. From each galaxy, we selected every minor satellite merger ($q > 3$) that

had a mass ratio between 3 and 20 that occurred within $z = 0.5 - 2$.

We find that 70% (18/26) of MW-mass galaxies in R25 experience multiple minor mergers occuring within 1 Gyr of each other. Of this population, one galaxy experiences a peak in SMBH activity associated with the merger event which then quenches within a few hundred Myrs, similar to our two quenched GM simulations. This quenched galaxy is one of 8 MW-mass galaxies that are quenched at z = 0 in the simulation. The total number of galaxies in R25 is therefore too small to make a meaningful statistical statement. Nevertheless, the existence of a single example within such a small volume confirms that the minor merger and AGN scenario we have outlined will arise completely naturally and contribute to quenching in LCDM cosmologies. Future analyses based on larger volume simulations can confirm this result.

2.4 Summary and Conclusions

Using the genetic modification technique of[260], we've created a suite of genetically modified galaxies using an initial "Organic" MW-mass galaxy with an LMC-mass satellite at $z = 0$. We use the GM process to create galaxies within DM halos with identical large scale structure environments and nearly-identical halo growth histories but for slight variations in their satellite accretion history. The result is a set of four MW-mass halos with accretion histories which have been modified in this controlled way. Despite their overall similarities, we find significant differences in their baryonic evolution. Two of these galaxies remain star forming and two become quenched at $z = 1$. By examining the two quenched cases, we determine that a pair of minor satellite interactions at $z = 1$, concurrent with the peak SMBH accretion rate in the galaxy, can fully quench its star formation until $z = 0$.

In the two quenched galaxies, the genetic modification process results in a change to the timing of early satellite mergers. Thus, the two satellites interact with the main galaxy within a period of $\sim$ 100 Myrs at $z = 1$. The first satellite merges with the main galaxy, adding to the fuel available to the SMBH, while the second passes through the main galaxy in a flyby. These minor satellite interactions disrupt the disk, and are followed by a peak of

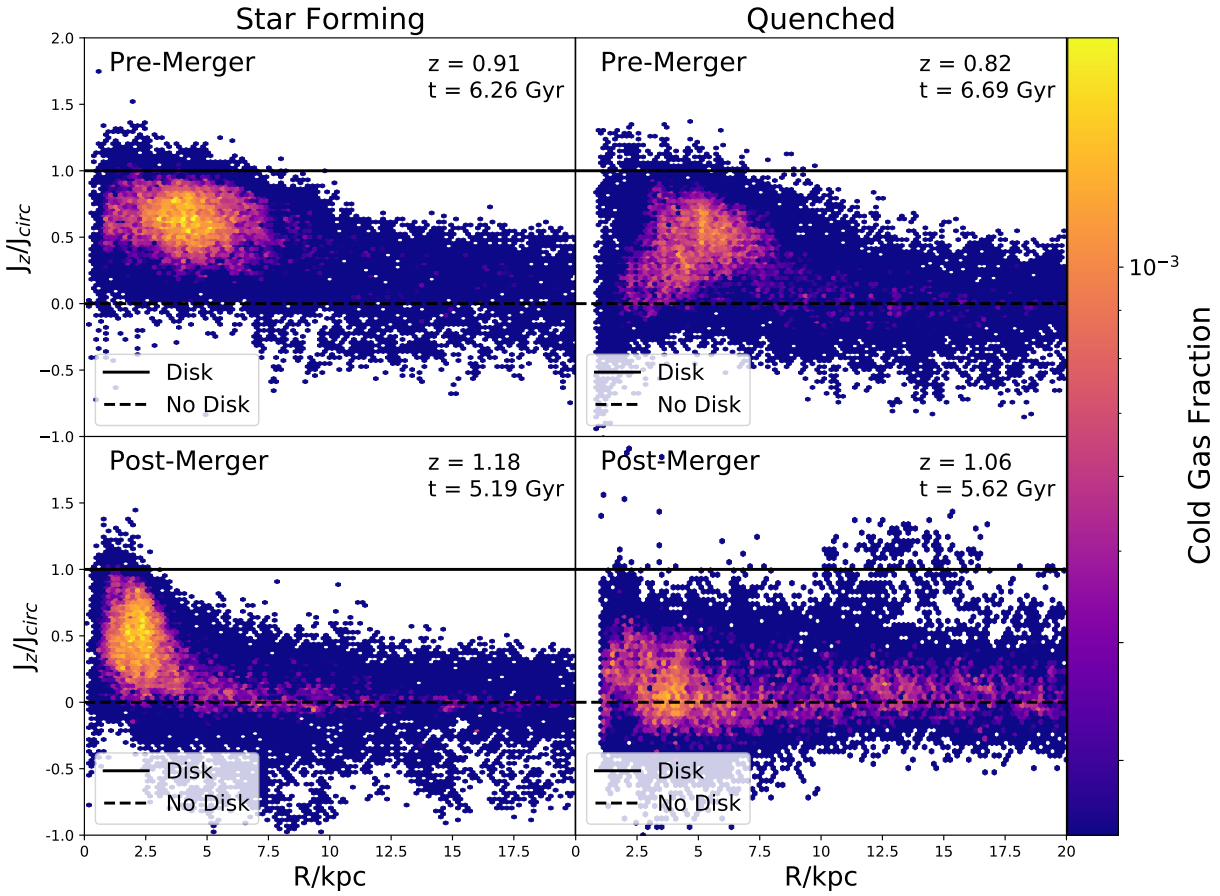

Figure 2.9: Plots of the circularity parameter $jz/jcirc$ of the cold gas ($T < 10^5$ K) for the star forming MW-mass galaxy, GM1, and a quenched MW-mass galaxy, GM2, around the time of the satellite merger in each galaxy. Gas that has $jz/jcirc$ closer to 1 is rotationally supported (i.e. in a disk), while gas with $jz/jcirc$ closer to 0 is dispersion supported. *(Top:)* Prior to the satellite mergers which result in GM2 quenching, both galaxies have fairly stable gaseous disk components. *(Bottom:)* After the interaction and mergers occur, however, the star forming galaxy *(Left)* retains a stable disk. You can also see compaction of the gas in the post-merger case[71]. Meanwhile the quenched galaxy *(Right)* at the post-merger time lacks a stable cold gas disk.

SMBH activity within a few hundred Myrs.

The timing of these events is roughly consistent with the rapid delay times observed between mergers and AGN activity by Schawinski et al. 2014[273]. They examined GALEX SFRs and SDSS colors of a sample of galaxies from the Galaxy Zoo Citizen science project[178] and found that early-type galaxies are quenched by rapid processes ($t_{quench} < 250$ Myrs). Other observational results find longer quenching timescales using similar methods e.g.[272;289].

To better understand our results on a broader scale, we estimate the number of these nearly simultaneous events within a cosmological volume that eventually quench a MW-mass galaxy. In a sample of 26 isolated MW-mass galaxies from the ROMULUS25 simulation, there are 10 galaxies that quench by $z = 0$ and one experiences multiple minor mergers that coincide with a peak in SMBH accretion that result in a quenched galaxy.

Given current observational capabilities, assessing the impact of minor mergers on star formation history remains a challenge. However, work disentangling minor merger effects on SF galaxies has been ongoing[185] and references therein and JWST will likely improve upon these observations in the future.

Major mergers ($q < 3$) between massive galaxies have long been thought to be the primary means by which spiral galaxies transform into ellipticals[75;128;142;272;293;297]. In addition, these mergers drive starbursts and fuel central SMBHs, where the latter process may suppress star formation in the remnant galaxy[131;245;253;267]. The tidal torques, combined with the angular momentum of infalling gas, funnel gas into the center of the galaxy, which subsequently increases the accretion rate of the SMBH[18;78;133]. However, recent observational and theoretical studies have called into question the efficacy of major mergers in driving SMBH fueling[74;87;126;127;301;340]. For example, Del Moro et al. 2016[74] examined a sample of luminous mid-IR quasars and found no direct evidence linking SFRs and AGN luminosity.

While previous work has explored the galaxy-scale physical consequences of major mergers, the role of minor merger disruption in galactic evolution and SMBH fueling is less understood but see:[50;133;166;225;317]. A recent simulation study by Hani et al. 2020[123] explores the relationship between mergers and galaxy evolution. They find that both major ($q \lesssim 3$) and minor mergers ($q \gtrsim 3$) can significantly increase the sSFR of the post-merger galaxy. However, the enhancement of the sSFR is a factor of ~ 2 for minor mergers ($q \sim 3 - 10$) and ~ 2.5 for major mergers. While Hani et al. 2020[123] do not find that galaxy mergers are globally quenching their post-merger galaxies, they conclude that the strongest merger-driven galaxies become quenched faster than their control galaxies.

We therefore explore the role of minor mergers, in tandem with the feedback of the SMBH,

as drivers for quenching massive galaxies. The closely timed interaction of the minor merger and flyby ultimately disrupt the galaxy disk, and drive gas into the vicinity of the SMBH, thereby fueling it[167]. Thus, it is the sequence and combination of these events that occur during a short period of few hundred Myrs —the SMBH fueling and subsequent feedback coupled with the disruption of the disk —that fully quench both MW-mass galaxies in GM2 and GM3 by $z = 1$. Our study has revealed a complex story where the dual impact of two minor mergers, and the increased SMBH fueling that these mergers drive, create a viable pathway for quenching in MW-mass galaxies and supports the growing evidence that the mechanisms that quench a galaxy are numerous and varied.

Chapter 3

NOT SO HEAVY METALS: BLACK HOLE FEEDBACK ENRICHES THE CIRCUMGALACTIC MEDIUM

Portions of this chapter were originally published in collaboration with Jessica K. Werk, Michael Tremmel, Andrew Pontzen, Charlotte Christensen, Thomas Quinn, and Akaxia Cruz in the September 2019 edition of The Astrophysical Journal (Sanchez, N. N., Werk, J. K., Tremmel, M., et al. 2019, The Astrophysical Journal, 882, 8; 2019 ©American Astronomical Society, DOI: 10.3847/1538-4357/ab3045), and are reproduced below with the permission of the American Astronomical Society.

Summary

We examine the effects of supermassive black hole (SMBH) feedback on the circumgalactic medium (CGM) using a cosmological hydrodynamic simulation ROMULUS25;[323] and a set of four zoom-in "genetically modified" Milky Way-mass galaxies sampling different evolutionary paths. By tracing the distribution of metals in the CGM, we show that O VI is a sensitive indicator of SMBH feedback. First, we calculate the column densities of O VI in simulated Milky Way-mass galaxies and compare them with observations from the COS-Halos Survey. Our simulations show column densities of O VI in the CGM consistent with those of COS-Halos star forming and quenched galaxies. These results contrast with those from previous simulation studies which typically underproduce CGM column densities of O VI. We determine that a galaxy's star formation history and assembly record have little effect on the amount of O VI in its CGM. Instead, column densities of O VI are closely tied to galaxy halo mass and black hole growth history. The set of zoom-in, genetically modified Milky Way-mass galaxies indicates that the SMBH drives highly metal-enriched material out into its host galaxy's halo which in turn elevates the column densities of O VI in the CGM.

3.1 Introduction

The circumgalactic medium (CGM), the extended region of gas surrounding galaxies out to their virial radii, is richly structured and composed of the raw materials and by-products of galaxy evolution. Due to its extremely diffuse nature, the CGM is the component of a galaxy that presents perhaps the greatest challenge to extragalactic observers. The most sensitive probes of the predominantly ionized gas in the CGM are background QSO sightlines. The spectra of these background QSOs show the absorption signature of a foreground galaxy's halo e.g.[12;30]. Such studies provide an inherently one-dimensional picture of the gas, typically along only a single sightline. Other observational techniques of studying the CGM include: stacking analyses, which combine between hundreds and thousands of spectra and/or images to detect the faint signals of CGM[227;300;373;375;376]; "down-the-barrel" spectroscopy, which employs a galaxy's own starlight as the background source for CGM absorption[37;125;184;261]; and emission line maps, which search for the few photons emitted directly by CGM gas[49;124;243]. Additionally X-ray observations by Chandra and XMM Newton have been used to help constrain the extent and nature of the hot, 10^6 K CGM e.g.[6;7;217;372].

Significant progress in the study of the $z \lesssim 1$ CGM followed the 2009 installation of the UV-sensitive Cosmic Origins Spectrograph (COS) on the *Hubble Space Telescope HST*,[114]. Numerous successful absorption-line surveys with COS have reported a structurally complex, multiphase medium with column densities and covering fractions of metal ions and hydrogen depending strongly on galaxy properties e.g.[38;39;143;152;176;241;306;327;332]. For example, while actively star-forming galaxies exhibit a highly-ionized component to their CGM characterized by strong O VI absorption out to at least 150 kpc, non-star-forming, elliptical galaxies show weak or no detections of O VI[331]. However, these same passive galaxies exhibit a high incidence of strong H I absorption in their CGM, as much cold, bound gas as their star-forming counterparts[143;240;314]. These results emphasize that the processes that transform galaxies from star-forming disks to passive ellipticals *do* affect the physical state of the CGM, but *do not* completely deplete it of cool, 10^4 K gas.

Numerous studies of the CGM indicate that it hosts a substantial fraction of a galaxy's baryons e.g.[152;241;358]. Overall, the observational studies on the low-redshift CGM all highlight the driving role played by gas in the galactic halo in shaping the evolution of stars and gas in the disks. It is clear that understanding the CGM is crucial for understanding the complex nature of galaxy evolution and growth.

The widespread O VI absorption in MW-mass halos, referenced above, has presented a particularly intriguing puzzle for theorists e.g.[195;214;222;302;309]. Oppenheimer et al. 2016[222] argue that the O VI bimodality in SF vs non-SF halos arises due to collisionally-ionized O VI acting as tracer of the virial temperature of gas in these galaxy halos. In this scenario, galaxies with $M_* \gtrsim 10^{11}$ $M_\odot$ would have more of their oxygen in a more ionized phase such as O VII and O VIII. This hypothesis is supported by observations of non-SF galaxies in the COS-Halos sample, which show lower O VI column densities, reportedly due to the intrinsically higher virial temperatures of these generally more massive, red ellipticals. In contrast, Suresh et al. 2017[309] argue that O VI is built up by supermassive black holes (SMBH), which can physically modify the CGM via outflows and heat it to $10^{5.5-5.8}$ K, the temperature at which the fraction of oxygen as O VI is maximized. Meanwhile, Oppenheimer et al. 2018[221] suggests that photo-ionizing energy from a flickering AGN might be required to raise the column densities of OVI within the virial radius to observed levels. These two pictures differ greatly in terms of the physical processes that give rise to widespread O VI in the CGM. In one, O VI traces the hot halo that forms in conjunction with the galaxy through gravitational processes. In the other, pc-scale processes in the inner, central galaxy provide enough heat and energy to impact the physical state of extended halo gas out to 100 kpc.

With respect to the picture put forward by Suresh et al. 2017[309], it is not unreasonable to propose that a galaxy's SMBH influences the content of its CGM. Galaxy properties in general have been shown to be strongly tied to the evolution of its central SMBH. Relations such as the M-σ and the bulge mass-BH mass correlation[94;190] indicate that the SMBH and its host galaxy halo *co-evolve*[106;167;249;347] and references therein. However, the direct mechanisms for SMBH-CGM impact remain unclear.

SMBHs have been proposed to effect the CGM in a variety of ways. First, feedback from the active SMBH may inject energy into the surrounding material, raising temperatures, resulting in collisionally- and photo-ionized metals in the gas[186;193;221]. Additionally, the SMBH may physically push multiphase gas out of the galaxy. Some of this material may end up falling back into the galaxy as part of the "recycling" of the CGM[330], enriching CGM gas with metals from the center of the galaxy, or may leave the CGM entirely and instead enrich the intergalactic medium (IGM).

In tandem with observational progress on characterizing the CGM, cosmological hydrodynamic simulations have become a powerful tool for examining the physics driving the multiphase nature of the CGM[52;97;99;136;177;214;222;280;305;309]. Despite significant effort, few of these studies are able to match the observed properties of the CGM. For example, most previous studies underpredict the column densities of O VI found by COS-Halos including the aforementioned studies,[136;219;222;309]. Nonetheless, these studies have led to important physical insights. Using the smooth particle hydrodynamic code GADGET-2[219;295], Ford et al. 2014[97] found that the presence of O VI in the CGM likely arises from metals ejected very early on in the galaxy's evolution. More recently, Nelson et al. 2018[214] matched the COS-Halos observations using the IllustrisTNG simulations and determined that the amount of O VI the CGM can depend on a variety of galactic properties including sSFR. In particular, they find that BH feedback (specifically, their low-accretion, kinetic-feedback mode) plays a crucial role in setting the amount of O VI in the CGM by affecting the amount of metal mass ejected by the galaxy.

Motivated by previous theoretical and observational work, we use two sets of simulations to study circumgalactic O VI: the cosmological volume, ROMULUS25[323], and three "genetically modified" variations of a zoom-in Milky-Way (MW) mass galaxy[236;260] selected from a cosmological volume. These genetically modified zoom-in galaxies are run with and without the implementation of BH physics to test the effect of SMBH feedback on the CGM. To compare our results with observations, we rely primarily on data from the COS-Halos Survey. Although several other surveys have examined the CGM around a wide-range of galax-

ies e.g.[39;67;152;270;306], COS-Halos[332] remains the best-studied, uniformly-selected sample of MW-mass host galaxies to-date, and one of the few to focus on O VI. Furthermore, COS-Halos tabulates CGM gas column densities along with spectroscopically and photometrically-determined galaxy properties (e.g. SFR, M_*) allowing for a straightforward comparison between our simulations and the data.

Ultimately, we examine the effects of both environmental and internal galaxy processes on the physical state and content of the CGM. Specifically, we address how the star formation and assembly history of the galaxy impact the content of the CGM and how SMBH activity imprints itself on the CGM. Using these zoom-in simulations in tandem with the ROMULUS25 simulation, we illuminate the roles that stellar evolution and SMBH feedback play in setting the properties of the CGM of MW-mass galaxies.

In Section 3.2, we describe the underlying physics used in our two galaxy samples. Section 3.3 details our results from examining the CGM in ROMULUS25 and comparisons with the zoom-in galaxies and observations. We discuss these results and their implications for future studies in Section 3.4. In Section 3.5, we summarize and offer conclusions.

3.2 Simulation Parameters

3.2.1 ChaNGa Physics

Both ROMULUS25 (hereafter R25) and our set of zoom-in galaxies were run using the smoothed particle hydrodynamics N-body tree code, Charm N-body GrAvity solver ChaNGa,[196]. ChaNGa includes the same models for a cosmic UV background, star formation (using a Kroup IMF), 'blastwave' SN feedback, and low temperature metal line cooling as previously used in GASOLINE[281;303;350;352]. Neither ROMULUS25 or the zoom-in simulations utilize metal cooling as the resolution of these simulations is too large to consider individual star forming regions. Instead, our simulations use a low temperature extension to the cooling curve such that only gas below 10^4 K cools proportionally to the metals in the gas. Gas above this threshold cools only via H/He, Bremsstrahlung, and inverse Compton. This lack

of metal cooling in our model likely causes our galaxies to over predict O VI by approximately 0.3 dex[281]; however, as our study compares total quantities of oxygen between simulations and the relative motions of metals, the relative values of N_{OVI} between simulations remains valid.

ChaNGa includes an improved SPH formalism which includes a geometric density approach in the force expression[351]. This update to the hydrodynamic treatment includes thermal diffusion[281] and reduces artificial surface tension allowing for better resolution of fluid instabilities[111;196;254].

Additional improvements have been made to the BH formation, accretion, and feedback models as well an improved prescription for dynamical friction[321;323]. BH seed formation is tied to dense, extremely low metallicity gas to better estimate SMBH populations in a wide range of galaxies. Sub-grid models for both dynamical friction—to better simulate realistic SMBH dynamical evolution and mergers—and accretion have been implemented. The new SMBH accretion model considers angular momentum support from nearby gas allowing for more physical growth compared to Bondi-Hoyle prescription alone or other methods that require additional assumptions or free parameters[8;258]. Angular momentum support is taken into account in the accretion equation:

$$\dot{M} \propto \frac{\pi (GM)^2 \rho c_s}{(v_\theta^2 + c_s^2)^2}, \tag{3.1}$$

where v_θ is the rotational velocity of the gas surrounding the BH and is informed by the angular momentum support of the gas on the smallest, resolvable scale. However, when bulk motion dominates over rotational motion, the formula reverts to the original Bondi-Hoyle. Thermal SMBH feedback energy is imparted on the nearest 32 gas particles according to a kernel smoothing and is determined by the accreted mass, $\dot{M}$, as:

$$E = \epsilon_r \epsilon_f \dot{M} c^2 dt, \tag{3.2}$$

where $\epsilon_r = 0.1$ and $\epsilon_f = 0.02$ are the radiative and feedback efficiency, respectively, and dt represents one black hole (BH) timestep, during which the accretion is assumed to be constant.

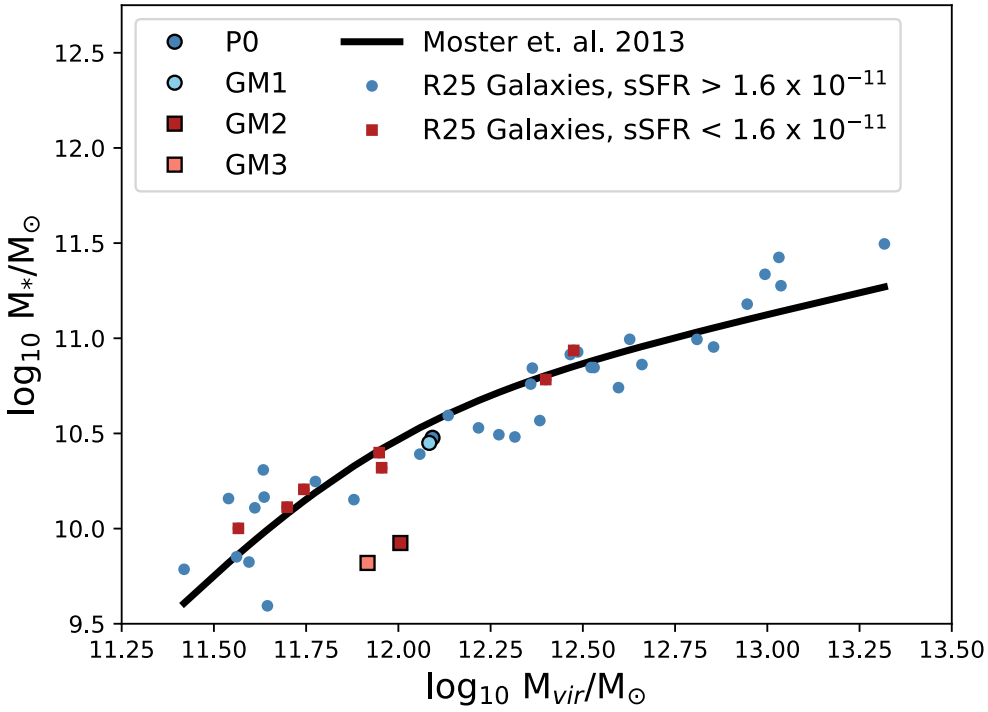

Figure 3.1: We show that the 39 galaxies from R25 in our sample, which are selected along the distribution of COS-Halos stellar masses within the range (3×10^9 $M_\odot$ —3×10^{11} $M_\odot$). Including the corrections of Munshi et al. 2013[204], the galaxies follow the stellar mass-halo mass (SHMH) relation up to $\sim 10^{13}$ above which they are slightly higher than predicted. Red squares and blue circles represent passive and star forming galaxies, respectively. The 4 zoom-in galaxies with BH physics are outlined in black.

Cooling is briefly ($\sim 10^{4-5}$ years) shut off immediately after AGN feedback events.[323] Our SMBH feedback prescription is also shown to be able to produce large scale outflows[236;319].

All our simulations were run with a ΛCDM cosmology from the most recent Planck collaboration utilizing $\Omega_0 = 0.3086$, $\Lambda = 0.6914$, h = 0.6777, $\sigma_8 = 0.8288$ and have Plummer equivalent force softening lengths of 250 pc. For simulating the cosmic reionization energy, both simulations have a Haardt et al. 2012[119] UV background applied at $z \sim 9$ through the evolution to low-redshift. For our purposes, we've defined the CGM in each simulated galaxy as all the gas inside the galaxy's virial radius, defined as the radius at which the density is 200 times the critical density, ρ_c, where $\rho/\rho_c = 200$ (R_{200}), and outside a spherical 10 kpc from its center.

3.2.2 ROMULUS25 *Cosmological Volume*

The ROMULUS25[323] R25 simulation is a 25 Mpc cosmological volume which includes galaxy halos within the mass range 10^9 —10^{13} $M_\odot$. R25 has a mass resolution of 3.4×10^5 $M_\odot$ and 2.1×10^5 $M_\odot$ for DM and gas particles, respectively. Galaxies in R25 have been shown to lie along the M_{BH}-M_* and stellar mass-halo mass relation (Figure 3.1, though slightly higher than predicted for the highest mass galaxies), and are consistent with observations of star formation and SMBH accretion histories at high redshift[323]. Both our M_{halo} and M_* measurements use the corrections from Munshi et al. 2013[204]. Additionally, Tremmel et al. 2017[323] shows that SMBH physics is a necessary component for reproducing the evolution of MW-mass galaxies as well as quenching in massive galaxies. For our study, we focus galaxies in R25 that fall within the stellar mass range of COS-Halos: 3×10^9 $M_\odot$ and 3×10^{11} $M_\odot$ and populate a similar distribution of stellar masses.

With these selection criteria in place, our sample includes 39 galaxies. Using the specific star formation (sSFR = SFR/M_*) cut of COS-Halos, 32 of these galaxies are star forming (sSFR $> 1.64 \times 10^{-11}$ yr^{-1}) and 7 are passive at $z \sim 0.17$. The sSFR of COS-Halos (previously $>10^{-11}$ yr^{-1}) has been corrected by a factor of 1.64 to account for the fact that COS-Halos uses a Salpeter IMF while our simulations use a Kroupa IMF[169]. This correction only affects the categoration two of our R25 galaxies. We further note that this fraction of passive galaxies is a conservative estimate. However, by $z = 0$, the quenched fraction in R25 is about 40 % for the highest mass galaxies[319].

3.2.3 Zoom-In Galaxies: Patient 0 and its Genetic Modifications

While R25 gives a cosmological context to our analysis, we examine our set of genetically modified zoom-in galaxies to better understand the physical and phenomenological processes that influence the CGM. To select our MW-mass galaxy, we ran an initial dark-matter-only simulation in a 50-Mpc-on-a-side cosmological volume. From this simulation, we selected a MW-analog ($M_{vir} = 9.9 \times 10^{11}$ $M_\odot$) halo at z=0 as our "Patient 0" (hereafter P0) and

Table 3.1: Zoom-In Galaxies Modification

Sim	Satellite Dark Matter Mass ($M_\odot$) at $z = 1$
P0	7.3×10^{10}
GM1	5.9×10^{10}
GM2	4.0×10^{10}
GM3	2.5×10^{10}

then re-simulated it at a higher resolution with baryons. We additionally required that the galaxy be >2 Mpc away from another MW- or higher mass galaxy. Finally, we selected our P0 for the satellite galaxy ($M_{sat} = 2 \times 10^{10}$ $M_\odot$) contained within its virial radius at $z = 0$ which acts as a proxy for a LMC satellite. Selecting a MW-analog galaxy in halo mass allows us to compare directly with the COS-Halos observations, which observed $\sim$ L^* galaxies. For the subsequent, "genetically modified" (GM) zoom-in runs, we use the method of genetic modification of Pontzen et al. 2017[236] which creates a set of very similar initial conditions that result in galaxy simulations which keep the large scale structure and cosmological conditions consistent (as in P0), while resulting in slight modifications to their accretion histories[260]. In our work, we uses the GM technique to decrease the mass of the satellite which exists at $z = 0$ in P0 and shrank its mass *prior* to when it enters the galaxy at $z = 1$. To create the modified set of initial conditions, we determined which elements in the linear overdensity field of the initial condition grid map to the particles in the satellite.

We then decreased the mean overdensity of these elements in the initial linear vector, all the while, maintaining the mean overdensity of the elements mapping to the main halo to preserve the final mass. We note that the effect of changing the satellite mass for the GM galaxies with BH physics does produces a shift in the dark matter mass of the halo (decreases $\leq$ 20%). The physical reason for this drop is that AGN feedback suppresses DM accretion following a particularly strong expulsion of gas. Additionally, the inclusion

Table 3.2: Properties of Zoom-In Galaxies *with BHs* at z = 0.17

Sim	Halo Mass ($M_\odot$)	Gas Mass ($M_\odot$)	Stellar Mass ($M_\odot$)	CGM Gas Mass ($M_\odot$)	R_{vir} (kpc)	T_{vir} (K)
P0	9.9×10^{11}	1.1×10^{11}	5.0×10^{10}	9.3×10^{10}	277.0	5.5×10^5
GM1	9.7×10^{11}	9.9×10^{10}	4.7×10^{10}	8.5×10^{10}	274.9	5.4×10^5
GM2	8.1×10^{11}	6.9×10^{10}	1.4×10^{10}	6.9×10^{10}	259.2	4.8×10^5
GM3	6.6×10^{11}	5.1×10^{10}	1.1×10^{10}	5.1×10^{10}	241.7	4.2×10^5

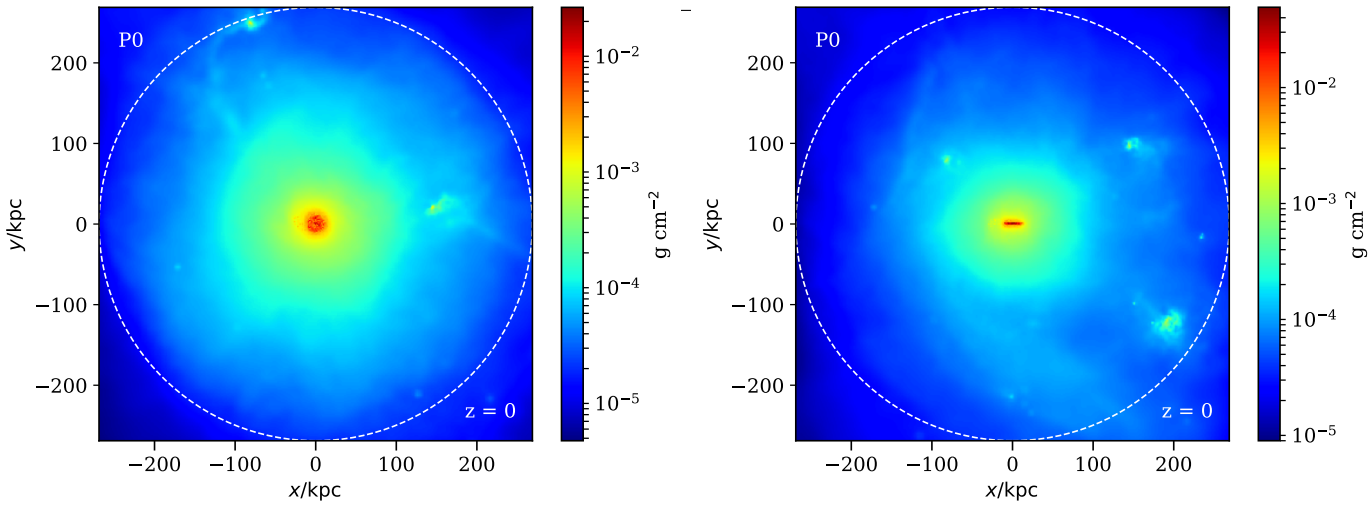

Figure 3.2: A face-on and edge-on view of our Patient 0 galaxy in projected gas density at $z = 0$.. The virial radius is designated by the white-dashed circle.

of baryonic physics can result in a decrease in total halo mass[204] which helps account for this drop. However, as the difference between our halo masses ($\sim$ 0.2 dex) is much smaller than our stellar masses ($\sim$ 0.2 dex), to a good approximation, we clearly explore the effect of changing M_* with fixed M_{halo}.

3.2.4 Zoom-In Galaxies: With BH Physics

At $z = 0$, our P0 galaxy is a star forming galaxy with a disk (Figure 3.2). P0 has an incoming satellite at $z = 0$ with an original mass of 7.34×10^{10} $M_\odot$ (mass ratio, q = 0.12) *prior* to entering the main halo's virial radius at $z \sim 1$. For each GM galaxy simulation, we

Table 3.3: Properties of Zoom-In Galaxies *without BHs* at z = 0.17

Sim	Halo Mass ($M_\odot$)	Gas Mass ($M_\odot$)	Stellar Mass ($M_\odot$)	CGM Gas Mass ($M_\odot$)	R_{vir} (kpc)	T_{vir} (K)
P0noBH	9.8×10^{11}	8.2×10^{10}	7.9×10^{10}	7.5×10^{10}	276.1	5.4×10^5
GM1noBH	9.9×10^{11}	8.7×10^{10}	7.4×10^{10}	8.0×10^{10}	276.2	5.5×10^5
GM2noBH	9.6×10^{11}	8.8×10^{10}	7.0×10^{10}	8.0×10^{10}	274.0	5.3×10^5
GM3noBH	8.4×10^{11}	7.1×10^{10}	7.3×10^{10}	6.4×10^{10}	261.9	4.9×10^5

systematically shrink this satellite halo's mass prior to its entry into the main halo (Table 3.1). GM1 results in a similar disked, star forming galaxy, while GM2 and GM3 become quenched at $z \sim 1$ (Table 3.2).

Patient 0 and its 3 GM simulations have mass resolutions of 1.4×10^5 $M_\odot$ and 2.1×10^5 $M_\odot$ for DM and gas particles, respectively. The DM field in these galaxies is simulated at twice the gas resolution to reduce noise in the potential near the galactic center[237] and more accurately trace BH dynamics[321].

While these GM galaxies are generated using the same method as Pontzen et al. 2017[236], their study examines a different set of galaxies. The three galaxies in Pontzen et al. 2017[237] were run to $z = 2$ and have $M_{Halo} \sim 10^{12}$ $M_\odot$. They each have incoming satellites whose masses are both increased and decreased prior to merging with the main galaxy, as in our galaxies. We note that the genetic modifications performed on the galaxies of Pontzen et al. 2017[237] were different from the ones implemented here. In their case, it was an enhanced merger (increased satellite's mass) that resulted in a quenched galaxy, rather than a shrunken satellite mass as we implement here. However, in our quenched galaxies, we see that the mass is compensated by faster, early accretion to account for maintaining the main halos' final masses.

3.2.5 Zoom-In Galaxies: Without BH Physics

One key benefit of the individual zoom-in galaxies includes the ability to remove or adjust the parameters affecting our galaxies. This capability allows us to test different theoretical models which would be too computationally expensive to do with a large volume like R25. In particular, we may exploit this utility to understand directly the effects of the SMBH. To isolate the effect of the SMBH on the CGM, all four of the zoom-in simulations (P0 and its 3 GMs) were re-simulated at the same resolution and with all the same physics *excluding* BH formation, feedback, and dynamical friction (Table 3.3). Black hole seed formation was disabled and the BH feedback and accretion efficiency parameters set to 0.

3.2.6 Zoom-In Galaxies: Quenching in GM2 and GM3

The top panel of Figure 3.3 shows star formation histories of the four zoom-in galaxies with BH physics included. P0 and GM1 are in light and dark blue, respectively, while GM2 and GM3 are shown similarly in dark and light red. Their star formation histories demonstrate that, unlike P0 and GM1 which remain star forming throughout their history, GM2 and GM3 become quenched at $z \sim 1$. Contrastingly, the lower panel of Figure 3.3 shows the star formation histories of the four zoom-in galaxies without BH physics and all four of their histories remain star forming and are fairly similar. The immediate quenching seen in the upper panel for GM2 and GM3, which occurs just after the merger of the satellite with the main halo, *does not* take place in the simulations of GM2 and GM3 without BH physics, consistent with Pontzen et al. 2017[236]. Significant outflows after the time of the merger (z $\sim$ 1) result in the quenching we see in GM2 and GM3 due to the combination of minor merger interactions that occur at this time as well as a peak in the SMBH accretion as a result of fueling from the infalling satellites. See Chapter 3 for a detailed analysis of the quenching mechanism.

Pontzen et al. 2017[236] previously explored the relationship between BH feedback and mergers and its effect on quenching, using the same genetic modification technique as we

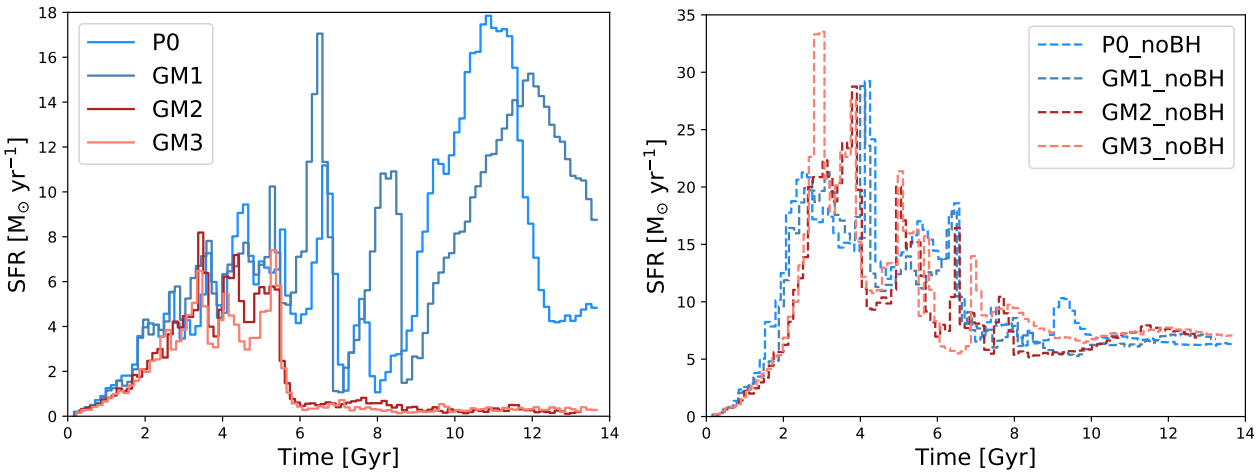

Figure 3.3: The star formation histories for the zoom-in galaxies: Patient 0 and its 3 GM galaxies with BH physics (*Left*) and without BH physics (*Right*). In the galaxies including BH physics, P0 and GM1 remain star forming throughout their histories while GM2 and GM3 become quenched at $z \sim 1$. Without BH physics, all four galaxies remain star forming until $z = 0$.

use for the GM galaxies in our study. They determine that SMBH feedback is critical to quenching a galaxy, which is consistent with our finding that quenched galaxies arise only in simulations that include SMBHs (Figure 3.3). Pontzen et al. 2017[236] argue that mergers can disrupt the cold disk of the galaxy, allowing SMBH feedback to more strongly suppress star formation in the disk and keep the galaxy in a state of quiescence. Mergers have also been shown to help funnel gas into the region of the SMBH allowing for more direct accretion[131;213;253;267].

We further examine the effects of the BH by looking to the accreted mass and accretion rates of the BHs. The upper panel in Figure 3.4 (colors as in Figure 3.3) shows the cumulative accreted SMBH mass as a function of time. Here we see that the accreted mass growth in the quenched galaxies, GM2 and GM3, is similar to that of the star forming galaxies. However, more significant differences arise in the lower panel of Figure 3.4, which depicts the SMBH accretion rates as a function of time. From this figure, we can see an increase of accretion occurs for both quenched galaxies near the time of the merger (z $\sim$ 1, t $\sim$ 6 Gyr). In particular, for the two quenched galaxies GM2 and GM3 (shown in dark and light red, respectively), we see that the accretion rate peaks about a Gyr earlier than for the star

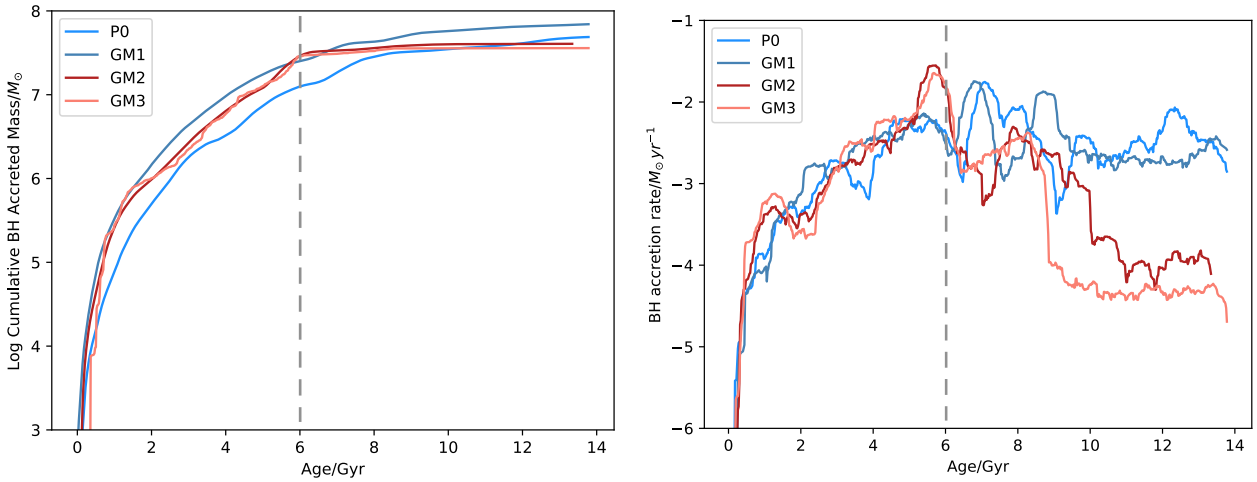

Figure 3.4: SMBH accreted mass (*Left*) and SMBH accretion rates (*Right*) for our 4 zoom-in galaxies. Colors as in Figure 3.3. The accreted mass of all the SMBHs are comparable. However, both quenched galaxies also have a sharp peak in accretion rate around the time of the most significant merger (z $\sim$ 1, t $\sim$ 6 Gyr), indicated by the dashed grey line.

forming galaxies. The accretion rate in the quenched galaxies continues to drop after this point, while the SMBH in each star forming galaxy continues to accrete. Although the BH's activity and growth are not directly affected by the changing mass of the incoming satellite, together the modified satellite mass and effect of the BH make a significant impact on the star formation history of the galaxy. Thus, while the peak accretion rates are similar in quenched and unquenched cases, the resulting energy couples differently to the galaxies and only in the latter case do they lead to a reduction in later inflows.

This set of galaxies was produced from very similar initial conditions and therefore have near-identical large scale filamentary feeding. However, they illustrate very different star formation and accretion histories and allow us to directly examine how assembly history may imprint itself on the CGM. Additionally, they allow us to concretely confirm the result of Pontzen et al. 2017[236] that the effect of a SMBH, while not the only requisite, is *vital* to the quenching process in galaxies.

3.3 Results

With the simulations we've described, we examine the effects of stellar evolution and SMBH feedback on setting the contents and physical state of the CGM in MW-mass galaxies.

Individual halos in the ROMULUS25 cosmological volume and in the individual zoom-in galaxies are extracted using the Amiga Halo Finder (AHF)[164] and central SMBH positions and velocities are defined relative to the center position and inner 1 kpc center-of-mass velocity of their host halo, respectively. All zoom-in galaxies have their most major merger occurring at $z \sim 1$ (mass ratio = M_{halo}/M_{sat}, q <10) and an additional merger occurs (q $\sim$ 10) close to $z = 0.2$, though this time varies slightly across the simulations (See Section 3.3.2).

The CGM of each individual galaxy halo (within the 39 selected R25 galaxies and our zoom-ins) is defined as the mass enclosed within the virial radius, but further than a spherical radius of 10 kpc away from the center. While the genetic modification process results in galaxies with similar final masses in the absence of strong ejective feedback, we find that the mass of the CGM correlates with the mass of the halo when BH physics is included. P0, which results in the most massive halo at $z \sim 0$, has the most mass in its CGM, while GM3 results in the least massive CGM mass and halo mass (Table 3.2).

3.3.1 O VI as a Tracer of Virial Temperature Material

Column densities of O VI are calculated using the analysis software Pynbody[234]. Oxygen enrichment from supernovae and winds is traced throughout the integration of the simulation and ionization states are calculated during post-processing, assuming optically thin conditions, a Haardt et al. 2012[119] ultraviolet radiation field at $z = 0$, and collisional ionization equilibrium. Recent papers have raised concerns that this UV background is too weak[165;283]. However, as we will soon demonstrate, the O VI in our simulations is predominantly collisionally ionized, so our choice of UV background does not affect our results. We use the CLOUDY software package[93;305] to create models with varying temperature, density, and redshift to determine O VI fractions for all the gas in each simulated galaxy. Figure 3.5 shows the column densities of O VI as a function of radius for our 39 R25 MW-mass galaxies. Red and grey solid lines represent the column densities of quenched and star forming galaxies within the R25 sample, respectively. The COS-Halos dataset is plotted on top in black,

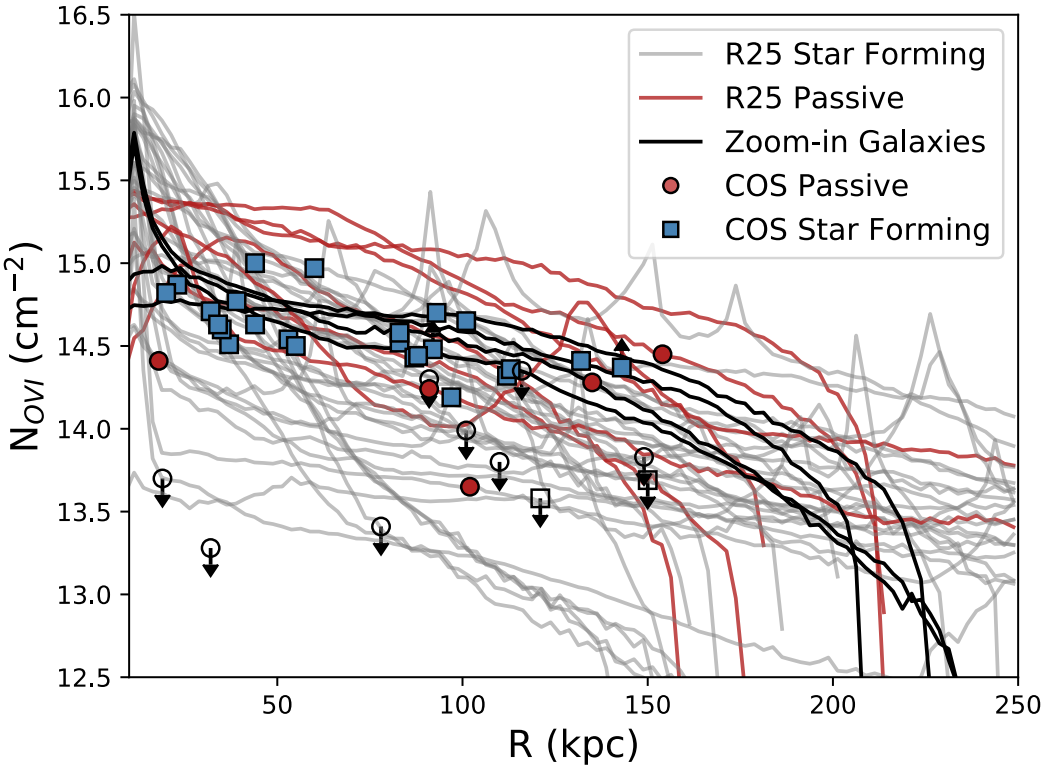

Figure 3.5: Mean column densities of O VI as a function of radius for all 39 of the galaxies in R25 which fall within the COS-Halos stellar mass range and our family of zoom-in galaxies. All galaxies are examined at $z = 0.17$. Solid grey and red lines indicate R25 star forming and quenched galaxy column densities, respectively. Solid black lines describe the column densities of our four zoom-in galaxies. Filled circles and squares indicate star forming and passive galaxies from the COS-Halos Survey dataset. Unfilled markers indicate upper limits.

with red squares and blue circles distinguishing between elliptical and spiral galaxies. Upper limits are designated with arrows and unfilled markers. The column densities of O VIfor the four zoom-in GM galaxies are shown in solid black lines.

Figure 3.5 shows that our simulations reliably reproduce the column densities of O VI in the CGM. While this agreement is a substantial improvement over previous simulations, which significantly underpredict NOVI, we stress that the lack of high temperature metal-line cooling in our simulations could be artificially boosting O VI abundances. However, given that the inclusion of high temperature metal cooling would only decrease the cooling time of gas by a factor of ~ 2 at temperatures and metallicities relevant to this study[281], it is unlikely to be the dominant effect in setting N_{OVI}, particularly when compared to AGN and

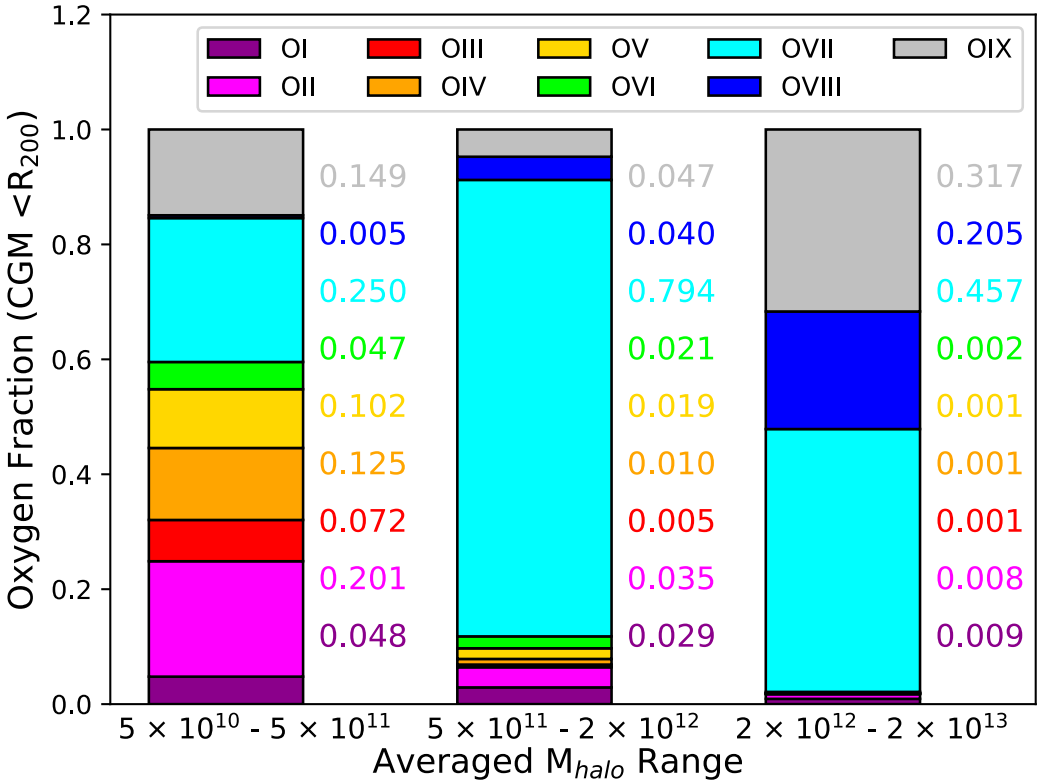

Figure 3.6: Average oxygen ion fractions in the CGM of R25 within 3 M_{halo} range bins: 5 $\times$ 10^{10} —5 $\times$ 10^{11}, 5 $\times$ 10^{11} —2 $\times$ 10^{12}, and 2 $\times$ 10^{12} —2 $\times$ 10^{13}. O VI is shown by green bars. The individual ion fractions are given in their corresponding colors to the right of each bar, ascending in order from least to most ionized such that O VI is fourth ionization fraction from the top. The average O VI fraction decreases as halo mass increases.

halo mass, which we demonstrate can change NOVI by factors of 10 or more. We see this in both the R25 galaxies, which in addition to providing evidence for this initial result also gives cosmological credence to our suite of GM galaxies, and our four GM galaxies that include BH physics. Most significantly, we note that *the column densities of O VI in the CGM of these galaxies does not depend on the assembly history of the galaxy.* All of our galaxies well match the O VI observations despite their differing assembly histories.

Following Figure 10 of Oppenheimer et al. 2016[222], Figure 3.6 shows the average ionization fractions for all the ionization states of oxygen within three mass ranges: low mass (5 $\times$ 10^{10} —5 $\times$ 10^{11} $M_{\odot}$), Milky Way-mass (5 $\times$ 10^{11} —2 $\times$ 10^{12} $M_{\odot}$), and high mass (2 $\times$ 10^{12} —2 $\times$ 10^{13} $M_{\odot}$). These three mass ranges include galaxies in R25 outside our sample

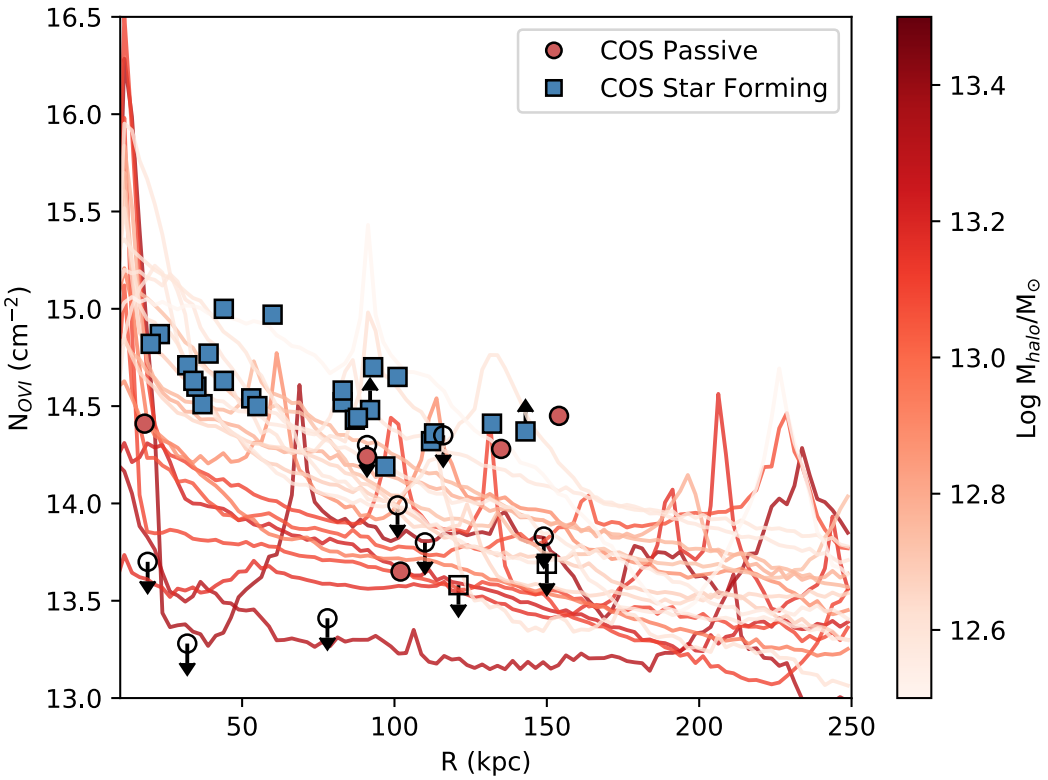

Figure 3.7: Column density profiles of O VI in the high mass ($M_{vir} > 2 \times 10^{12}$ $M_\odot$) galaxies of R25 at z = 0.17.

of 39 COS-Halo mass galaxies. Dark purple, light purple, red, orange, yellow, green, light blue, dark blue, and gray indicate the oxygen ions, O I, O II, O III, O IV, O V, O VI, O VII, O VIII, and O IX, respectively. The average ion fraction for each ion of oxygen is shown to the right of each column for the designated mass bin in its corresponding color. Ion fractions are in order from the top, highest to lowest. From the figure, we see that the O VI fraction (in green) decreases from the MW-mass range to the high mass regime due to the increase in virial temperature of higher mass galaxies, which moves from a value close to the ionization peak for O VI, T $\sim 10^{5.5} K$, to $10^{6.3}$ K. Similarly, Figure 3.7 shows the column densities of O VI for only the highest mass galaxies in R25 (2×10^{12} <M_{halo} <2×10^{13} $M_\odot$). Lines of N_{OVI} are colored by halo mass, with light red being the least massive and dark red denoting the highest mass galaxies. COS-Halos observations are plotted on top as in Figure 3.5. Figure 3.7 confirms that as galaxy virial mass increases, column densities of O VI decrease. This

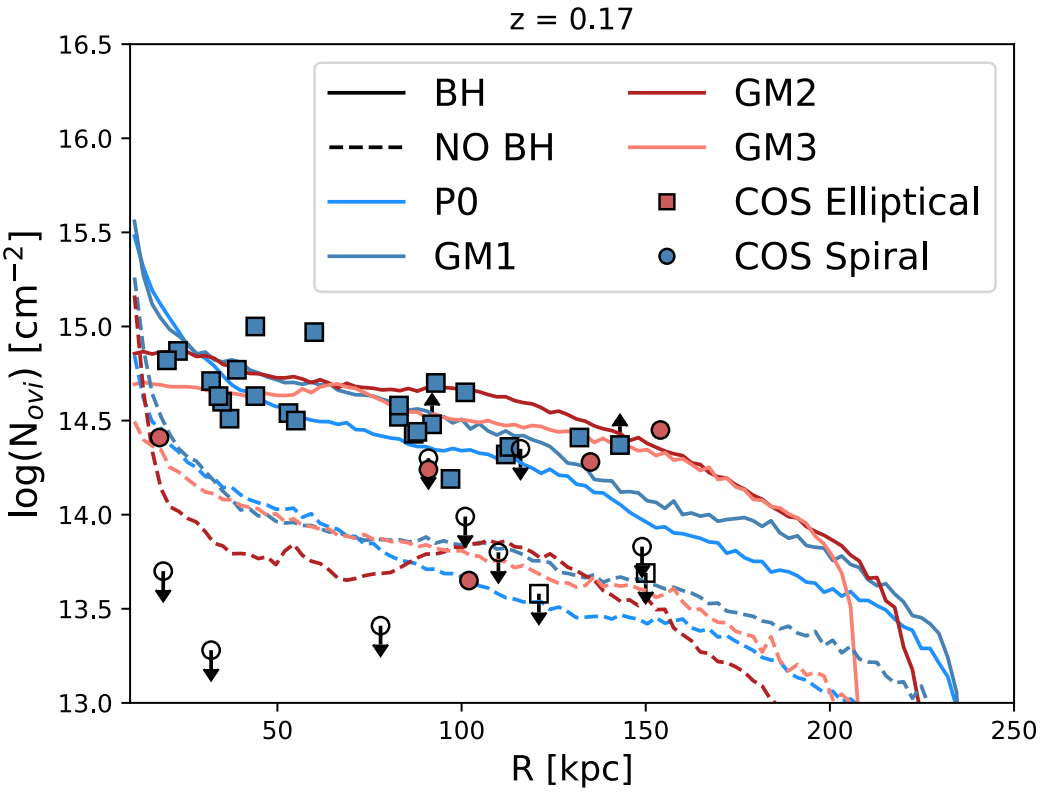

Figure 3.8: Column density profiles of O VI in our 4 zoom-in galaxies with (solid lines) and without (dashed lines) BH physics. P0 and GM1, our two star forming galaxies are marked in light blue and dark blue, respectively. Our quenched galaxies, GM2 and GM3, are labeled in dark red and light red, respectively. These column densities show that the BH is essential to shaping the O VI in the CGM of star forming and passive galaxies alike.

finding is consistent with the results of Oppenheimer et al. 2016[222] which determined that O VI acts as a tracer for the virial temperature of a galaxy. From this study, we determine that the star formation properties of the galaxy do not correlate with the evolution of O VI in the CGM. This result does not include local photoionization effects from the galaxy's star formation or AGN on the CGM. When these effects are included, especially the effect of 'AGN flickering,' Oppenheimer et al. 2018[221] finds a significant increase in CGM OVI column density. Instead, it appears that the mass of the galaxy, as it affects its virial temperature (Table 3.2), plays a more significant role in determining the column density of O VI seen in the CGM of the R25 galaxies.

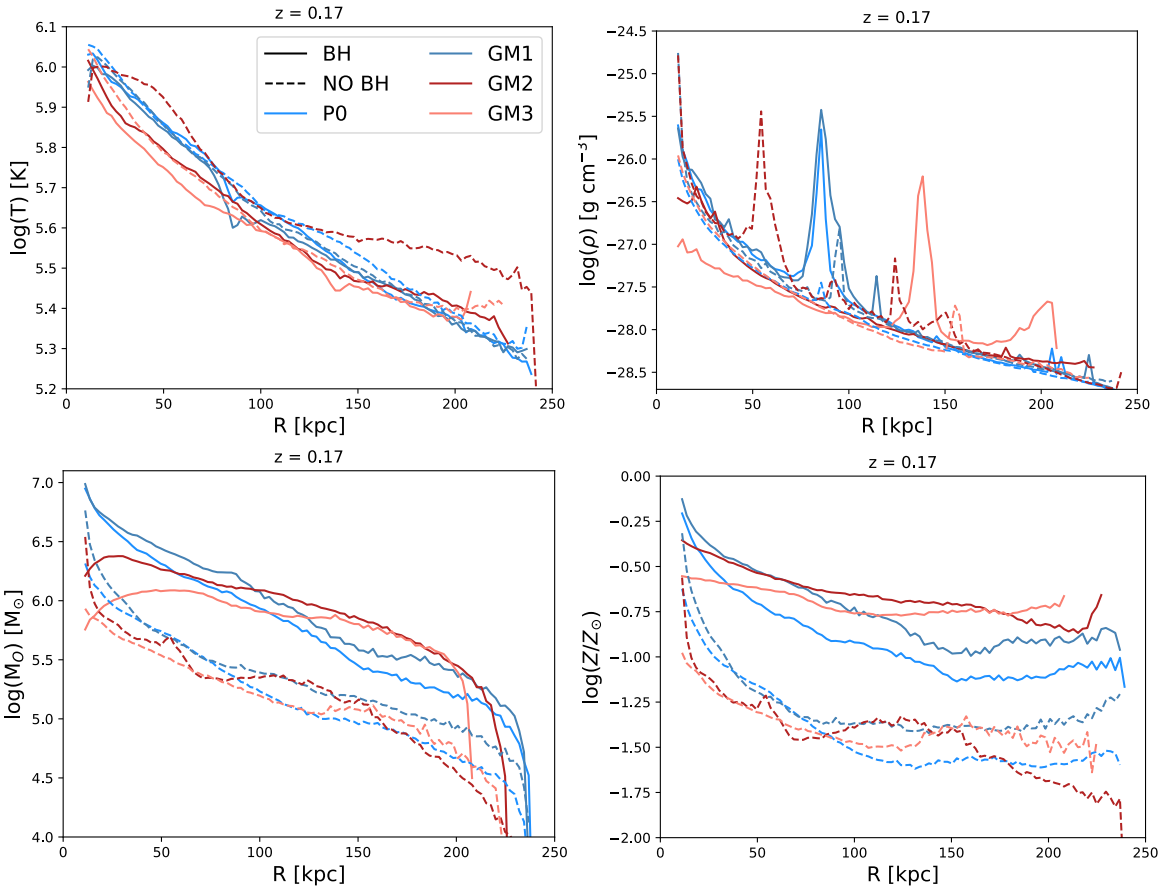

Figure 3.9: *Clockwise from Upper Left:* Temperature, density, metallicity, and total oxygen mass profiles of the CGM of our 4 zoom-in galaxies with and without BH physics at $z = 0.17$, the average redshift of COS-Halos. Colors and linestyles as in Figure 3.8. Solid and dashed lines designate simulations with and without BH physics, respectively.

3.3.2 Metal Transport by the SMBH

With both the R25 galaxies and zoom-in GMs, we have been able to examine the effects of star formation on the CGM. However, the zoom-in galaxies additionally offer us a controlled environment with which to more directly probe the impact of BH physics on the CGM. We examine the column densities of O VI in the CGM in our 4 zoom-in galaxies *without* BH physics and compare them to the cases where BH physics is included. Figure 3.8 shows the column densities of O VI in the CGM of all four of our zoom-in galaxies with BH physics (solid lines) and without (dashed lines). P0 and GM1 are light and dark blue, respectively, with GM2 and GM3 in dark and light red, as before. We can see that in the cases where BH physics is not included (dashed lines), the values of N_{OVI} are significantly lower implying

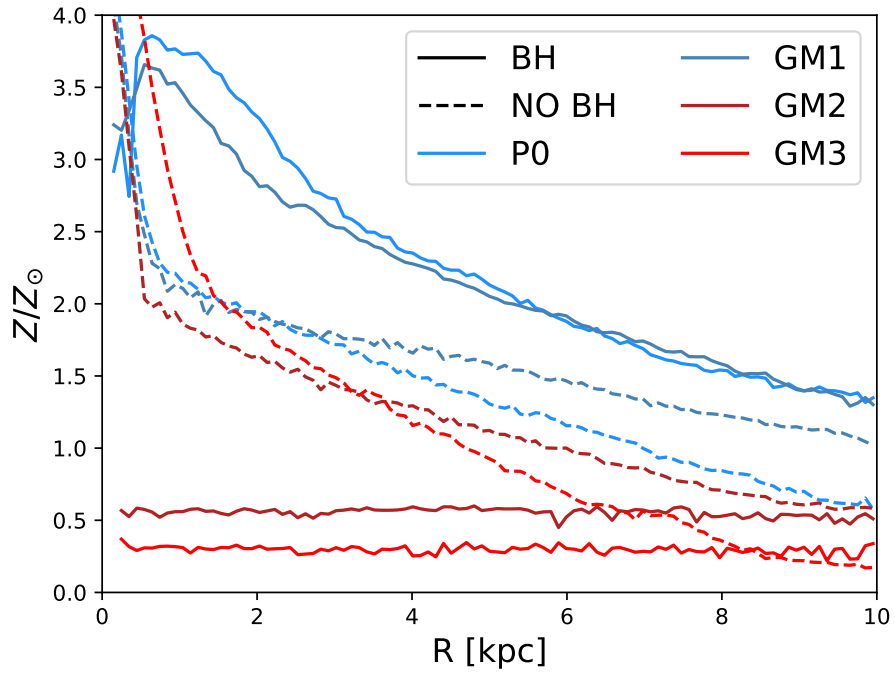

Figure 3.10: Metallicity profile of the gas within the disk of our 4 zoom-in galaxies with and without BH physics. Colors and line styles as in Figure 3.8. Without the BH physics, metals remain trapped near the center of the disk with no mechanism to propagate out into the CGM.

that the presence of the SMBH must play an important role in populating O VI in the CGM. We look to the temperature, oxygen mass, density, and metallicity of the CGM to investigate the cause of this decrease in O VI.

Figure 3.9 shows the temperature (*Upper Left*), density (*Upper Right*), total mass in oxygen (*Bottom Left*), and metallicity (*Bottom Right*) profiles of CGM in our 4 GMs with and without BH physics (colors and line styles as in Figure 3.8). From the upper plots in Figure 3.9, we see that the temperatures and densities of the CGM in our GM galaxies are not significantly changed by the lack of a SMBH. However, as we examine the bottom panels, we note a distinct difference. The CGM of the galaxies without BH physics have significantly less oxygen mass and are lower in metallicity. It appears that rather than energetically changing the temperature or physical modifying the gas density in the CGM, the lack of BH physics in these galaxies results in CGM with significant lack of metals. We look to the disk

of the galaxy for more clues about this difference. Figure 3.10 (colors and line styles as in Figure 3.8) shows that, in the galaxies without BH physics (dashed lines), there is a large reservoir of metals being created near the center of the disk that is not being propogated outwards. It is the lack of SMBH feedback in these galaxies that is resulting in CGM that are severely lacking in metals.

Figure 3.11 shows the phase diagrams of the CGM of the 4 zoom-in galaxies both with (*Left Column*) and without BH physics (*Right Column*). Examining the CGM phase diagrams for the GMs that include BH physics, we note the following key differences. First, there is decreasing overall mass from the uppermost (P0) to lowermost (GM3) figure. We can attribute this difference to the slight decrease in total halo mass from P0 to GM3 (Table 3.2) and to the fact that both GM2 and GM3 are quenched galaxies.

Second, the amount of cool, dense gas (T $<10^{4.5}$, n_H $>10^{-3}$) in each galaxies' CGM varies. We attribute this to various characteristics of each simulation. In particular, for P0 and GM1 with BH physics much of this gas comes from some disk gas present at our definition of the CGM boundary, $R = 10$ kpc. For GM2 with BH physics, this gas comes primarily from incoming satellite galaxies. We attribute the same reasoning to the 4 galaxies without BH physics which also have a similar structure in their CGM phase diagrams (as we explore below).

Finally, there is a significant lack of hot, dense gas (T $>10^{5.5}$, n_H $>10^{-3}$) in the phase diagrams of GM2 and GM3, our quenched galaxies. To study this final difference, we explore the CGM phase diagrams that *exclude* BH physics (*Right Column* of Figure 3.11). We note that the overall shapes of these phase diagrams are somewhat similar to the star forming galaxies *with* BH physics. All four of these galaxies remain star forming throughout their evolution (Figure 3.3b). The similarities end there, however, as the merger histories of these galaxies are characterized by a late-z merger which occurs at slightly varying times for the 4 galaxies without BH physics. This late-z merger is separate from the modified satellite which is still present at $z = 0$ in each galaxy's halo.

P0 has its last significant merger (q $\sim$ 10, where q = M_{halo}/M_{sat}) at $z \sim 0.7$. GM1

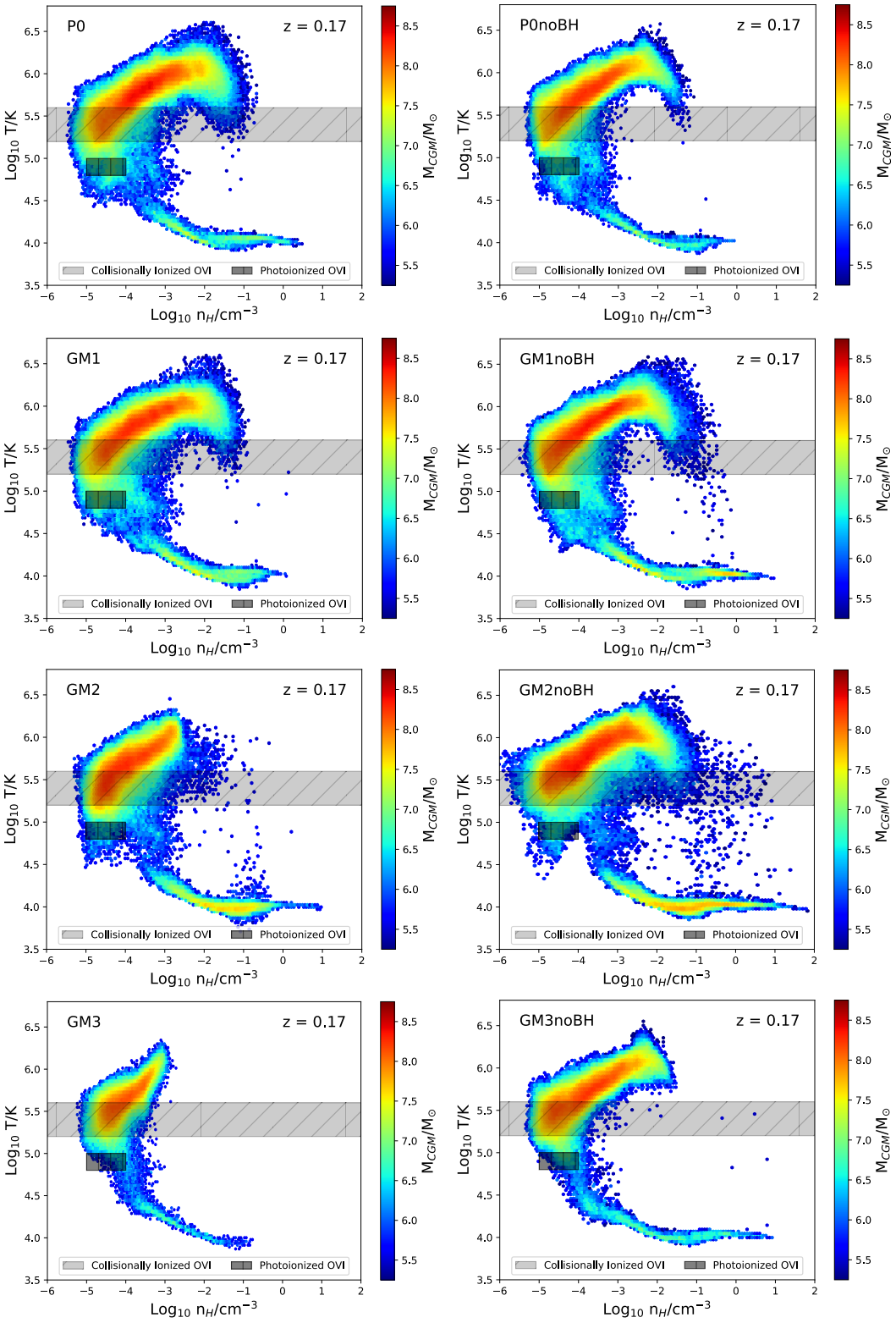

Figure 3.11: Phase diagrams of the temperature and density of the two star forming zoom-in galaxies, P0 (*Top row*) and GM1 (*Second row*), and the two quenched galaxies, GM2 (*Third row*) and GM3 (*Bottom row*). The phase diagrams of galaxies with BH hole physics vary quite widely between the star forming (P0 and GM1) and quenched cases (GM2 and GM3), particularly in the highest temperature and density gas. However, the phase diagrams of the galaxies without BH physics appear more similar, as are their star formation histories. Semi-transparent light and dark gray boxes span the region of collisionally and photo-ionized O VI as temperature and density regions where fractions of O VI are larger than 0.05 %.

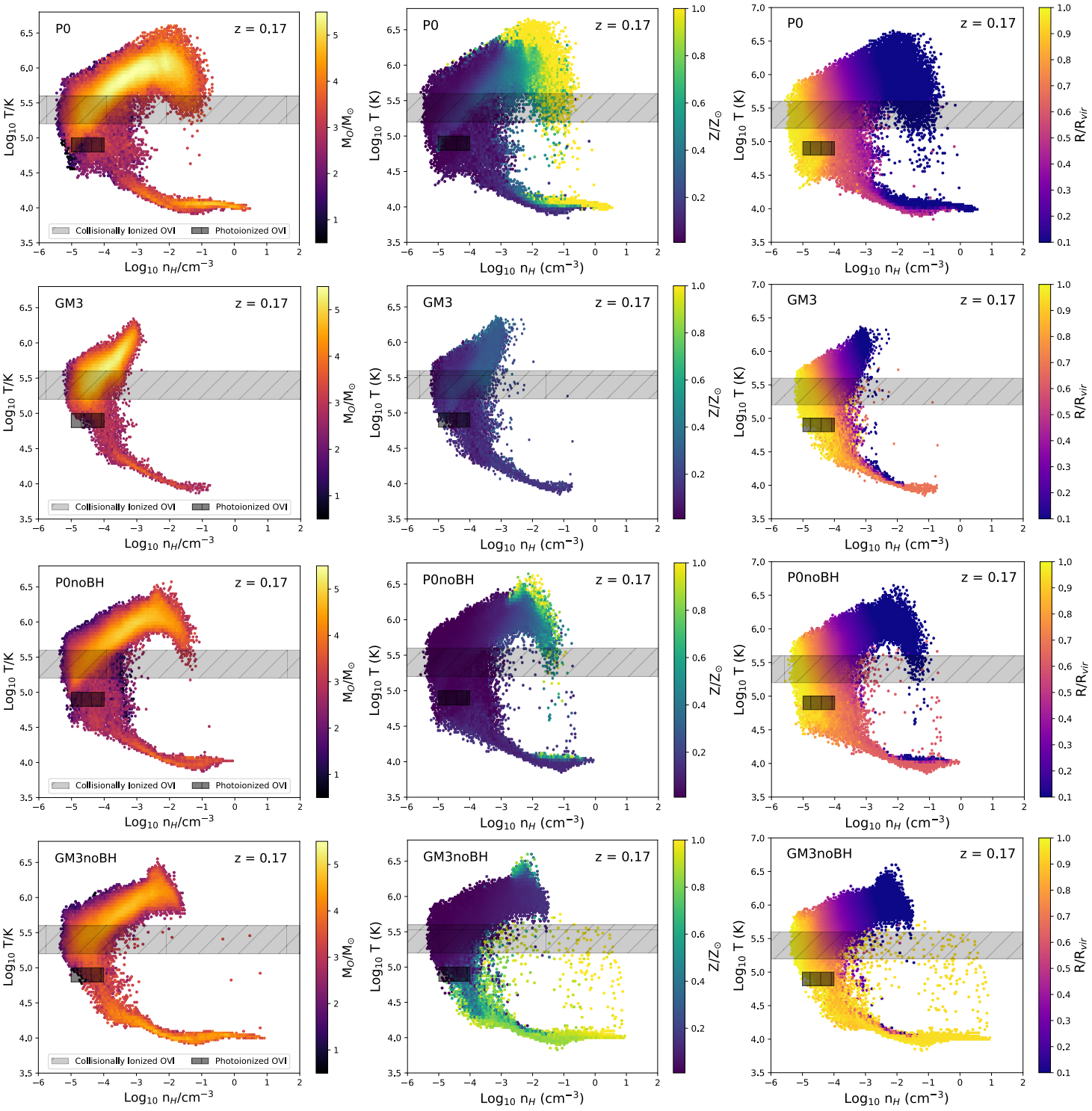

Figure 3.12: Phase diagrams of the temperature and density of the star forming, P0, and quenched, GM2, with BH physics (*Top two rows* and the same two galaxies without (*Lower two rows*). *Left:* The phase diagrams of these galaxies weighted by the total oxygen mass in each bin. *Middle:* The same phase diagram showing temperature and density, however, the colorbar is weighted by the average metallicity of the gas in each bin. We note that the high density, high temperature gas we see in the star forming P0, is also the highest metallicity gas in the CGM. *Right:* Similarly, a phase diagram with the colorbar now weighted by the average distance from the center of the galaxy of the gas particles in each bin.

has a similar minor satellite merger at $z \sim 0.5$ which increases the amount of metal in the CGM (up to ~ 2 % compared to P0), but by $z = 0.17$, the satellite galaxy has merged fully with the galaxy of the main halo. Only 0.1 % of the highest metallicity gas remains outside of 20 kpc from the galaxy, or about 10^6 $M_\odot$. In GM2, the minor satellite galaxy merger occurs at $z \sim 0.17$ causing a large swell in the amount of metal enrichment seen in the CGM. This high metallicity gas ($M_{Z>0.8Z_\odot,R>20kpc} = 2.3 \times 10^9$ $M_\odot$) accounts for 3 % of the total CGM gas mass, the majority of which is outside of 20 kpc from the main halo's disk (still concentrated in the region of the satellite galaxy). This satellite in GM3 doesn't fully merge with the main halo until almost $z \sim 0$. We note that similar, late-z mergers are present in the zoom-in galaxies with BH physics. However, their effect is less significant due to the metal enrichment caused by the SMBH.

There is a lack of the hot, dense gas in the quenched galaxies. However, we do see the hot, dense gas feature in the CGM phase diagrams of the galaxies *without* BH physics, which all result in star forming, disked galaxies. Figure 3.12 examines this difference with the same CGM phase diagrams of P0 and GM3 weighted by oxygen mass, metallicity, and distance from the center of the galaxy, with (*Two Upper Rows*) and without (*Two Lower Rows*) BH physics. The hot, dense gas in P0 with BH physics (*Upper Row*) appears to be mostly comprised of high metallicity gas that is close to the disk (R <50 kpc). Quantifying properties of this gas, we find that 3 % of the CGM gas has metallicity $Z > 0.8$ $Z_\odot$ at $z = 0.17$. Furthermore, of this 3 %, nearly 30 % is farther than 20 kpc from the center of the galaxies. For GM1, the CGM is comprised of 6.7 % gas with $Z > 0.8$ $Z_\odot$ with 55 % of that gas farther than 20 kpc. Contrastingly, a negligible amount of the CGM of both GM2 and GM3 have $Z > 0.8$ $Z_\odot$ at $z = 0.17$. The CGM of the four galaxies without BH physics also have small amounts of gas with $Z > Z_\odot$, from 0.2 % in P0noBH to 0.1 % in GM3noBH, when discounting the contribution from the satellite merger at $z \sim 0.2$. These percentages of high metallicity gases in P0 and GM1 with BH physics point to metal exchange in the galaxy that is strongly dependent on the SMBH. This result is consistent with our discussion of Figure 3.10 and with Nelson et al. 2018[214] who also find that metal mass ejection due to the BHs

in their simulations is key to their results (See Section 3.4 for more details).

The lack of high metallicity gas in the CGM phase diagrams of the galaxies with no BH physics (Figure 3.12, *Right Column*) implies that metals are not being driven out of the disk. We find that feedback does not play a significant role in directly heating or excavating the CGM gas. Instead the SMBH's feedback is pivotal in *transporting the metals* from the center of the galaxy out into the CGM.

3.4 Discussion

Our results are broadly consistent with those of Oppenheimer et al. 2016[222] who use a suite of EAGLE simulated galaxies to examine the bimodality of O VI column densities in star forming and quenched galaxies discovered by Tumlinson et al. 2011[331]. They argue that the star forming galaxies with M_{halo} = 10^{11} - 10^{12} $M_{\odot}$ are most likely to exhibit high fractions of O VI because they have a virial temperature, T $\sim$ $10^{5.5}$, which corresponds to the maximum O VI ionization fraction in collisional ionization equilibrium. Meanwhile, their quenched galaxies (M_{halo} = 10^{12} - 10^{13} $M_{\odot}$) have high enough virial temperatures such that the dominant ionization state of oxygen is not O VI but rather O VII or above. Oppenheimer et al. 2016[222] argues that the O VI content is not a tracer of star formation directly, but rather a more direct thermometer for the temperature of the halo.

We note that the quenched galaxies in our sample have slightly smaller M_{halo} than our star forming galaxies, unlike those in Oppenheimer. This difference explains the lack of bimodality in our sample. While all 4 of our zoom-in galaxies with BH physics have virial temperatures which maximize O VI, we looked at a sample of R25 galaxies that spanned a mass range extending to M_{halo} = 2 $\times$ 10^{13} $M_{\odot}$ to test the [Oppenheimer et al. 2016[222] bimodality argument.

Figure 3.7 directly shows that the column densities of O VI in the R25 sample indeed act as thermometer for the temperature of the halo. Furthermore, in Figure 3.6 we show that as the virial temperature increases in the R25 sample, oxygen is likely to be ionized to a higher ionization state than O VI. Examining galaxies within low, MW-, and high mass bins from

the R25 suite, we see that the column densities of O VI decrease as the temperature which maximizes O VI ($T = 10^{5.5}$) is surpassed by the virial temperatures of these halos.

This lack of bimodality contrasts with the findings of Suresh et al. 2017[309] and Nelson et al. 2018[214]. Suresh et al. 2017[309] examined a sample of star forming and quenched galaxies from the moving mesh-based Illustris simulation[344]. The column densities of O VI in these galaxies reproduce the bimodality seen in Tumlinson et al. 2011[331], wherein star forming galaxies have higher column density of O VI than quenched galaxies of the same mass. However, they find the total column densities of O VI are lower than expected based on the COS-Halos observations. Suresh et al. 2017[309] argue that the bimodality arises due to the effect of AGN feedback in their model rather than O VI acting as a temperature gauge for the halo virial temperature. To arrive at this result, Suresh et al. 2017[309] ran smaller simulation volumes which did not use their AGN prescription. In these smaller volumes, the bimodality disappeared.

In comparison, Nelson et al. 2018[214] uses IllustrisTNG[183;209] to examine the O VI bimodality. This updated version of Illustris uses a new "multi mode" BH feedback model which allows for a thermal "quasar" mode at high accretion rates and a kinetic "wind" mode at low accretion rates. With this new AGN accretion model, the column densities of O VI in their galaxies match the COS-Halos observations and show the same bimodality as Tumlinson et al. 2011[331] and Suresh et al. 2017[309]. Specifically, Nelson et al. 2018[214] finds that there is likely more O VI in the CGM of galaxies if their galaxy has any of the following characteristics: higher gas fraction, higher sSFR, higher gas metallicity, bluer color, or a less massive BH. In addition, they conclude that the energy injected by their AGN in the kinetic feedback mode (low accretion rate) can significantly affect the O VI content of the CGM. They also conclude that BH feedback in this mode directly affects the O VI and results in higher O VI columns in star forming galaxies. They attribute this affect to the ejection of metal mass from the central galaxy and (to a lesser extent) the heating of CGM gas by energy infusion from the SMBH.

Despite differences in their methods, both studies attribute the existence of a bimodality

in the O VI column densities to the SMBH feedback in their simulations. We see no such effect. Our 4 zoom-in GM galaxies all have very similar characteristics (Table 3.2 and Figure 3.4) and we do not see significant differences between their column densities of O VI. Our results are consistent with those of Nelson et al. 2018[214] in that the SMBH is responsible for enriching the CGM by physically driving metals out of the disk.

In our study, we establish that the SMBHs at the center of our galaxies are crucial for ejecting metal-enriched material out into the CGM, thereby elevating the column densities of O VI. This result implies that galaxies with lower mass BHs—and therefore less BH feedback—are likely to have lower metallicity gas in their CGM. In contrast, galaxies with higher mass BHs will have more metal-enriched CGM material. We may infer that varying BH properties result in the large distribution of CGM metallicities measured by observers[175;241;370]. The lower right panel of Figure 3.9 shows that within our 4 zoom-in galaxies, we span a range of metallicities from -1.25 to solar, nearly the full range seen in observational studies.

We predict that the early growth of the BH's mass (or more specifically, its accretion history) correlates directly with CGM metallicity. The lower panel of Figure 3.4 shows the accretion history of the SMBHs in our 4 zoom-ins. While the accretion histories are similar up to z $\sim$ 1, they have significant differences at later times. This result is consistent with the idea that the CGM metal budget is built up at early times through BH feedback, while later BH feedback does not significantly change the amount of O VI in the CGM of their host galaxies. Using *HST*/COS observations, Berg et al. 2018[27] (COS-AGN) examines the kinematics of cool gas in the CGM of both AGN and non-AGN host galaxies. They find no signature of recent AGN activity in the inner ($\lesssim$ 160 kpc) CGM of their sample, but do find kinematic differences at high impact parameters. They interpret this difference as an indicator that the CGM is built up by activity in the host galaxy at early times.

While many studies, both theoretical and observational, have sought to connect galaxy star formation rates, ISM content, and environments to CGM properties, there has been no observational study to explore a direct link between SMBH properties and the CGM. Future observations of the CGM in galaxies with well-known SMBH masses could attempt

to address this missing link.

3.5 Summary and Conclusion

We have examined the effects of SMBH feedback and star formation history on the column densities of O VI in the CGM of galaxies with stellar masses between 3×10^9 —3×10^{11} $M_\odot$. To do so, we have used the cosmological volume ROMULUS25 and a zoom-in galaxy with 3 genetic modifications run with and without BH physics.

In our simulations, we determine that the SMBH transports metals into the CGM. Previous studies have examined the effect of AGN heating on the CGM as a way to raise ambient gas to a temperature that optimizes the production of O VI[186;193;309]. Others have proposed that SMBH feedback may physically push outflows of gas from the galaxy, resulting in a higher mass CGM and therefore higher column densities of O VI. Neither of these cases is what we see in our simulations. *Instead, our SMBH feedback propagates metal mass (but not total gas mass) into the outer halo. Furthermore, we find that O VI column densities depend on the virial temperature of the galaxy halo.* Relatedly, we determine that the presence of a SMBH alone cannot quench a galaxy. Rather a SMBH and additional factors, such as the presence of a satellite galaxy and/or previous mergers, are necessary for a galaxy to quench.

The combined results of our large R25 cosmological simulation and our zoom-in galaxies with BH physics imply a mechanism by which column densities of O VI are set primarily by the virial temperature of the host galaxies and accretion history of the SMBH. However, we do not include a photo-ionization prescription in our simulations, which may have a small effect on the O VI content close to the disk of the galaxy. Furthermore, we find that O VI column densities in the CGM of our galaxies are not significantly affected by the evolution of the stellar disk. Their phase diagrams also show significant differences in response to their overall assembly histories, showing more overall and higher metallicity gas in the star forming cases. Despite these gas phase differences, the column densities of O VI remain unchanged. We conclude that the physical conditions that give rise to widespread O VI absorption in the CGM are not set by whether a galaxy quenches, but instead are driven by early SMBH

feedback and the virial temperature of the galaxy halo.

Chapter 4

THE SCATTER MATTERS: SMBH DEVIATION FROM M-σ INFORMS THE METAL CONTENT OF THE CGM

Portions of this chapter are intended to be published in The Astrophysical Journal in collaboration with Michael Tremmel, Jessica K. Werk, Charlotte Christensen, Grace Telford, Michael Tremmel, Thomas Quinn, Jennifer Mead, Ray Sharma, and Alyson Brooks.

Summary

By comparing a supermassive black hole's (SMBH) mass to the properties of its stellar population, we explore the BH feedback's impact on metal retention and flow into and through the circumgalactic medium (CGM) of simulated galaxies of Milky Way-mass and below. We examined 140 galaxies from the 25 Mpc cosmological volume, ROMULUS25, between the masses of 3×10^9 – 3×10^{11} $M_\odot$. We measured the metals retained in each component of the galaxy (disk and CGM) by comparing the amount of metals in each region to the metals expected to form through stellar evolution. By calculating the theoretically expected mass of each SMBH based on the M-σ relationship, we determined the deviation from M-σ for each SMBH (i.e. how over- or under-massive a SMBH is compared to their host stellar dispersion). We find that SMBHs which are *over-massive* compared to their host galaxy (BH masses above the M-σ relation) are 20-40% more effective at removing metals from their disks than under-massive SMBHs. This effect is even stronger in galaxies that are quenched by z = 0. Non-star-forming galaxies at z = 0 can retain up to 20% *less* of the metals that they originally form compared to galaxies of similar mass that remain star forming. Additionally, *over-massive* BHs begin accreting material earlier than their *under-massive* counterparts. Our results indicate that SMBHs which are *over-massive* are more effective at both regulating star formation in the center of their galaxies and moving metals out from the disk into the CGM and IGM.

4.1 Introduction

The vastly different scales between the event horizon of a supermassive black hole (SMBH) and its host galaxy have been creatively described as the difference between a grain of sand and the entirety of the Saharan Desert A difference of approximately 10 orders of magnitude[271]. While the size difference between the objects makes their interaction surprising, more and more evidence continues to connect the evolution and properties of galaxy hosts to their SMBHs[94;106;120;182;249;263]. Of the relations drawn between the SMBH and its host galaxy, the M-σ remains the most fundamental.[167] and citations therein

The M-σ relation describes the relationship between a SMBH's mass and the velocity dispersion of its host galaxy's bulge. A tight correlation across three orders of magnitude, this observed relation is theorized to tie together the growth of a SMBH–during its tenure as an active galactic nuclei (AGN)–and the energy-driven winds which its accretion disk drives resulting in the removal of the gas necessary for continued star formation. In this way, the energetics of the SMBH work to regulate the star formation in the bulge of the galaxy, until such time that it is no longer accreting (and thus driving powerful outflows) which then allow gas accretion and star formation to resume.

Despite showing the strong correlation of this relation, the scatter in the M-σ relation has driven observers and theorists alike to find explanations for the deviation of galaxies and SMBHS from this theoretical predication. At the high mass end, we see scatter with more over-massive BHs residing in the massive ellipticals above $\sim 10^{13}$ $M_{\odot}$.[80;85;201;212;337] While scatter on the lower end of the relation has driven an examination into the variable pathways that drive BH growth[112;197;248;349].

While a concerted effort has gone into explaining the physical processes that result in the scatter on the M-σ[112;197;248;279;349], the impact on a galaxy whose SMBH deviates from the M-sigma relation has not been well constrained, especially within the circumgalactic medium.

Since the installation of the Cosmic Origin Spectrograph (COS) on HST in the early

2010s, the impact of the SMBH's feedback on the phase and metallicity of CGM gas has been a critical outstanding question in galactic evolution. Simulations were initially hard-pressed to match the observational surveys taken with COS such as COS-Halos[332;357]. Measurements of high ions like OVI were too low, and low ions were difficult to replicate in the simulated environment[222;309].

Many cosmological simulations have also worked to update the gas physics in their codes to better characterize the low density, multiphase medium of the CGM; furthermore, recent work has focused on connecting the impact of energetic feedback of a galaxy's SMBH to the diffuse CGM. Broadly, simulations have shown that the SMBH can impact the CGM in a multitude of ways: heating and evacuating gas to quench star formation in the disk IllustrisTNG and EAGLE simulations[215;222;309], driving metal rich gas out of galaxy centers and enriching the CGM with metals IllustrisTNG and ROMULUS25[216;266], as well as evacuating CGM gas out into the IGM EAGLE[221]. Another study of the EAGLE simulations finds that more gas is flowing out of the halo virial radius than from the ISM of central galaxies[198], while[223] finds that CGM mass fraction declines after explosive episodes of AGN-driven feedback in galaxies from both EAGLE and IllustrisTNG.

Interestingly,[68] ties the expulsion of gas by SMBH-driven outflows to the scatter in the halo gas fraction, f_{CGM}, at fixed M_{200}. They find that galaxies with more massive BHs (within a fixed halo mass bin) reside within more gas-poor halos and that galaxies with under-massive BHs retain a higher gas fraction as well as show elevated star formation rates. In a follow up study,[69] show that the evacuation of CGM gas by SMBH feedback is a critical step in the morphological evolution and quenching of their galaxies. Furthermore, they determine that the BH mass is tied to the dark matter halo binding energy, wherein galaxies with more tightly (loosely) bound halos host BH which are more (less) massive and thereby eject more (less) material from the CGM. These results point to an intrinsic connection between black hole masses and the evolution of the CGM. We follow this line of investigation to further our understanding of how the deviation of a SMBH's mass from theoretical expectations impacts its host halo gas.

In our paper, we examine how deviation in SMBH mass from M-σ changes the overall effectiveness of a SMBH in terms of gas and metal flow into the CGM. We explore this change across two orders of magnitude in mass, including Milky Way-mass galaxies and down to 3 $\times$ 10^9 $M_\odot$ in stellar mass. Our study also includes comparisons between our simulations and observational constrains such as metal retention fractions and expected column densities of high and low ions in the CGM.

This paper is organized as follows: Section 2 introduces our simulations and the galaxy selection process, and Section 3, we describe our results. In Section 4, we compare our findings to obsrvational data and discuss a broader context and their implications. Finally, in Section 5, we summarize our conclusions.

4.2 Simulation Parameters

All of the galaxies examined in this paper were selected from the ROMULUS25 (R25) simulation, a 25 Mpc cosmological volume, run with the smoothed particle hydrodynamics N-body tree code, Charm N-body Gravity solver ChaNGa[196]. ChaNGa adopts its models for cosmic UV background, star formation based on a Kroupa IMF, and 'blastwave' supernova feedback from the well-tested GASOLINE code[281;303;350;352].

ChaNGa includes updated SPH formalism which updates the force expression to include a geometric density approach[351]. This new hydrodynamics treatment includes thermal diffusion[281] and reduces artificial surface tension to result in improve resolution of fluid instabilities[196;254].

R25 does not include a full treatment of metal cooling due to a resolution limit too large to consider individual star forming regions[56]. Nevertheless, we include a low temperature extension to the cooling curve which allows only gas below 10^4 K to cool proportionally to the metals in the gas. Gas above 10^4 K cools only by H/He, Bremsstrahlung, and inverse Compton effects. (See Tremmel et al. 2017 for full details.) Sanchez et al. 2019 describes how a lack of full metal cooling treatment may over-predict the amount of individual ions measurements; however, as we only consider the relative total metals between galaxies in our

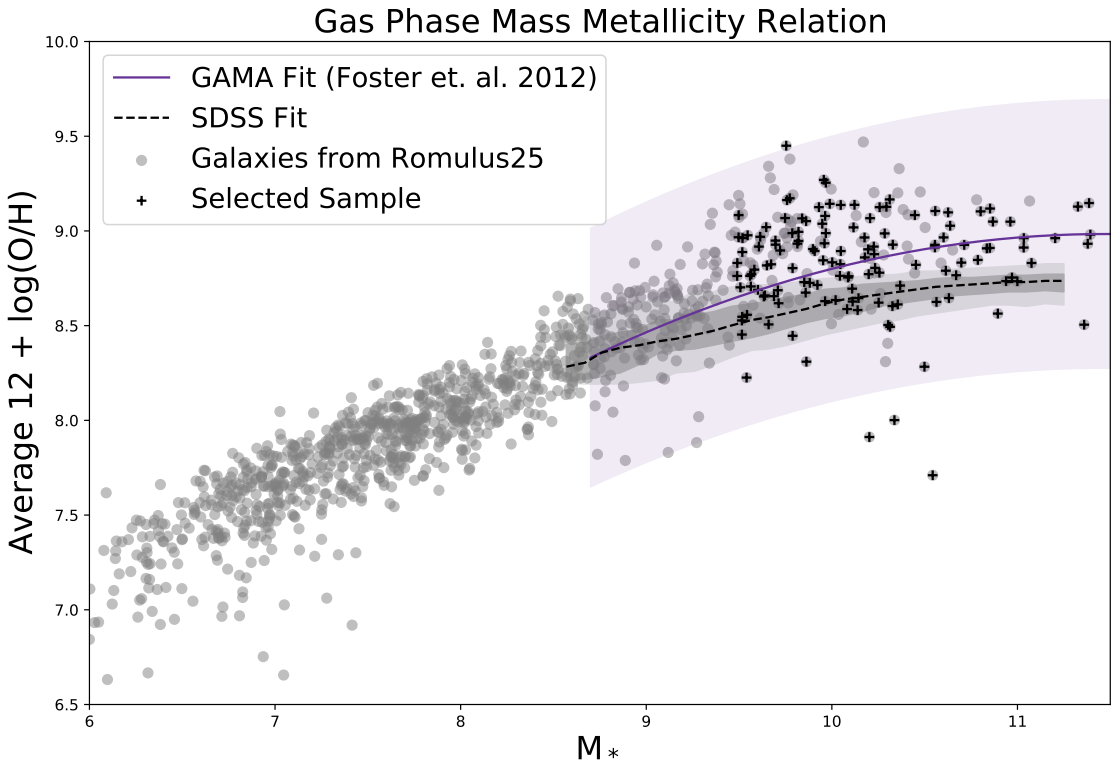

Figure 4.1: The relation between the stellar mass and gas phase metallicity for our sample (black crosses) and a wider selection of ROMULUS25 galaxies (grey circles). The black dashed line indicates the SDSS fit relation[159;232;326] and the purple solid line indicates the same relation from the Galaxy and Mass Assembly (GAMA) survey[101]. Our sample of galaxies ($3 \times 10^9 < M_* < 3 \times 10^{11}$) fit well within the errors of the expected gas-phase metallicity of the galaxies from the GAMA survey, but over-predict the amounts expected from SDSS.

suite of galaxies, our results remain valid.

R25 includes updated black hole formation, accretion, and feedback prescriptions. BH formation ties seeds to dense and extremely low metallicity gas to more effectively estimate SMBH populations in a variety of galaxy mass regimes. The SMBH accretion model is based on Bondi-Hoyle, but includes a consideration for angular momentum support from nearby gas. This update allows for more physically motivated growth than Bondi-Hoyle alone[8;257]. An updated dynamical friction prescription has been included to better track SMBH growth and dynamical evolution. Thermal SMBH feedback imparts energy on the nearest 32 gas particles according to a kernel smoothing and is based on accreted mass, $\dot{M}$, via:

$$E = \epsilon_r \epsilon_f \dot{M} c^2 dt, \tag{4.1}$$

where $e_f = 0.1$ and $e_r = 0.02$ are the feedback and radiative efficiency, respectively. Accretion is assumed to be constant for one black hole timestep, dt, and cooling is shut off immediately after feedback events. This SMBH feedback prescriptions has been shown to successfully produce large scale outflows[236;325]. Finally, an updated dynamical friction prescription has been included to better track SMBH growth and dynamical evolution[321]. For additional details about BH prescriptions, see[323].

R25 was run with a Λ CDM cosmology with $\Omega_m = 0.3086$, $\Omega_\Lambda = 0.6914$, h = 0.67, $\sigma_8 = 0.77$[3]. R25 has a Plummer equivalent force softening length of 250 pc and has a UV background applied at z $\sim$ 9 through the evolution to $z = 0$[119].

R25 consistently matches the stellar mass-halo mass[200], and SMBH-stellar mass relation using stellar mass and halo mass corrections from[204]. It has also been shown to match the M-σ relation[252]. Figure 4.1 shows the stellar mass and gas phase metallicity relation for galaxies selected from R25. Grey circles show galaxies across five orders of magnitude and black crosses indicate the sample of galaxies we will analyze throughout this paper (See Section 4.2.1 below).

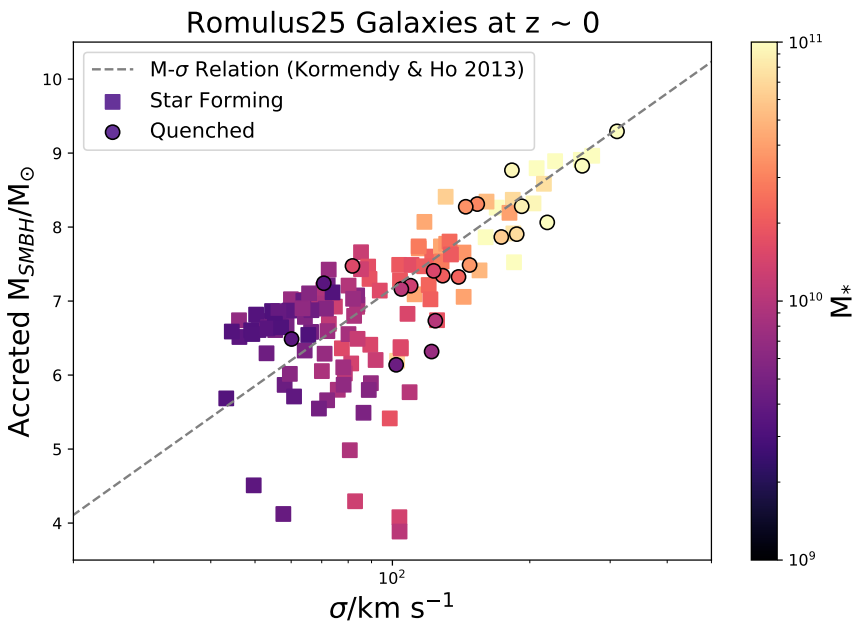

Figure 4.2: The M-σ relation for the 140 galaxies within ROMULUS25 that are within the COS-Halos stellar mass range and that contain a SMBH. Star forming galaxies are denoted by squares and quenched galaxies (sSFR ¡ 1.6 $\times$ 10^{-11} $M_\odot$ yr^{-1}) are shown as circles. Points are colored by the stellar mass of the galaxy. The spread of the galaxies fall along the empirical M-σ relation[167], grey dashed line, though we note that our sample tend to lie slightly above the line[252].

4.2.1 Galaxy Sample Selection: ROMULUS25 *Galaxies from the COS-Halos Mass Range*

For comparison with observations, we selected our sample of galaxies using a roughly L^* stellar mass range well inspected by observations (COS-Halos, CGM^2) of 3 $\times$ 10^9 $M_\odot$ >M_* >3 $\times$ 10^{11} $M_\odot$. Within ROMULUS25, there are 282 galaxies within this stellar mass range at z $\sim$ 0. We further refined our selection to remove galaxies that we considered satellites. We defined satellites as galaxies within 300 kpc of another more massive galaxy. Using this definition, our final sample consisted of 140 galaxies. There are 119 star forming (specific star formation rates, sSFR ¿ 1.6 $\times$ 10^{-11}) galaxies in our sample and 21 are quenched (sSFR ¡ 1.6 $\times$ 10^{-11}) at $z \sim 0$.

Figure 4.2 shows the M-σ relation for our 140 galaxies. Our sample fall along the line produced using the M-σ equation of[167]:

$$\frac{M_\bullet}{10^9 M_\odot} = \left(0.309^{+0.037}_{-0.033}\right)\left(\frac{\sigma}{200\ km\ s^{-1}}\right)^{4.38\pm0.29} \tag{4.2}$$

where $M_\bullet$ represents the mass of the SMBH and σ indicates the stellar dispersion of the

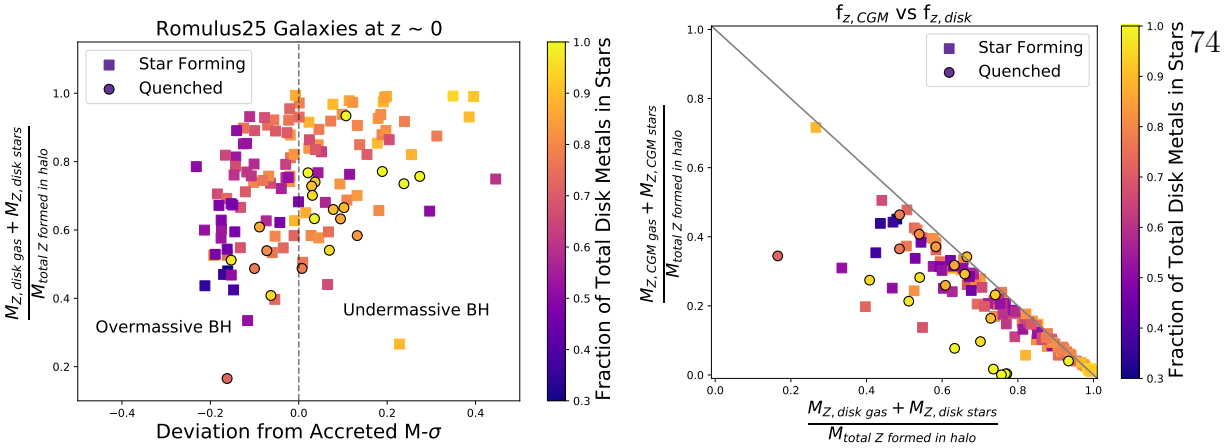

Figure 4.3: *Left:* The metal retention, f_z, of each of the 140 galaxies within ROMULUS25 as a function of their deviation from the M-σ relation. Points are colored by the fraction of total disk metals contained in stars. SMBHs which are over-massive compared to their host galaxies (left of the grey, dashed line) stellar population (BH masses above the M-σ relation) are 20-40% more effective at removing metals from the disk. This effect is even stronger in quenched galaxies. Non-star-forming galaxies at $z = 0$ can retain up to 20% less of the metals that they originally form compared to galaxies of similar mass that remain star forming. *Right:* The metal retention in the CGM, $f_{Z,CGM}$, as a function of the metals retained in the disk, $f_{Z,disk}$. The grey solid line indicated the one-to-one line where halos that fall along the line still retain all the metals formed in their galaxies, while galaxies below the line have lost metals to the IGM. From this figure, we see that in most cases, the metals that are ejected from the disk remain in the CGM with few galaxies having lost metals to the IGM. We find that the SMBH in our simulations don't evacuate the gas and metals from their CGM, instead enriching them.

galaxy's bulge.

4.3 Results

4.3.1 Metal Retention

We find the metal retention fraction, the metals retained by the central $0.1R_{vir}$ of each galaxy, correlates with the deviation of each galaxy's central SMBH from the M-σ relation (Figure 4.3).

Metal retention fractions are calculated using the formula:

$$f_Z = \frac{M_{Z,g,present} + M_{Z,*,present}}{M_{Z,formed}} \tag{4.3}$$

where $M_{Z,g,present}$ and $M_{Z,*,present}$ are the amount of mass contained in metals or stars, respectively, within the central $0.1R_{vir}$ at $z = 0$. $M_{Z,formed}$ indicates the amount of metals

formed throughout the simulation from stars residing anywhere in the halo by $z = 0$.

The deviation from M-σ is calculated based on the distance between each galaxy's location on the M-σ relation (Figure 4.2) and the theoretical line of[167], indicated by the dashed grey line at 0.0.

Galaxies with over-massive SMBHs retain significantly less metals within their disks, star forming galaxies losing up to $\sim 60\%$ of their metals from the disk, and quenched galaxies as much at $\sim 80\%$. Galaxies with under-massive black holes retain most, if not all of their metals within the disk, with most of those metals locked in stars (yellow points). Meanwhile, galaxies with under-massive SMBHs have a majority of their metals locked in the gas phase (purple points).

We can determine where the metals lost by each galaxy end up in the right hand panel of Figure 4.3. It compares the metal retention in the CGM to the metal retention in the disk. We find that the majority of our star forming galaxies keep nearly all of their metals within the disk and CGM with only up to $\sim 10\%$ of their metals being lost to the IGM. Only 7% (8/119) of these SF galaxies lose more that 10% of their metals to the IGM. Meanwhile, all but one quenched galaxy have lost some metals to the IGM, nearly half of which have lost more than 20%. Furthermore, by comparing the color of the points, we can see that in the star forming galaxies which keep most of their metals, those metals are stored in stars within the disk (yellow points). The galaxies that lose more of their metals to the CGM (purple points) have more of the metals in their disk contained within the gas phase.

The left panel of figure 4.4 similarly shows the metal retention of the CGM as a function of the metal retention in the disk, now colored by each galaxy's deviation from M-σ. Red symbols indicate galaxies with over-massive black holes and blue galaxies contain under-massive black holes. We find that the galaxies that retain the most metals in their disks (Left figure, bottom right) have under-massive black holes. Additionally, these are the same galaxies in the right panel of Figure 4.3 that maintain all their metals within stars. In contrast, the galaxies with over-massive BHs are those which lose the most metals to the CGM and IGM from the disk.

The right panel of 4.4 shows the fraction of baryons in the CGM as a function of the baryonic fraction in the disk. Comparing the left and right panels in this figure, we see that the metals in the galaxy do not follow the baryonic component. I.e. the different trends we see between these plots tells us that the motion of the metals is not strictly following the motion of the gas and stars. Instead, we see a distinct trend for the metal retention that points to interactions from the SMBH. We discuss the implications of this result below in Section 4.4.

We calculated the metallicity gradient of each of our galaxies, splitting the sample into two bins which included all the galaxies with over-massive black holes (deviation from M-σ <0) and those with under-massive SMBHs (deviation from M-σ >0). Figure 4.5 shows the averaged metallicity gradient for all the galaxies with over-massive BHs (red) and those with under-massive BHs (blue). We see that, on average, galaxies with under-massive BHs are more likely to have a concentration of metals built up in their centers. By comparison, galaxies with over-massive BHs have fewer metals in their centers and have an overall flatter metallicity gradient on average.

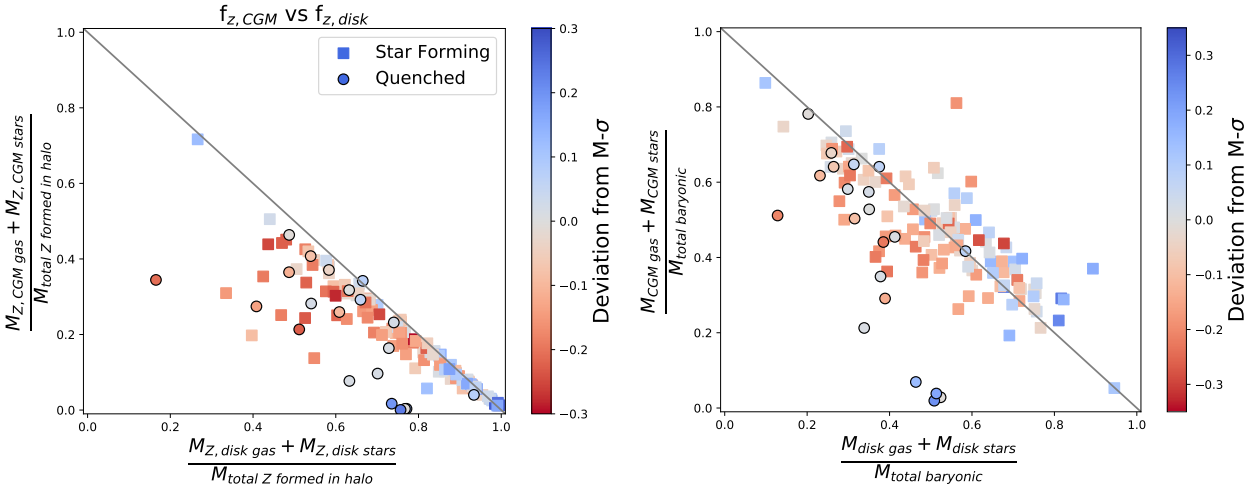

Figure 4.4: *Left* The metal retention of gas and stars in the *CGM* of each of the 155 galaxies within ROMULUS25 as a function of the metal retention of gas and stars in the *disk*. *Right* Fraction of total baryonic mass in the CGM as a function of the fraction of total baryonic mass in the disk. Points are colored by the deviation in M-σ.

4.3.2 Column Densities

To make some predictions about expected column densities, we first selected only the star forming galaxies from our sample due to the small number statistics of our quenched galaxies. Then we subdivided the SF galaxies into the two sets: galaxies with under-massive black holes and galaxies with over-massive black holes. Finally, we selected a matching pairs from each set with similar stellar masses and SFHs. This selection resulted in a subsample of 64 galaxies, 32 each with over- or under-massive SMBH, from which we could specifically isolate differences due to the SMBH mass excess.

For each of these 64 galaxies we calculated the C IV column densities as a function of radius and calculated the median value (Figure 4.6). We find that there is more abundant C IV in the CGM of galaxies with over-massive SMBHs than those with under-massive SMBHs. This difference is as large a dex at a few tens of percent of the virial radius, with an average difference of 0.5 dex between 0.1 to 0.8 R_{vir}.

Future HST/COS surveys will be able to determine whether these predictions hold for observations. COS-Halos[355], one such future survey, will connect the UV absorption measurements made with COS to dynamically-resolved SMBH measurements for galaxies in the line-of-sight of the background quasar. We discuss the implications of this result and compare our predictions to those from other simulations in Section 4.4.

4.4 Discussion

4.4.1 BHs Primarily Drive Metals into the CGM not the IGM

Our results paint a consistent picture of galaxy evolution wherein galaxies that accrete more gas grow central SMBHs that are over-massive compared to their stellar dispersion (an approximation for their potential) and these over-massive BHs are more effective at ejecting metals from the center of their host galaxies (Figure 4.5).[279] determined that galaxies with over-massive black holes formed earlier and comparable to lower stellar densities. We see similar indications of star formation suppression in our galaxies hosting over-massive black

holes. These results are also consistent with[69] who found that in a sample of galaxies from EAGLE and IllustrisTNG those with over-massive black holes formed within dark matter halos with tightly bound centers and were characterized by systematically lower star formation rates.

Despite these similarities, we find a distinct result in our sample of galaxies compared to[69]. They find that the galaxies in their sample with over-massive BHs negatively correlate with the fraction of total gas in their CGM. I.e. galaxies with BHs that are over massive evacuate more of their CGM. In contrast, the galaxies that host over-massive black holes in our sample do host a smaller total baryon fraction than the hosts of under-massive BHs, *but* the over-massive BH hosts host a higher fractions those baryons in the CGM. In other words, the over-massive BHs in our galaxies are effective at evacuating both gas and especially metals from their disk, but they are not adept at evacuating material out of the CGM and into the intergalactic medium.

This distinction is likely due to the difference in the implementation of BH feedback. We expand on these details below.

To confirm the BHs role in driving metal out of the center of the galaxy, we refer to the work of[266], which explored the metal content of the CGM in a set of 4 galaxies run with the same code and similar conditions to ROMULUS25. In that paper, they compare 4 galaxy simulations with and without black hole physics and find that the galaxies without BH physics end up with a concentration of metals in their centers as we see here in the galaxies with under-massive BHs. Figure 4.5 above is very similar to their Figure 10. The consistencies between these simulations leads us to determine that the SMBH, which was responsible for ejecting metals from the galaxies in[266], is also key in ejecting metals from the galaxies with over-massive BHs in our sample.

This result also helps explain what we see in the galaxies with under-massive BHs. These galaxies, which accrete less gas, have SMBHs which grow less. These under-massive BHs are less effective at regulating star formation which results in two of the characteristics we see. First, more metals end up locked in both the the gas and stars at the center of the galaxies.

Second, more stars have formed at the center of these galaxies. This point further confirms one for the results of[279] which noted that the hosts of under-massive black holes followed nearly identical evolutionary tracks to galaxies without black holes.

We further compare our results to those of[69] which find that galaxies with over-massive BHs have a lower fraction of baryons locked in their CGM due to the evacuation of gas by black hole feedback both for IllustrisTNG galaxies and those in EAGLE. Interestingly, we find the opposite. Figure 4.7 shows the fraction of baryons in CGM gas, defined as in[69] by:

$$f_{CGM} = \frac{M_{gas,T>10^4K}}{M_{vir}}. \tag{4.4}$$

We find that the galaxies in our simulations that host over-massive black holes have the highest fraction of baryons in their CGM in addition to having more metal enriched CGM gas (Figure 4.3). It's worth noting that the right hand panel of Figure 4.4 shows that these over-massive BH hosts have fewer baryons overall compared to their counterpart galaxies despite having more of those baryons in the CGM. This distinct differences between our findings and those of[69] are likely due to the differences in the implementation of sub-grid BH physics.

In the EAGLE simulation, AGN feedback[36] is implemented via stochastic, isotropic heating applied to gas particles ($\Delta T_{AGN} = 10^{8.5}$ K) and the AGN feedback efficiency was chosen to reproduce the z = 0 scaling relation between galaxy stellar mass and their central SMBH masses. The energy injection rate is: $f_{AGN}\dot{m}_{acc}c^2$ where $\dot{m}_{acc}$ is the BH accretion rate and $f_{AGN} = 0.015$ is a fixed value where f_{AGN}^2 determines the fraction of available energy coupled to the ISM. AGN feedback is the primary form of self-regulation in EAGLE once a hot CGM has formed, limiting the impact of stellar-driven winds out of the galaxy[42].

In IllustrisTNG, AGN feedback is implemented in two modes: high accretion rates drive a feedback mode which injects energy thermally, heating nearby gas cells to the BH using an efficiency of $f_{AGN,thm} = 0.02$. Meanwhile, feedback associated with low accretion rates inject energy kinetically with a random direction chosen for each inject event. The efficiency of the kinetic mode, $f_{AGN,kin}$, scales with local gas density up to 0.2. Kinetic AGN energy is

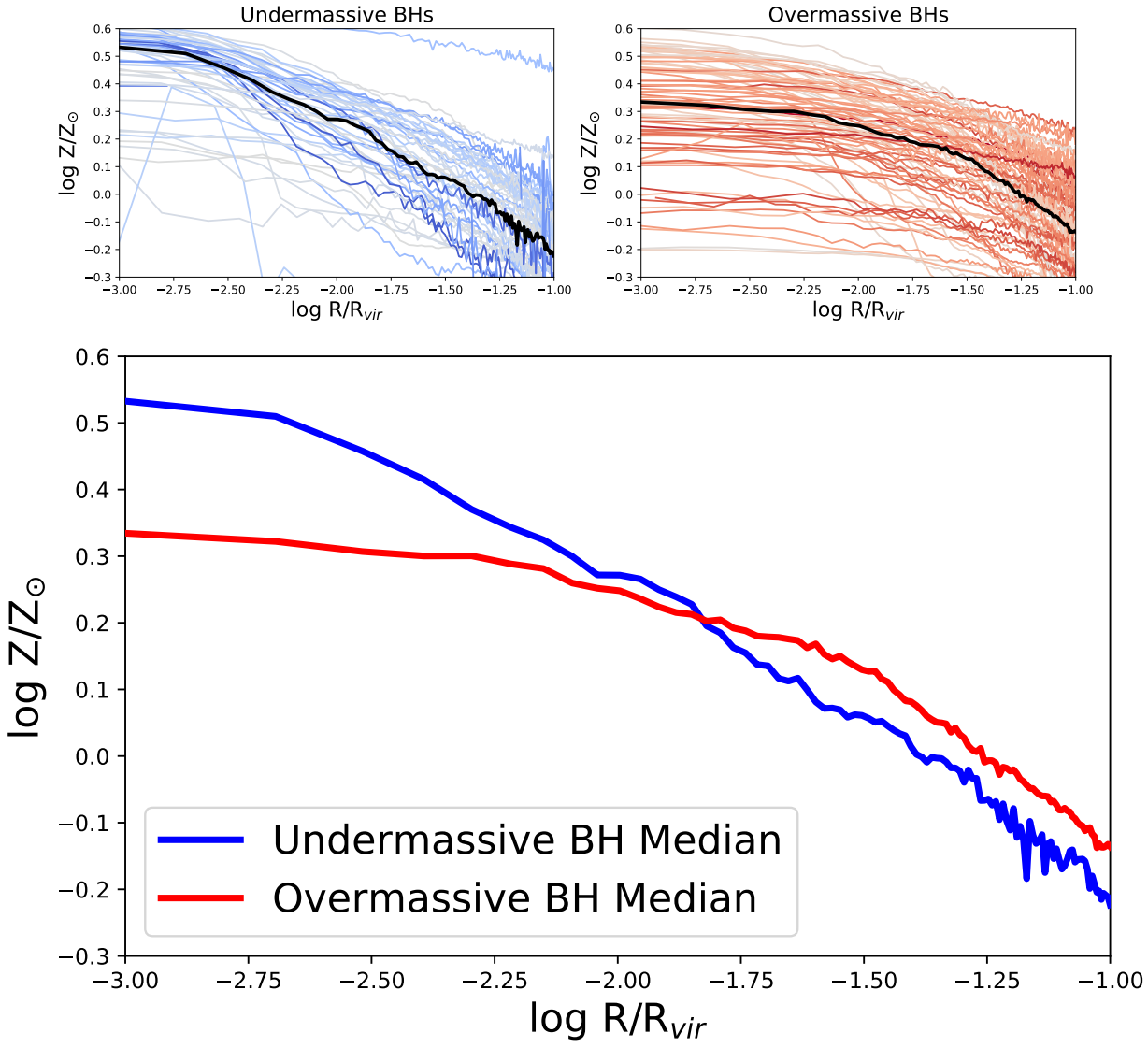

Figure 4.5: The log of the averaged metallicity gradients for all the over-massive (red) and under-massive (blue) galaxies in our sample, focusing on the central $0.1R_{vir}$ that we use to calculate our metal retetion values. Overall, galaxies with over-massive black holes show a flatter distribution of metals with no strong build up of metals in the center. By comparison, galaxies with under-massive black holes tend to have a build up of super-solar metal-rich gas at their centers and a steeper metallicity gradient.

coupled to the hydrodynamic scheme such that the injection velocity is determined by the mass of gas associated with the inject region. Additionally, the coupling efficiency of kinetic

feedback is reduced at low gas densities in order to avoid runaway feedback. The threshold between high and low accretion scales as a function of the BH mass and is written in terms of the Eddington ratio:

$$\chi = min[0.1, \chi_0(m_{BH}/10^8 M_\odot)^2] \tag{4.5}$$

where $\chi_0 = 0.002$. Regardless of mass, a BH can inject feedback via the thermal mode at sufficiently high accretion rates[354]; however, once a BH reaches the pivot mass of $10^8 M_\odot$, this mode becomes rare thereby setting this mass as the transition between thermal and kinetic feedback modes.

It is therefore interesting to note that in the galaxies of these two simulation suites,[69] find that the SMBHs effectively eject gas and metals from the CGM out into the IGM, resulting in smaller f_{CGM} values. In contrast, the SMBHs in our galaxies do not appear to evacuate gas and metals from the CGM, driving galaxy-scale outflows that can enrich the CGM of their hosts, but are unlikely to drive material out past the virial radius.

4.4.2 Predictions for Future CGM Surveys

From Figure 4.6, we predict that surveys like COS-Holes will see a distinction between the amount of C IV and other ions like O VI in the CGM of galaxies that host over- and under-massive central SMBHs. An observable test for these predictions could come in the form of future HST/COS observations, specifically those like COS-Holes[355] that will pair UV absorption measurements to dynamical BH mass measurements. With such observations, we will additionally be able to determine whether or not SMBH are evacuating gas in the CGM of their hosts. Furthermore, metal line measurements paired with dynamical BH mass estimates would allow us to determine whether SMBHs that are over- or under-massive play different roles in setting the metal content of the CGM.

One case of note is M31.[311] measured the disk of the Andromeda Galaxy had lost up to 66% of the metals formed by its stellar population. Therefore, the metal retention of the disk, $f_{z,disk}$, is 38%, which is close to the lowest metal retention rates we find in our sample

(Figure 4.3). The galaxies with the lowest metal retention rates nearly all host over-massive black holes, which also appears to be the case for M31. M31 has a velocity dispersion in the bulge of 151-153 km/s[366;379] and a central SMBH mass of 1.4×10^8 $M_\odot$[25] which is 1.5× larger than expected based on equation 4.2[167].

While this is only one case, it demonstrates a clear example of galaxy with metals that have been ejected from the disk in the presence of a SMBH that is over-massive compared to its stellar dispersion. It remains clear that there is plenty of exciting work to be done connecting the flow of metals in a galaxy to the properties and effects of SMBHs.

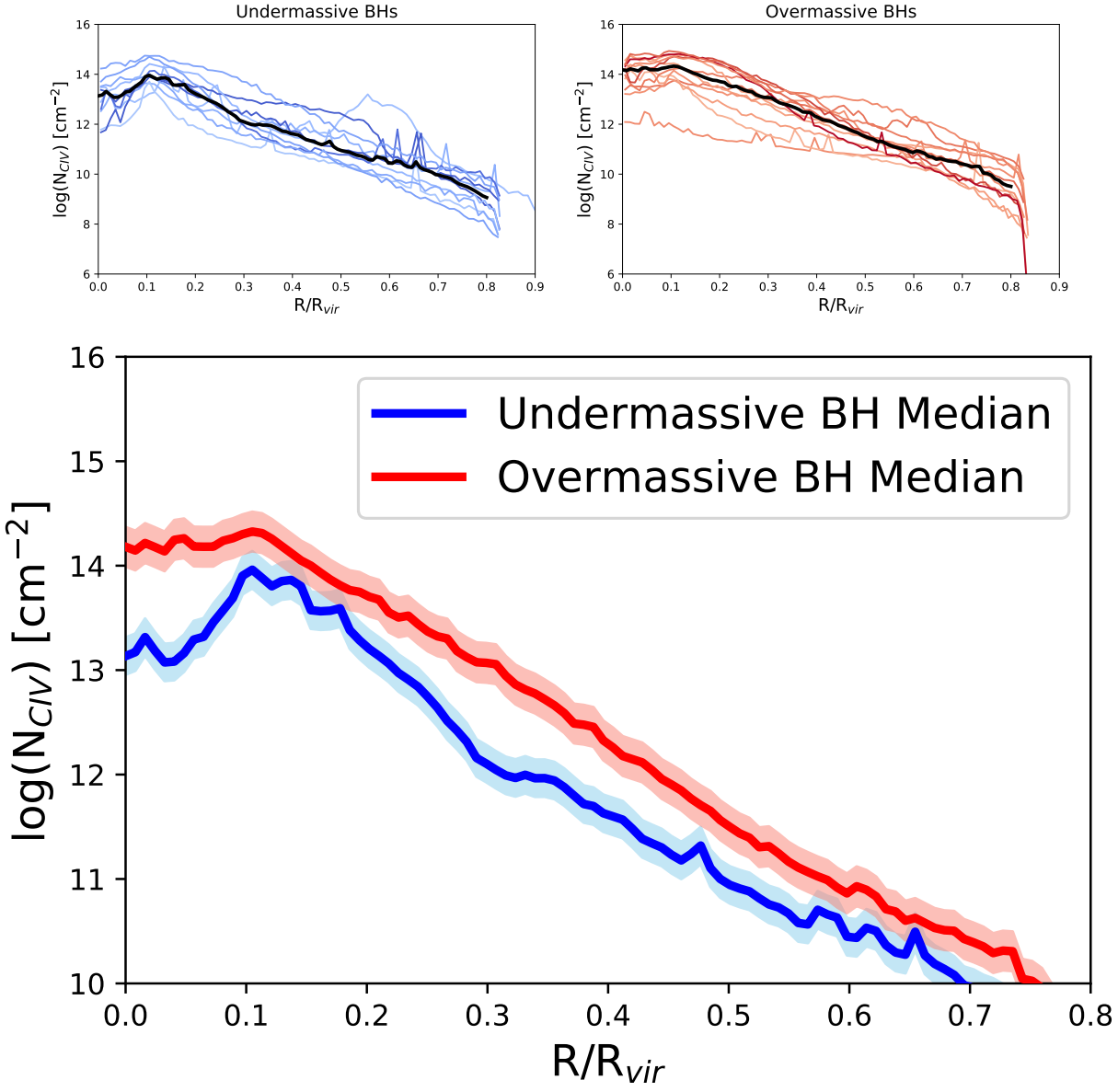

Figure 4.6: Column densities of C IV as a function of radius for subsample of stellar-mass-matched galaxies with over-massive (red) and under-massive (blue) SMBHs. The upper panels show N(C IV) for all 64 galaxies split between each subset of BH and the lower panel shows the median for each subset as well as the standard deviation of the median. Our measurements predict that upcoming UV absorption missions that include host galaxy SMBH information, such as the COS-Holes survey, will observe a difference in the amount of C IV in their CGM. Galaxies with over-massive black holes will contain up to 0.5 dex more C IV in their CGM gas than galaxies hosting under-massive black holes.

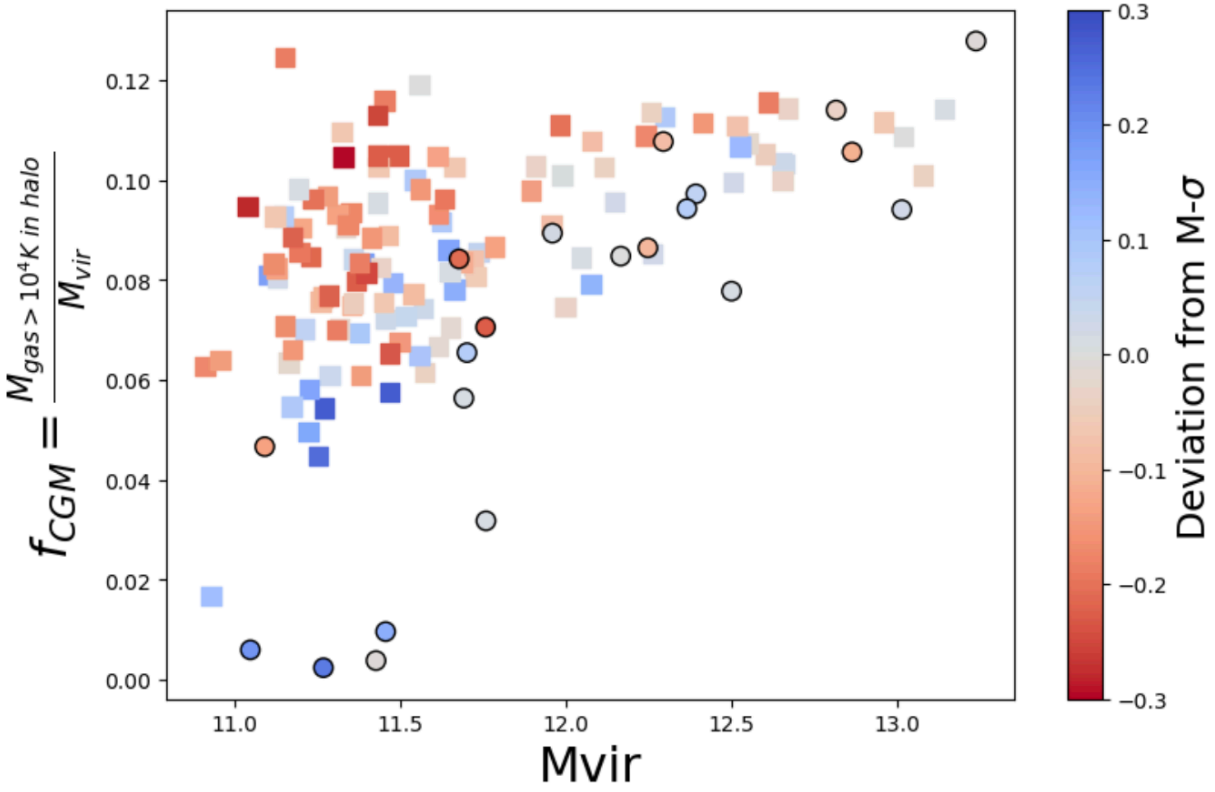

Figure 4.7: Measurements of the fraction of baryons in the CGM, as calculated in[69], as a function of the virial radius for all 140 of our galaxies. Points colored by deviation from M-σ as in Figure 4.4. We find that galaxies hosting over-massive SMBHs (red) contain a high fraction of baryons in their CGM, in addition to containing more enriched gas in the CGM (Figure 4.3).

Chapter 5

CONCLUSIONS: LOOKING TOWARDS THE FUTURE

5.1 Summary

The primary goal of this dissertation has been to understand the different roles of stellar feedback, SMBH feedback, and environment play in setting different observable properties of the CGM, specifically how environment, accretion history, and SMBH feedback can impact the global properties of the CGM (Chapter 2); how measurements of O VI in the CGM vary based on differing star formation histories and BH physics implemention (Chapter 3), and where enrichment from the stars in the galaxy disk end up due to feedback processes (Chapter 4).

Throughout this work, I have motivated the benefits and caveats of using my suite of ChaNGa simulations, including all galaxies from ROMULUS25 and the set of zoom-in galaxies run using the GM technique. The GM process allowed us to create galaxies from nearly identical initial conditions and these subsequent simulations, with such similar starting characteristics, created a critical test case for the effects of star formation history on the CGM. Similarly, testing the original GM galaxies with a sample that does not include BH physics allowed us directly test its effect on the metal enrichment of the CGM. Exploring the cause of the differing star formation histories, the subtly changed minor merger interaction, gave us a unique view into the possible quenching mechanisms of Milky Way-mass galaxies.

The various subsamples of galaxies I explored from ROMULUS25 added necessary components to my work. In understanding the quenching mechanism of the GM galaxies, it provided critical cosmological context and was used to determine how likely such a case would be in the observable universe. By measuring the column densities of O VI from a sample of L* galaxies in ROMULUS25, we confirmed that the star formation rate plays a less significant role that halo mass in setting the amount of O VI in the CGM of these galaxies. Finally, we used a much larger sample of galaxies, still centered on the Milky Way-mass regime, to determine that the accreted mass of the SMBH at each galaxy's center can be used to inform the metal content of both the ISM and CGM of the galaxies.

By furthering our understanding of the critical role SMBH feedback plays in setting

the nature of circumgalactic gas, this research makes important strides in broadening our understanding of the interdependent and complex mechanisms driving galaxy evolution. Nevertheless, our understanding of precisely how to best implement the energetics of feedback sources and how they couple to gas remains incomplete[96].

5.2 Connecting The Dots

The chapters of my work individually highlight the processes of quenching in Milky Way-mass galaxies, compare to metal line observations of the CGM, and predict measurements for future observational surveys. Together, they further develop a deep connection between the growth and evolution of SMBHs and their host galaxies as well the gas accretion and motion throughout time.

Chapter 2 shows not only an additional mechanism for driving quenching in Milky Way-mass galaxies, but also the impact of quenching processes on CGM gas. I.e. the removal and disruption of the cold gas supply from the disk.

Chapter 3 shows how early enrichment of the CGM by AGN feedback is observable in both quenched and star forming galaxies, despite varying star formation histories. It also shows that the SMBH is a critical component in enriching the CGM, far more than stellar feedback in our simulations.

Finally, Chapter 4 brings all this together by exploring a specific quality of the SMBH, how massive it is in comparison to the potential of the host galaxies and how this quality impacts the effectiveness of its enrichment of the surrounding CGM.

Together, the body of my work shows that the CGM of Milky Way-mass galaxies in simulations is in particular an interesting place to explore the impact of feedback on gas physics, and that the SMBH play a key role in driving the evolution of these galaxies.

5.3 Future Work: Isolating Processes in Galaxy Evolution

One of the key obstacles to quantifying the role of feedback on gas is that galaxy evolution is complicated and chaotic by nature. The complex interactions of a galaxy with its

environment, such as mergers and accretion, make it challenging to study and disentangle the different feedback processes at play. To shed light on this problem, we must continue advance novel techniques like the genetic modification process to cosmological simulations and carry out multi-epoch, multi- wavelength observational studies of the CGM.

Recent studies of simulated galaxies have shown that the circumgalactic medium is particularly sensitive to feedback prescriptions which makes it a good test laboratory for continued feedback process studies[328]. Though simulations have struggled to replicate the complicated multi-phase structure of the CGM, the varying implementations of feedback processes make differentiating the different sources building up the multi-phase CGM even more difficult. Different simulation prescriptions show different results, some heating and evacuating gas from the CGM[224], others enriching the CGM with metals from the disk[216;266;309], and quenching galaxy star formation[75;265;286].

So, the same problem arises: Galaxy evolution is complex and interdependent. Assembly history impacts star formation as well as SMBH growth, which in turn impacts star formation and accretion history, which impacts the CGM, and so on. Therefore it is critical to create better, controlled tests which can disentangle not only the differences between stellar and SMBH feedback processes but that can also isolate the impact of a galaxy's assembly and accretion history.

One way to attempt to solve this problem is with high-resolution cosmological simulations with reliable gas tracking, metal cooling, and advanced stellar and SMBH feedback prescriptions that allow for the controlled numerical tests. I plan to develop a new generation of genetically modified galaxies to just that.

5.4 Future Work: More CGM Observations and Better, More Controlled Simulations

In preparation to move on to my postdoc this Fall, I have designed two suites of genetically modified simulations that are currently being run with the same N-body+smoothed particle hydrodynamics code CHANGA[196]. However, the improved resolution in our simulations will

allow for the inclusion of upgraded physics, such as better ISM modeling, full treatments for metal cooling and H2 abundances, and the implementation of a super bubble feedback model[154] for both supernovae and SMBH feedback. Additional improvements to the SMBH physics have been included, such as the direct collapse of black hole seeds based on local gas properties and more realistic interactions between the SMBH and multi-phase gas, including gas rich mergers, at earlier times. The new GM suites will also include variations in the models for SMBH accretion and feedback to further explore the connection between star formation history, assembly history, and the impact of the SMBH.

These two suites of GM galaxies will be a powerful tool to distinguish the different processes that impact the observable properties of the CGM. While one will focus on isolating stellar and SMBH feedback effects from one another and from individual late-z mergers, the other will give us the power to trace differences due to the overall accretion history and how that varies along the axis of modified assembly histories. The full set of GM simulations will contain all the information needed to disentangle and isolate the tracers that couple feedback to the complex, multi-phase structure of the CGM.

Nevertheless, while there have been many advances in understanding of the physics of the CGM, ongoing observations are critical. The upcoming COS-Holes[355] survey will give us incredible insight into how the CGM is impacted by SMBH characteristics at previously observerd UV wavelengths. New observations at unobserved wavelengths will also be key however. For example, recent studies of the X-ray emission lines in L* galaxies have shown points of improvements for current feedback models. Amidst both star forming and quiescent galaxies in this mass range, the effectiveness of feedback prescriptions has been called into question with stellar feedback prescriptions that are too weak and SMBH feedback which may be too strong[54].

As of now, there is no end in sight to work needed to disentangle the details of this multiphase region. As a statement, it is not meant to be a deterrent, but in fact the opposite, and this author looks forward to a future full of research possibilities.

BIBLIOGRAPHY

[1] Aarseth, S. J., Turner, E. L., & Gott, J. R., I. 1979, The Astrophysical Journal, 228, 664

[2] Abadi, M. G., Moore, B., & Bower, R. G. 1999, Monthly Notices of the Royal Astronomical Society, 308, 947

[3] Ade, P. A., Aghanim, N., Arnaud, M., et al. 2016, Astronomy and Astrophysics, 594, arXiv:1502.01589

[4] Agertz, O., Kravtsov, A. V., Leitner, S. N., & Gnedin, N. Y. 2013, Astrophysical Journal, 770, arXiv:1210.4957

[5] Akins, H. B., Christensen, C. R., Brooks, A. M., et al. 2020, arXiv, arXiv:2008.02805

[6] Anderson, M. E., & Bregman, J. N. 2010, Astrophysical Journal, 714, 320

[7] Anderson, M. E., Bregman, J. N., & Dai, X. 2013, Astrophysical Journal, 762, arXiv:1211.5140

[8] Anglés-Alcázar, D., Davé, R., Faucher-Giguère, C.-A., Özel, F., & Hopkins, P. F. 2017, Monthly Notices of the Royal Astronomical Society, 464, 2840

[9] Anglés-Alcázar, D., Faucher-Giguère, C.-A., Kereš, D., et al. 2016, Mnras, 000, 0

[10] —. 2017, Monthly Notices of the Royal Astronomical Society, 470, 4698

[11] Applebaum, E., Brooks, A. M., Christensen, C. R., et al. 2020, arXiv:2008.11207

[12] Bahcall, J. N., & Spitzer, Lyman, J. 1969, The Astrophysical Journal, 156, L63

[13] Bahé, Y. M., & McCarthy, I. G. 2015, Monthly Notices of the Royal Astronomical Society, 447, 969

[14] Baldassare, V. F., Dickey, C., Geha, M., & Reines, A. E. 2020, arXiv:2006.15150

[15] Baldry, I. K. 2004, in AIP Conference Proceedings, Vol. 743 (AIP), 106–119

[16] Baldry, I. K., Balogh, M. L., Bower, R. G., et al. 2006, Monthly Notices of the Royal Astronomical Society, 373, 469

[17] Balogh, M. L., Babul, A., & Patton, D. R. 1998, 000, 1

[18] Barnes, J. E., & Hernquist, L. 1996, The Astrophysical Journal, 471, 115

[19] Barro, G., Faber, S. M., Dekel, A., et al. 2016, The Astrophysical Journal, 820, 120

[20] Behroozi, P. S., Conroy, C., & Wechsler, R. H. 2010, Astrophysical Journal, 717, 379

[21] Behroozi, P. S., Wechsler, R. H., & Conroy, C. 2013, Astrophysical Journal, 770, arXiv:1207.6105

[22] Belfiore, F., Maiolino, R., Maraston, C., et al. 2016, Monthly Notices of the Royal Astronomical Society, 461, 1

[23] Bell, E. F., McIntosh, D. H., Katz, N., & Weinberg, M. D. 2003, The Astrophysical Journal Supplement Series, 149, 289

[24] Bell, E. F., Wolf, C., Meisenheimer, K., et al. 2004, The Astrophysical Journal, 608, 752

[25] Bender, R., Kormendy, J., Bower, G., et al. 2005, The Astrophysical Journal, 631, 280

[26] Benson, A. J., Bower, R. G., Frenk, C. S., et al. 2003, The Astrophysical Journal, 599, 38

[27] Berg, T. A. M., Ellison, S. L., Tumlinson, J., et al. 2018, Monthly Notices of the Royal Astronomical Society, 478, 3890

[28] Berger, M., & Colella, P. 1989, Journal of Computational Physics, 82, 64

[29] Berger, M. J., & Oliger, J. 1984, Journal of Computational Physics, 53, 484

[30] Bergeron, J. 1986, \Aap, 155, L8

[31] Bigiel, F., Leroy, A. K., Walter, F., et al. 2011, Astrophysical Journal Letters, 730, arXiv:1102.1720

[32] Binney, J. 1977, The Astrophysical Journal, 215, 483

[33] Blanton, M. R., Hogg, D. W., Bahcall, N. A., et al. 2003, 186

[34] Bondi, H., & Hoyle, F. 1944, Monthly Notices of the Royal Astronomical Society, 104, 273

[35] Booth, C. M., Agertz, O., Kravtsov, A. V., & Gnedin, N. Y. 2013, Astrophysical Journal Letters, 777, arXiv:1308.4974

[36] Booth, C. M., & Schaye, J. 2009, Monthly Notices of the Royal Astronomical Society, 398, 53

[37] Bordoloi, R., Lilly, S. J., Knobel, C., et al. 2011, The Astrophysical Journal, 743, 10

[38] Bordoloi, R., Tumlinson, J., Werk, J. K., et al. 2014, Astrophysical Journal, 796, arXiv:1406.0509

[39] Borthakur, S., Heckman, T., Tumlinson, J., et al. 2015, Astrophysical Journal, 813, 46

[40] —. 2016, The Astrophysical Journal, 833, 1

[41] Bower, R. G., Benson, A. J., Malbon, R., et al. 2006, Monthly Notices of the Royal Astronomical Society, 370, 645

[42] Bower, R. G., Schaye, J., Frenk, C. S., et al. 2017, Monthly Notices of the Royal Astronomical Society, 465, 32

[43] Boylan-Kolchin, M., Ma, C. P., & Quataert, E. 2008, Monthly Notices of the Royal Astronomical Society, 383, 93

[44] Brammer, G. B., Whitaker, K. E., Dokkum, P. G. V., Marchesini, D., & Labb, I. 2010, 5, 173

[45] Brooks, A. M., Governato, F., Quinn, T., Brook, C. B., & Wadsley, J. 2009, The Astrophysical Journal, 694, 396

[46] Bruce, V. A., Dunlop, J. S., Mortlock, A., et al. 2016, Monthly Notices of the Royal Astronomical Society, 458, 2391

[47] Burchett, J. N., Tripp, T. M., Prochaska, J. X., et al. 2019, The Astrophysical Journal, 877, L20

[48] Butsky, I. S., Fielding, D. B., Hayward, C. C., et al. 2020, The Astrophysical Journal, 903, 77

[49] Cantalupo, S., Arrigoni-Battaia, F., Prochaska, J. X., Hennawi, J. F., & Madau, P. 2014, Nature, 506, 63

[50] Carlberg, R. G., Lake, G., & Norman, C. A. 1986, The Astrophysical Journal, 300, L1

[51] Cejda, B. D., Hensel, N. H., & Council on Undergraduate Research (U.S.). 2009, Undergraduate research at community colleges, 72

[52] Cen, R. 2013, Astrophysical Journal, 770, 1

[53] Chadayammuri, U., Bogdan, A., Oppenheimer, B., et al. 2022, arXiv:2203.01356

[54] Chadayammuri, U., Tremmel, M., Nagai, D., Babul, A., & Quinn, T. 2020, 17, 1

[55] Choi, E., Somerville, R. S., Ostriker, J. P., Naab, T., & Hirschmann, M. 2018, The Astrophysical Journal, 866, 91

[56] Christensen, C., Quinn, T., Governato, F., et al. 2012, Monthly Notices of the Royal Astronomical Society, 425, 3058

[57] Christensen, C. R., Davé, R., Governato, F., et al. 2015, arXiv:1508.00007

[58] —. 2016, The Astrophysical Journal, 824, 57

[59] Cicone, C., Maiolino, R., Sturm, E., et al. 2014, Astronomy and Astrophysics, 562, 1

[60] Cohen, B., & Lee, I.-s. 1979, J Bone Joint Surg Am, 36, 1

[61] Cole, S., Aragon-Salamanca, A., Frenk, C. S., Navarro, J. F., & Zepf, S. E. 1994, Monthly Notices of the Royal Astronomical Society, 271, 781

[62] Cox, T. J., Dutta, S. N., Di Matteo, T., et al. 2006, The Astrophysical Journal, 650, 791

[63] Croton, D. J., Springel, V., White, S. D., et al. 2006, Monthly Notices of the Royal Astronomical Society, 365, 11

[64] Croton, D. J., Stevens, A. R. H., Tonini, C., et al. 2016, The Astrophysical Journal Supplement Series, 222, 22

[65] Cruz, A., Pontzen, A., Volonteri, M., et al. 2020, 11, 1

[66] Dalla Vecchia, C., & Schaye, J. 2012, Monthly Notices of the Royal Astronomical Society, 426, 140

[67] Danforth, C. W., Keeney, B. A., Tilton, E. M., et al. 2016, The Astrophysical Journal, 817, 111

[68] Davies, J. J., Crain, R. A., McCarthy, I. G., et al. 2019, Monthly Notices of the Royal Astronomical Society, 485, 3783

[69] Davies, J. J., Crain, R. A., Oppenheimer, B. D., & Schaye, J. 2020, Monthly Notices of the Royal Astronomical Society, 491, 4462

[70] Dekel, A., & Birnboim, Y. 2006, Monthly Notices of the Royal Astronomical Society, 368, 2

[71] Dekel, A., & Burkert, A. 2014, Monthly Notices of the Royal Astronomical Society, 438, 1870

[72] Dekel, A., & Silk, J. 1986, The Astrophysical Journal, 303, 39

[73] Dekel, a., Birnboim, Y., Engel, G., et al. 2009, Nature, 457, 451

[74] Del Moro, A., Alexander, D. M., Bauer, F. E., et al. 2016, Monthly Notices of the Royal Astronomical Society, 456, 2105

[75] Di Matteo, T., Springel, V., & Hernquist, L. E. 2005, Nature, 433, 604

[76] Di Matteo, T., Springel, V., & Ilernquist, L. 2005, Nature, 433, 604

[77] Di Teodoro, E. M., & Peek, J. E. G. 2021, arXiv:2110.01618

[78] D'Onghia, E., Burkert, A., Murante, G., & Khochfar, S. 2006, Monthly Notices of the Royal Astronomical Society, 372, 1525

[79] Dubois, Y., Peirani, S., Pichon, C., et al. 2016, Monthly Notices of the Royal Astronomical Society, 463, 3948

[80] Dubois, Y., Volonteri, M., Silk, J., et al. 2015, Monthly Notices of the Royal Astronomical Society, 452, 1502

[81] Eastwood, D. S., Khochfar, S., & Trew, A. 2019, Monthly Notices of the Royal Astronomical Society, 488, 2006

[82] Efstathiou, G. 1979, Monthly Notices of the Royal Astronomical Society, 187, 117

[83] —. 1992, Monthly Notices of the Royal Astronomical Society, 256, 43P

[84] Eisenstein, D. J., & Loeb, A. 1995, The Astrophysical Journal, 443, 11

[85] Emsellem, E., Cappellari, M., Krajnović, D., et al. 2011, Monthly Notices of the Royal Astronomical Society, 414, 888

[86] Fabian, A. 2012, Annual Review of Astronomy and Astrophysics, 50, 455

[87] Fanidakis, N., Baugh, C. M., Benson, A. J., et al. 2012, 2820, 2797

[88] Feldmann, R., Hopkins, P. F., Quataert, E., Faucher-Giguère, C. A., & Kerěs, D. 2016, Monthly Notices of the Royal Astronomical Society: Letters, 458, L14

[89] Feldmann, R., & Mayer, L. 2014, Monthly Notices of the Royal Astronomical Society, 446, 1939

[90] —. 2015, Monthly Notices of the Royal Astronomical Society, 446, 1939

[91] Feldmann, R., Quataert, E., & Hopkins, P. F. 2017, 1072, 1050

[92] Ferland, G. J., Korista, K. T., Verner, D. A., et al. 1998, Publications of the Astronomical Society of the Pacific, 110, 761

[93] Ferland, G. J., Porter, R. L., Van Hoof, P. A. M., et al. 2013, Revista Mexicana de Astronomia y Astrofisica, 49, 137

[94] Ferrarese, L., & Merritt, D. 2000, The Astrophysical Journal, 539, L9

[95] Fielding, D., Quataert, E., & Martizzi, D. 2018, Monthly Notices of the Royal Astronomical Society, 481, 3325

[96] Fielding, D. B., Tonnesen, S., DeFelippis, D., et al. 2020, The Astrophysical Journal, 903, 32

[97] Ford, A. B., Davé, R., Oppenheimer, B. D., et al. 2014, Monthly Notices of the Royal Astronomical Society, 444, 1260

[98] Ford, A. B., Oppenheimer, B. D., Davé, R., et al. 2013, Monthly Notices of the Royal Astronomical Society, 432, 89

[99] Ford, A. B., Werk, J. K., Davé, R., et al. 2016, Monthly Notices of the Royal Astronomical Society, 459, 1745

[100] —. 2016, Monthly Notices of the Royal Astronomical Society, 459, 1745

[101] Foster, C., Hopkins, A. M., Gunawardhana, M., et al. 2012, 1

[102] Fraternali, F., & Tomassetti, M. 2012, Monthly Notices of the Royal Astronomical Society, 426, 2166

[103] Gabor, J. M., Davé, R., Finlator, K., & Oppenheimer, B. D. 2010, Monthly Notices of the Royal Astronomical Society, 407, 749

[104] Gallazzi, A., Brinchmann, J., Charlot, S., & White, S. D. M. 2007, Monthly Notices of the Royal Astronomical Society, 383, 1439

[105] Gaspari, M., Ruszkowski, M., & Oh, S. P. 2013, Monthly Notices of the Royal Astronomical Society, 432, 3401

[106] Gebhardt, K., Kormendy, J., Ho, L. C., et al. 2000, The Astrophysical Journal, 543, L5

[107] Gill, S. P. D., Kneb, A., & Gibson, B. K. 2004, Monthly Notices of the Royal Astronomical Society, 351, 399

[108] Ginder, S. a., Kelly-Reid, J. E., & Mann, F. B. 2014, First Look (Provisional Data) (NCES 2015-012). U.S. Department of Education. Washington, DC: National Center for Education Statistics, 1

[109] Girichidis, P., Naab, T., Walch, S., et al. 2016, The Astrophysical Journal, 816, L19

[110] Governato, F., Brook, C. B., Brooks, A. M., et al. 2009, Monthly Notices of the Royal Astronomical Society, 398, 312

[111] Governato, F., Weisz, D., Pontzen, A., et al. 2015, Monthly Notices of the Royal Astronomical Society, 448, 792

[112] Graham, A. W., & Scott, N. 2015, Astrophysical Journal, 798, 1

[113] Grand, R. J., Gómez, F. A., Marinacci, F., et al. 2017, Monthly Notices of the Royal Astronomical Society, 467, 179

[114] Green, J. C., Froning, C. S., Osterman, S., et al. 2012, Astrophysical Journal, 744, arXiv:1110.0462

[115] Gunn, J. E., & Gott, J. Richard, I. 1972, The Astrophysical Journal, 176, 1

[116] Guo, Q., White, S., Boylan-Kolchin, M., et al. 2011, Monthly Notices of the Royal Astronomical Society, 413, 101

[117] Guo, Y., Maiolino, R., Jiang, L., et al. 2020, arXiv:2001.05473

[118] Gupta, A. C. 2017, Galaxies, 6, 1

[119] Haardt, F., & Madau, P. 2012, The Astrophysical Journal, 746, 125

[120] Haehnelt, M. G., Natarajan, P., & Rees, M. J. 1998, Monthly Notices of the Royal Astronomical Society, 300, 817

[121] Hafen, Z., Faucher-Giguère, C. A., Anglés-Alcázar, D., et al. 2019, Monthly Notices of the Royal Astronomical Society, 1272, 1248

[122] Haiman, Z., Spaans, M., & Quataert, E. 2000, The Astrophysical Journal, 537, L5

[123] Hani, M. H., Gosain, H., Ellison, S. L., Patton, D. R., & Torrey, P. 2020, Monthly Notices of the Royal Astronomical Society, 493, 3716

[124] Hayes, M., Melinder, J., Östlin, G., et al. 2016, The Astrophysical Journal, 828, 1

[125] Heckman, T. M., Alexandroff, R. M., Borthakur, S., Overzier, R., & Leitherer, C. 2015, Astrophysical Journal, 809, 147

[126] Hewlett, T., Villforth, C., Wild, V., Mendez-abreu, J., & Rowlands, K. 2017, 17, 1

[127] Hirschmann, M., Naab, T., Somerville, R. S., Burkert, A., & Oser, L. 2012, 3222, 3200

[128] Hopkins, P. F., Hernquist, L., Cox, T. J., et al. 2006, The Astrophysical Journal Supplement Series, 163, 1

[129] Hopkins, P. F., Kereš, D., Oñorbe, J., et al. 2014, Monthly Notices of the Royal Astronomical Society, 445, 581

[130] —. 2014, Monthly Notices of the Royal Astronomical Society, 445, 581

[131] Hopkins, P. F., & Quataert, E. 2010, Monthly Notices of the Royal Astronomical Society, 407, 1529

[132] Hopkins, P. F., Quataert, E., & Murray, N. 2012, Monthly Notices of the Royal Astronomical Society, 421, 3522

[133] Hopkins, P. F., Somerville, R. S., Cox, T. J., et al. 2009, 814, 802

[134] Hopkins, P. F., Wetzel, A., Kereš, D., et al. 2018, Monthly Notices of the Royal Astronomical Society, 480, 800

[135] Hummels, C., Smith, B., & Silvia, D. 2016, arXiv:1612.03935

[136] Hummels, C. B., Bryan, G. L., Smith, B. D., & Turk, M. J. 2013, Monthly Notices of the Royal Astronomical Society, 430, 1548

[137] Hummels, C. B., Smith, B. D., Hopkins, P. F., et al. 2019, The Astrophysical Journal, 882, 156

[138] Huscher, E., Oppenheimer, B. D., Lonardi, A., et al. 2020, 000, arXiv:2005.06310

[139] Ilbert, O., Salvato, M., Le Floc'h, E., et al. 2010, The Astrophysical Journal, 709, 644

[140] Ilbert, O., McCracken, H. J., Le Fèvre, O., et al. 2013, Astronomy & Astrophysics, 556, A55

[141] Iyer, K. G., Tacchella, S., Genel, S., et al. 2020, 35, 1

[142] Johansson, P. H., Naab, T., & Burkert, A. 2009, 1, 802

[143] Johnson, S. D., Chen, H. W., & Mulchaey, J. S. 2015, Monthly Notices of the Royal Astronomical Society, 449, 3263

[144] Kang, X., Jing, Y. P., Mo, H. J., & Borner, G. 2005, The Astrophysical Journal, 631, 21

[145] Katz, N., & White, S. D. M. 1993, The Astrophysical Journal, 412, 455

[146] Kauffmann, G., White, S. D. M., & Guiderdoni, B. 1993, Monthly Notices of the Royal Astronomical Society, 264, 201

[147] Kauffmann, G., White, S. D. M., Heckman, T. M., et al. 2004, 731, 713

[148] Kauffmann, G., Heckman, T. M., White, S. D. M., et al. 2003, Monthly Notices of the Royal Astronomical Society, 341, 54

[149] Kauffmann, G., Heckman, T. M., Tremonti, C., et al. 2003, Monthly Notices of the Royal Astronomical Society, 346, 1055

[150] Kaufmann, T., Bullock, J. S., Maller, A., & Fang, T. 2008, Formation and Evolution of Galaxy Disks ASP Conference Series, 396, 439

[151] Kaviraj, S., Laigle, C., Kimm, T., et al. 2017, Monthly Notices of the Royal Astronomical Society, 467, 4739

[152] Keeney, B. A., Stocke, J. T., Danforth, C. W., et al. 2017, Astrophysical Journal Supplement Series, 230, 6

[153] Keller, B. W., Kruijssen, J. M., & Wadsley, J. W. 2020, Monthly Notices of the Royal Astronomical Society, 493, 2149

[154] Keller, B. W., Wadsley, J., Benincasa, S. M., & Couchman, H. M. P. 2014, Monthly Notices of the Royal Astronomical Society, 442, 3013

[155] Keller, B. W., Wadsley, J., & Couchman, H. M. 2015, Monthly Notices of the Royal Astronomical Society, 453, 3499

[156] Keller, B. W., & Wadsley, J. W. 2017, The Astrophysical Journal, 835, L17

[157] Keller, B. W., Wadsley, J. W., Wang, L., & Kruijssen, J. M. 2019, Monthly Notices of the Royal Astronomical Society, 482, 2244

[158] Keres, D., Katz, N., Weinberg, D. H., & David, R. 2005, Monthly Notices of the Royal Astronomical Society, 363, 2

[159] Kewley, L. J., & Ellison, S. L. 2008, The Astrophysical Journal, 681, 1183

[160] King, A., & Pounds, K. 2015, Annual Review of Astronomy and Astrophysics, 53, 115

[161] Kirby, E. N., Cohen, J. G., Guhathakurta, P., et al. 2013, Astrophysical Journal, 779, arXiv:1310.0814

[162] Klein, R. I., McKee, C. F., & Colella, P. 1994, The Astrophysical Journal, 420, 213

[163] Knebe, A., Green, A., & Binney, J. 2001, Monthly Notices of the Royal Astronomical Society, 325, 845

[164] Knollmann, S. R., & Knebe, A. 2009, The Astrophysical Journal Supplement Series, 182, 608

[165] Kollmeier, J. A., Weinberg, D. H., Oppenheimer, B. D., et al. 2014, The Astrophysical Journal, 789, L32

[166] Kormendy, J. 1989, The Astrophysical Journal, 342, L63

[167] Kormendy, J., & Ho, L. C. 2013, Annual Review of Astronomy and Astrophysics, 51, 511

[168] Krolik, J. H. 1999, The Astrophysical Journal, 515, L73

[169] Kroupa, P. 2001, Monthly Notices of the Royal Astronomical Society, 322, 231

[170] Kroupa, P., Tout, C. A., & Gilmore, G. 1993, Monthly Notices of the Royal Astronomical Society, 262, 545

[171] Krumholz, M. R., Dekel, A., & McKee, C. F. 2012, Astrophysical Journal, 745, arXiv:1109.4150

[172] Lang, P., Wuyts, S., Somerville, R. S., et al. 2014, The Astrophysical Journal, 788, 11

[173] Larson, R. B. 1974, Monthly Notices of the Royal Astronomical Society, 169, 229

[174] Larson, R. B., Tinsley, B. M., & Caldwell, C. N. 1980, The Astrophysical Journal, 237, 692

[175] Lehner, N., Howk, J. C., Tripp, T. M., et al. 2013, Astrophysical Journal, 770, arXiv:1302.5424

[176] Liang, C. J., & Chen, H. W. 2014, Monthly Notices of the Royal Astronomical Society, 445, 2061

[177] Liang, C. J., Kravtsov, A. V., & Agertz, O. 2018, Monthly Notices of the Royal Astronomical Society, 479, 1822

[178] Lintott, C., Schawinski, K., Bamford, S., et al. 2011, Monthly Notices of the Royal Astronomical Society, 410, 166

[179] López Fernández, R., González Delgado, R. M., Pérez, E., et al. 2018, Astronomy & Astrophysics, 615, A27

[180] Ma, J., & Baum, S. 2016, College Board Research, 1

[181] Madau, P., & Dickinson, M. 2014, 1

[182] Magorrian, J., Tremaine, S., Richstone, D., et al. 1998, The Astronomical Journal, 115, 2285

[183] Marinacci, F., Grand, R. J. J., Pakmor, R., et al. 2017, Monthly Notices of the Royal Astronomical Society, 466, 3859

[184] Martin, C. L. 2006, The Astrophysical Journal, 647, 222

[185] Maschmann, D., Melchior, A.-L., Mamon, G. A., Chilingarian, I. V., & Katkov, I. Y. 2020, Astronomy & Astrophysics, 1

[186] Mathews, W. G., & Prochaska, J. X. 2017, The Astrophysical Journal, 846, L24

[187] Mazzei, P., Rampazzo, R., Marino, A., et al. 2019, The Astrophysical Journal, 885, 165

[188] McAlpine, S., Harrison, C. M., Rosario, D. J., et al. 2020, Monthly Notices of the Royal Astronomical Society, 22, 1

[189] Mccarthy, I. G., Schaye, J., Bower, R. G., et al. 2011, Monthly Notices of the Royal Astronomical Society, 412, 1965

[190] Mcconnell, N. J., & Ma, C.-P. 2013, The Astrophysical Journal, 764, 184

[191] McGee, S. L., Balogh, M. L., Wilman, D. J., et al. 2011, Monthly Notices of the Royal Astronomical Society, 413, 996

[192] McNamara, B. R., & Nulsen, P. E. 2007, Annual Review of Astronomy and Astrophysics, 45, 117

[193] McQuinn, M., & Werk, J. K. 2017, arXiv:1703.03422v2

[194] —. 2018, The Astrophysical Journal, 852, 33

[195] —. 2018, The Astrophysical Journal, 852, 33

[196] Menon, H., Wesolowski, L., Zheng, G., et al. 2015, Computational Astrophysics and Cosmology, 2, 1

[197] Micic, M., Holley-Bockelmann, K., Sigurdsson, S., & Abel, T. 2007, Monthly Notices of the Royal Astronomical Society, 380, 1533

[198] Mitchell, P. D., Schaye, J., Bower, R. G., & Crain, R. A. 2020, Monthly Notices of the Royal Astronomical Society, 494, 3971

[199] Montero, F. R., Davé, R., Wild, V., Anglés-Alcázar, D., & Narayanan, D. 2019, Monthly Notices of the Royal Astronomical Society, 490, 2139

[200] Moster, B. P., Naab, T., & White, S. D. 2013, Monthly Notices of the Royal Astronomical Society, 428, 3121

[201] Moster, B. P., Somerville, R. S., Maulbetsch, C., et al. 2010, The Astrophysical Journal, 710, 903

[202] Mullaney, J. R., Alexander, D. M., Aird, J., et al. 2015, Monthly Notices of the Royal Astronomical Society: Letters, 453, L83

[203] Munshi, F., Brooks, A. M., Christensen, C., et al. 2019, The Astrophysical Journal, 874, 40

[204] Munshi, F., Governato, F., Brooks, A. M., et al. 2013, The Astrophysical Journal, 766, 56

[205] —. 2013, Astrophysical Journal, 766, arXiv:1209.1389

[206] Muratov, A. L., Kereš, D., Faucher-Giguère, C.-A., et al. 2017, Monthly Notices of the Royal Astronomical Society, 468, 4170

[207] —. 2017, Monthly Notices of the Royal Astronomical Society, 468, 4170

[208] Muzzin, A., Marchesini, D., Stefanon, M., et al. 2013, 18, doi:10.1088/0004-637X/777/1/18

[209] Naiman, J. P., Borkiewicz, K., & Christensen, A. J. 2017, Publications of the Astronomical Society of the Pacific, 129, 58008

[210] Naiman, J. P., Pillepich, A., Springel, V., et al. 2018, Monthly Notices of the Royal Astronomical Society, 477, 1206

[211] Nandra, K., & Iwasawa, K. 2007, Monthly Notices of the Royal Astronomical Society: Letters, 382, 2

[212] Natarajan, P. 2011, Bulletin of the Astronomical Society of India, 39, 145

[213] Nelson, D., Vogelsberger, M., Genel, S., et al. 2013, Monthly Notices of the Royal Astronomical Society, 429, 3353

[214] Nelson, D., Pillepich, A., Springel, V., et al. 2018, Monthly Notices of the Royal Astronomical Society, 475, 624

[215] Nelson, D., Kauffmann, G., Pillepich, A., et al. 2018, Monthly Notices of the Royal Astronomical Society, 477, 450

[216] Nelson, D., Pillepich, A., Springel, V., et al. 2019, 000, arXiv:1902.05554

[217] Nicastro, F., Mathur, S., Elvis, M., et al. 2005, Nature, 433, 495

[218] Noeske, K. G., Weiner, B. J., Faber, S. M., et al. 2007, The Astrophysical Journal, 660, L43

[219] Oppenheimer, B. D., & Davé, R. 2008, Monthly Notices of the Royal Astronomical Society, 387, 577

[220] Oppenheimer, B. D., Segers, M., Schaye, J., Richings, A. J., & Crain, R. A. 2017, eprint arXiv:1705.07897, 000, arXiv:1705.07897

[221] —. 2018, Monthly Notices of the Royal Astronomical Society, 474, 4740

[222] Oppenheimer, B. D., Crain, R. A., Schaye, J., et al. 2016, Monthly Notices of the Royal Astronomical Society, 460, 2157

[223] Oppenheimer, B. D., Bogdán, Á., Crain, R. A., et al. 2020, The Astrophysical Journal, 893, L24

[224] Oppenheimer, B. D., Davies, J. J., Crain, R. A., et al. 2020, Monthly Notices of the Royal Astronomical Society, 491, 2939

[225] Ostriker, J. P. 1980, Comments on Astrophysics, 8, 177

[226] Ostriker, J. P., & McKee, C. F. 1988, Reviews of Modern Physics, 60, 1

[227] Peek, J. E., Ménard, B., & Corrales, L. 2015, Astrophysical Journal, 813, 7

[228] Peeples, M. S., Werk, J. K., Tumlinson, J., et al. 2014, Astrophysical Journal, 786, doi:10.1088/0004-637X/786/1/54

[229] Peeples, M. S., Corlies, L., Tumlinson, J., et al. 2019, The Astrophysical Journal, 873, 129

[230] Peng, Y. J., Lilly, S. J., Kovač, K., et al. 2010, Astrophysical Journal, 721, 193

[231] Penny, S. J., Masters, K. L., Smethurst, R., et al. 2018, Monthly Notices of the Royal Astronomical Society, 476, 979

[232] Pettini, M., & Pagel, B. E. 2004, Monthly Notices of the Royal Astronomical Society, 348, 59

[233] Pointon, S. K., Kacprzak, G. G., Nielsen, N. M., et al. 2019, arXiv:1907.05557

[234] Pontzen, A., Rovskar, R., Stinson, G., R.;, W., & Reed, D.M.; and Coles, J. and Quinn, T. 2013, pynbody: Astrophysics Simulation Analysis for Python, doi:2013ascl.soft05002P

[235] Pontzen, A., & Tremmel, M. 2018, The Astrophysical Journal Supplement Series, 237, 23

[236] Pontzen, A., Tremmel, M., Roth, N., et al. 2017, Monthly Notices of the Royal Astronomical Society, 465, 547

[237] —. 2017, Monthly Notices of the Royal Astronomical Society, 465, 547

[238] Potter, D., Stadel, J., & Teyssier, R. 2017, Computational Astrophysics and Cosmology, 4, arXiv:1609.08621

[239] Press, W. H., & Schechter, P. 1974, The Astrophysical Journal, 187, 425

[240] Prochaska, J. X., Hennawi, J. F., Lee, K. G., et al. 2013, Astrophysical Journal, 776, arXiv:1308.6222

[241] Prochaska, J. X., Werk, J. K., Worseck, G., et al. 2017, arXiv:1702.02618

[242] —. 2017, The Astrophysical Journal, 837, 169

[243] Putman, M. E., Peek, J. E. G., & Joung, M. R. 2012, 491

[244] Quilis, V., Moore, B., & Bower, R. 2000, Science, 288, 1617

[245] Reddy, N. A., Steidel, C. C., Pettini, M., et al. 2008, The Astrophysical Journal Supplement Series, 175, 48

[246] Rees, M. J., & Ostriker, J. P. 1977, Mon. Not. R. astr. Soc, 179, 541

[247] Reeves, J. N., Sambruna, R. M., Braito, V., & Eracleous, M. 2009, Astrophysical Journal, 702, 2007

[248] Reines, A. E., Greene, J. E., & Geha, M. 2013, Astrophysical Journal, 775, arXiv:1308.0328

[249] Reines, A. E., & Volonteri, M. 2015, The Astrophysical Journal, 813, 82

[250] —. 2015, The Astrophysical Journal, 813, 82

[251] Rey, M. P., & Pontzen, A. 2018, Monthly Notices of the Royal Astronomical Society, 474, 45

[252] Ricarte, A., Tremmel, M., Natarajan, P., & Quinn, T. 2019, Monthly Notices of the Royal Astronomical Society, 489, 802

[253] Richards, G. T., Strauss, M. a., Fan, X., et al. 2006, The Astronomical Journal, 131, 2766

[254] Ritchie, B. W., & Thomas, P. A. 2001, Monthly Notices of the Royal Astronomical Society, 323, 743

[255] Robertson, B., Bullock, J. S., Cox, T. J., et al. 2006, The Astrophysical Journal, 645, 986

[256] Rosario, D. J., Santini, P., Lutz, D., et al. 2013, Astrophysical Journal, 771, arXiv:1302.1202

[257] Rosas-Guevara, Y., Bower, R. G., Schaye, J., et al. 2016, 17, 1

[258] Rosas-Guevara, Y. M., Bower, R. G., Schaye, J., et al. 2015, Monthly Notices of the Royal Astronomical Society, 454, 1038

[259] Rosdahl, J., Schaye, J., Dubois, Y., Kimm, T., & Teyssier, R. 2017, Monthly Notices of the Royal Astronomical Society, 466, 11

[260] Roth, N., Pontzen, A., & Peiris, H. V. 2016, Monthly Notices of the Royal Astronomical Society, 455, 974

[261] Rubin, K. H., Prochaska, J. X., Koo, D. C., et al. 2014, Astrophysical Journal, 794, arXiv:1307.1476

[262] Rupke, D. S. 2018, Galaxies, 6, arXiv:1812.05184

[263] Saglia, R. P., Opitsch, M., Erwin, P., et al. 2016, The Astrophysical Journal, 818, 47

[264] Salem, M., Bryan, G. L., & Hummels, C. 2014, Astrophysical Journal Letters, 797, 2

[265] Sanchez, N. N., Tremmel, M., Werk, J. K., et al. 2021, The Astrophysical Journal, 911, 116

[266] Sanchez, N. N., Werk, J. K., Tremmel, M., et al. 2019, The Astrophysical Journal, 882, 8

[267] Sanchez, N. N., Bellovary, J. M., Holley-Bockelmann, K., et al. 2018, The Astrophysical Journal, 860, 20

[268] Sanderbeck, P. R. U., McQuinn, M., D'Aloisio, A., & Werk, J. K. 2017, The Astrophysical Journal, 869, 159

[269] —. 2017, arXiv:1710.07295

[270] Savage, B. D., Kim, T. S., Wakker, B. P., et al. 2014, Astrophysical Journal, Supplement Series, 212, arXiv:1403.7542

[271] Savorgnan, G. A. D., & Graham, A. W. 2016, The Astrophysical Journal Supplement Series, 222, 10

[272] Schawinski, K., Dowlin, N., Thomas, D., Urry, C. M., & Edmondson, E. 2010, The Astrophysical Journal, 714, L108

[273] Schawinski, K., Urry, C. M., Simmons, B. D., et al. 2014, Monthly Notices of the Royal Astronomical Society, 440, 889

[274] —. 2014, Monthly Notices of the Royal Astronomical Society, 440, 889

[275] Schaye, J., Crain, R. A., Bower, R. G., et al. 2015, Monthly Notices of the Royal Astronomical Society, 446, 521

[276] Schiavi, R., Capuzzo-Dolcetta, R., Arca-Sedda, M., & Spera, M. 2020, Astronomy and Astrophysics, 642, 1

[277] Schramm, M., & Silverman, J. D. 2013, Astrophysical Journal, 767, doi:10.1088/0004-637X/767/1/13

[278] Semenov, V. A., Kravtsov, A. V., & Gnedin, N. Y. 2017, The Astrophysical Journal, 845, 133

[279] Sharma, R. S., Brooks, A. M., Somerville, R. S., et al. 2020, The Astrophysical Journal, 897, 103

[280] Shen, S., Madau, P., Aguirre, A., et al. 2012, Astrophysical Journal, 760, arXiv:1109.3713

[281] Shen, S., Wadsley, J., & Stinson, G. 2010, Monthly Notices of the Royal Astronomical Society, 407, 1581

[282] Shin, J., Woo, J.-H., & Mulchaey, J. S. 2016, The Astrophysical Journal Supplement Series, 227, 31

[283] Shull, J. M., Moloney, J., Danforth, C. W., & Tilton, E. M. 2015, Astrophysical Journal, 811, 3

[284] Sijacki, D., Springel, V., Di Matteo, T., & Hernquist, L. 2007, Monthly Notices of the Royal Astronomical Society, 380, 877

[285] Silk, J. 2013, Astrophysical Journal, 772, arXiv:1305.5840

[286] Silk, J., & Rees, M. J. 1998, Growth Lakeland, 4, 4

[287] Simmons, B. D., Urry, C. M., Schawinski, K., Cardamone, C., & Glikman, E. 2012, Astrophysical Journal, 761, doi:10.1088/0004-637X/761/1/75

[288] Simons, R. C., Kassin, S. A., Snyder, G. F., et al. 2019, The Astrophysical Journal, 874, 59

[289] Smethurst, R. J., Lintott, C. J., Simmons, B. D., et al. 2015, Monthly Notices of the Royal Astronomical Society, 450, 435

[290] Smith, M. C., Sijacki, D., & Shen, S. 2019, Monthly Notices of the Royal Astronomical Society, 485, 3317

[291] Snyder, G. F., Torrey, P., Lotz, J. M., et al. 2015, 1908, 1886

[292] Somerville, R. S., & Davé, R. 2015, Annual Review of Astronomy and Astrophysics, 53, 51

[293] Somerville, R. S., Hopkins, P. F., Cox, T. J., Robertson, B. E., & Hernquist, L. 2008, 506, 481

[294] Somerville, R. S., & Primack, J. R. 1999, 1110

[295] Springel, V. 2005, Monthly Notices of the Royal Astronomical Society, 364, 1105

[296] —. 2010, Monthly Notices of the Royal Astronomical Society, 401, 791

[297] Springel, V., Di Matteo, T., & Hernquist, L. 2005, The Astrophysical Journal, 620, L79

[298] —. 2005, Monthly Notices of the Royal Astronomical Society, 361, 776

[299] Springel, V., Pakmor, R., Pillepich, A., et al. 2018, Monthly Notices of the Royal Astronomical Society, 475, 676

[300] Steidel, C. C., Erb, D. K., Shapley, A. E., et al. 2010, Astrophysical Journal, 717, 289

[301] Steinborn, L. K., Hirschmann, M., Dolag, K., et al. 2018, 21, 1

[302] Stern, J., Faucher-Giguère, C.-A., Zakamska, N. L., & Hennawi, J. F. 2016, The Astrophysical Journal, 819, 130

[303] Stinson, G., Seth, A., Katz, N., et al. 2006, Monthly Notices of the Royal Astronomical Society, 373, 1074

[304] Stinson, G. S., Brook, C., Macciò, A. V., et al. 2013, Monthly Notices of the Royal Astronomical Society, 428, 129

[305] Stinson, G. S., Brook, C., Prochaska, J. X., et al. 2012, Monthly Notices of the Royal Astronomical Society, 425, 1270

[306] Stocke, J. T., Keeney, B. A., Danforth, C. W., et al. 2013, Astrophysical Journal, 763, arXiv:1704.00235

[307] Stopyra, S., Pontzen, A., Peiris, H., Roth, N., & Rey, M. P. 2021, The Astrophysical Journal Supplement Series, 252, 28

[308] Strateva, I., Ivezić, Ž., Knapp, G. R., et al. 2001, The Astronomical Journal, 122, 1861

[309] Suresh, J., Rubin, K. H. R., Kannan, R., et al. 2017, Monthly Notices of the Royal Astronomical Society, 465, 2966

[310] Telford, O. G., Werk, J. K., Dalcanton, J. J., & Williams, B. F. 2018, arXiv:1811.02589

[311] —. 2019, The Astrophysical Journal, 877, 120

[312] Terrazas, B. A., Bell, E. F., Pillepich, A., et al. 2019, 19, 1

[313] Thielemann, F.-K., Nomoto, K., & Yokoi, K. 1986, Astronomy and Astrophysics (ISSN 0004-6361), 158, 17

[314] Thom, C., Tumlinson, J., Werk, J. K., et al. 2012, Astrophysical Journal Letters, 758, arXiv:1209.5442

[315] Thomas, D., Maraston, C., Bender, R., & de Oliveira, C. M. 2005, The Astrophysical Journal, 621, 673

[316] Tombesi, F., Cappi, M., Reeves, J. N., & Braito, V. 2012, Monthly Notices of the Royal Astronomical Society: Letters, 422, 1

[317] Toomre, A., & Toomre, J. 1972, The Astrophysical Journal, 178, 623

[318] Tremblay, G. R., Combes, F., Oonk, J. B. R., et al. 2018, The Astrophysical Journal, 865, 13

[319] Tremmel, M., Governato, F., Volonteri, M., Pontzen, A., & Quinn, T. R. 2018, arXiv:1802.06783

[320] —. 2018, arXiv:1802.06783

[321] Tremmel, M., Governato, F., Volonteri, M., & Quinn, T. R. 2015, Monthly Notices of the Royal Astronomical Society, 451, 1868

[322] Tremmel, M., Karcher, M., Governato, F., et al. 2016, 19, 1

[323] —. 2017, Monthly Notices of the Royal Astronomical Society, 470, 1121

[324] Tremmel, M., Quinn, T. R., Ricarte, A., et al. 2019, Monthly Notices of the Royal Astronomical Society, 483, 3336

[325] —. 2019, Monthly Notices of the Royal Astronomical Society, 483, 3336

[326] Tremonti, C. A., Heckman, T. M., Kauffmann, G., et al. 2004, The Astrophysical Journal, 613, 898

[327] Tripp, T. M., Meiring, J. D., Prochaska, J. X., et al. 2011, Science, 334, 952

[328] Truong, N., Pillepich, A., Nelson, D., Werner, N., & Hernquist, L. 2021, 17, 1

[329] Trussler, J., Maiolino, R., Maraston, C., et al. 2020, Monthly Notices of the Royal Astronomical Society, 491, 5406

[330] Tumlinson, J., Peeples, M. S., & Werk, J. K. 2017, Annual Review of Astronomy and Astrophysics, 55, 389

[331] Tumlinson, J., Thom, C., Werk, J. K., et al. 2011, Science, 334, 948

[332] —. 2013, The Astrophysical Journal, 777, 59

[333] Turk, M. J., Smith, B. D., Oishi, J. S., et al. 2011, Astrophysical Journal, Supplement Series, 192, arXiv:1011.3514

[334] —. 2011, Astrophysical Journal, Supplement Series, 192, doi:10.1088/0067-0049/192/1/9

[335] Uhlig, M., Pfrommer, C., Sharma, M., et al. 2012, Monthly Notices of the Royal Astronomical Society, 423, 2374

[336] van den Bosch, F. C., Aquino, D., Yang, X., et al. 2008, Monthly Notices of the Royal Astronomical Society, 387, 79

[337] Van den Bosch, F. C., Yang, X., Mo, H. J., et al. 2007, Monthly Notices of the Royal Astronomical Society, 376, 841

[338] van der Wel, A., Franx, M., van Dokkum, P. G., et al. 2014, The Astrophysical Journal, 788, 28

[339] Veilleux, S., & Cecil, G. 2005, arXiv:0504435v3

[340] Villforth, C., Herbst, H., Hamann, F., et al. 2018, 13, 1

[341] Villforth, C., Sarajedini, V., & Koekemoer, A. 2012, Monthly Notices of the Royal Astronomical Society, 426, 360

[342] Vogelsberger, M., Genel, S., Sijacki, D., et al. 2013, Monthly Notices of the Royal Astronomical Society, 436, 3031

[343] Vogelsberger, M., Marinacci, F., Torrey, P., & Puchwein, E. 2020, Nature Reviews Physics, 2, 42

[344] Vogelsberger, M., Genel, S., Springel, V., et al. 2014, Monthly Notices of the Royal Astronomical Society, 444, 1518

[345] Voit, G. M., Meece, G., Li, Y., et al. 2017, The Astrophysical Journal, 845, 80

[346] Volonteri, M. 2012, Science, 337, 544

[347] Volonteri, M., & Bellovary, J. 2012, Reports on Progress in Physics, 75, 1

[348] —. 2012, Reports on progress in physics. Physical Society (Great Britain), 75, 124901

[349] Volonteri, M., & Natarajan, P. 2009, Monthly Notices of the Royal Astronomical Society, 400, 1911

[350] Wadsley, J., Stadel, J., & Quinn, T. 2004, New Astronomy, 9, 137

[351] Wadsley, J. W., Keller, B. W., & Quinn, T. R. 2017, Monthly Notices of the Royal Astronomical Society, 471, 2357

[352] Wadsley, J. W., Veeravalli, G., & Couchman, H. M. P. 2008, Monthly Notices of the Royal Astronomical Society, 387, 427

[353] Wang, L., Dutton, A. A., Stinson, G. S., et al. 2015, Monthly Notices of the Royal Astronomical Society, 454, 83

[354] Weinberger, R., Ehlert, K., Pfrommer, C., Pakmor, R., & Springel, V. 2017, Monthly Notices of the Royal Astronomical Society, 470, 4530

[355] Werk, J. K., Bentz, M. C., Burchett, J. N., et al. 2021, Connecting Galaxy Black Hole Mass with the State of the Circumgalactic Medium, HST Proposal. Cycle 29, ID. #16650

[356] Werk, J. K., Prochaska, J. X., Thom, C., et al. 2012, The Astrophysical Journal Supplement Series, 198, 3

[357] —. 2013, The Astrophysical Journal Supplement Series, 204, 17

[358] Werk, J. K., Prochaska, J. X., Tumlinson, J., et al. 2014, The Astrophysical Journal, 792, 8

[359] Werk, J. K., Prochaska, J. X., Cantalupo, S., et al. 2016, 24

[360] Werle, A., Fernandes, R. C., Asari, N. V., et al. 2020, 15, 1

[361] Wetzel, A. R., Hopkins, P. F., Kim, J.-h., et al. 2016, The Astrophysical Journal, 827, L23

[362] Wetzel, A. R., Tinker, J. L., & Conroy, C. 2012, Monthly Notices of the Royal Astronomical Society, 424, 232

[363] Whitaker, K. E., Van Dokkum, P. G., Brammer, G., & Franx, M. 2012, Astrophysical Journal Letters, 754, doi:10.1088/2041-8205/754/2/L29

[364] White, S. D. M. 1976, Monthly Notices of the Royal Astronomical Society, 177, 717

[365] White, S. D. M., & Rees, M. J. 1978, Monthly Notices of the Royal Astronomical Society, 183, 341

[366] Whitmore, B. C. 1980, The Astrophysical Journal, 242, 53

[367] Wiersma, R. P., Schaye, J., Theuns, T., Dalla Vecchia, C., & Tornatore, L. 2009, Monthly Notices of the Royal Astronomical Society, 399, 574

[368] Wilde, M. C., Werk, J. K., Burchett, J. N., et al. 2021, The Astrophysical Journal, 912, 9

[369] Woosley, S. E., & Weaver, T. A. 1995, The Astrophysical Journal Supplement Series, 101, 181

[370] Wotta, C. B., Lehner, N., Howk, J. C., O'Meara, J. M., & Prochaska, J. X. 2016, The Astrophysical Journal, 831, 1

[371] Wuyts, S., Förster Schreiber, N. M., van der Wel, A., et al. 2011, The Astrophysical Journal, 742, 96

[372] Yao, Y., Wang, Q. D., Penton, S. V., et al. 2010, Astrophysical Journal, 716, 1514

[373] York, D. G., Khare, P., Vanden Berk, D., et al. 2006, Monthly Notices of the Royal Astronomical Society, 367, 945

[374] Zahid, H. J., Dima, G. I., Kewley, L. J., Erb, D. K., & Davé, R. 2012, Astrophysical Journal, 757, doi:10.1088/0004-637X/757/1/54

[375] Zhang, H., Zaritsky, D., Werk, J., & Behroozi, P. 2018, The Astrophysical Journal, 866, L4

[376] Zhu, G., & Ménard, B. 2013, Astrophysical Journal, 773, arXiv:1304.0451

[377] Zinger, E., Pillepich, A., Nelson, D., et al. 2020, Monthly Notices of the Royal Astronomical Society, 499, 768

[378] Zolotov, A., Brooks, A. M., Willman, B., et al. 2012, The Astrophysical Journal, 761, 71

[379] Zou, H., Yang, Y. B., Zhang, T. M., et al. 2011, Research in Astronomy and Astrophysics, 11, 1093